EQUATION OF STATE FOR POLYTETRAFLUOROETHYLENE (PTFE) AND MIXTURES WITH PTFE

A Dissertation
Presented to
The Academic Faculty

By

Zhibo Wu

In Partial Fulfillment
Of the Requirements for the Degree
Doctor of Philosophy in the
School of Aerospace Engineering

Georgia Institute of Technology
August 2009

EQUATION OF STATE FOR POLYTETRAFLUOROETHYLENE (PTFE) AND MIXTURES WITH PTFE

Approved by:

Dr. Sathya Hanagud, Advisor
School of Aerospace Engineering
Georgia Institute of Technology

Dr. David L. McDowell
School of Mechanical Engineering
Georgia Institute of Technology

Dr. George Kardomateas
School of Aerospace Engineering
Georgia Institute of Technology

Dr. Nicoleta Apetre
School of Aerospace Engineering
Georgia Institute of Technology

Dr. Massimo Ruzzene
School of Aerospace Engineering
Georgia Institute of Technology

Date Approved: May 13, 2009

ACKNOWLEDGEMENTS

I am very grateful to my thesis advisor, Dr. Sathya V. Hanagud, for his close reviewing my research progress and day-by-day guidance during my Ph.D. study at Georgia Tech, and his reviewing and correcting my entire thesis manuscript. I would like to thank Dr. George Kardomateas, Dr. Massimo Ruzzene, Dr. David L. McDowell, and Dr. Nicoleta Apetre for their time in serving on my thesis committee and providing many highly valuable suggestions to improve the thesis. I would like to express my heartfelt respect to the Graduate Coordinator of School of Aerospace Engineering, Dr. Jeff Jagoda, for his great attention to my Ph.D. study and his help on various policies related to registration and tuition waiver.

I would like to show my heartfelt gratitude to Dr. Xia Lu, for her advice and encouragement, which helped me to overcome countless difficulties when I began my Ph.D. study. I also want to thank my friends, Dr. Tianci Jiang, Roussislava Zaharieva, Akash Dixit and Derek Reding for sharing their knowledge with me and morally supporting me through the years.

Lastly, on a more personal note, I am most grateful to my husband, Yuan, for his love and support through the years.

TABLE OF CONTENTS

LIST OF TABLES

LIST OF FIGURES

SUMMARY

Aerospace structural materials are usually classified for their strength characteristics and the beneficial strength to weight ratios. In aerospace structural design, the strength implies resistance to loads experienced during the service life of the aerospace structure. These loads include fatigue loads and extreme loads that are expected during maneuvers. These structural materials are also expected to resist environmental conditions that result in corrosion failure, stress corrosion failure and other environmentally induced damage conditions. Thus, such structural materials are expected to have a single function of resisting loads experienced during the service life of the structure. However, the research work of the past few years is directed to explore the potential of new materials that are capable of providing more than one basic function of strength. Very often the additional functions such as the functions of sensing and actuation are considered. The focus of this work is to explore the potential of the second function of energetic characteristics. Thus, the dual functional materials have both the structural characteristics and energetic characteristics. Sometimes these materials are cited in the literature as the reactive material structures or dual functional structural energetic materials. The dual functions of such materials are realized by a synthesis of granular composites of reactive materials, binders, structural reinforcements and voids. Specific reactive materials that are considered include thermite mixtures, intermetallic combinations and oxidizing metals.

The goals of this work, however, are not to explore new techniques of synthesis of the structural energetic materials or reactive material structures. The objectives are to discuss multiscale models that are used to characterize the constitutive relations of the

granular composite materials with dual functions. Usually, the determination of both the constitutive relations with all the needed parameters and chemical reaction characteristics are by the use of experiments. In this work, however, the goals are to explore the potential of different structural energetic materials that are made from different combinations of reactive materials, different binders and voids. In such exploratory studies, it is necessary to consider different ratios of the basic ingredients. Because the dual functional energetic structural materials are used in applications where the resulting structure encounters high intensity impact loads, impact and penetration into selected targets and shock induced chemical reactions, it is also necessary to consider large or finite deformations of these materials. The experimental techniques that are used consist of techniques such as the gas gun tests and flyer plate impact tests. To accomplish the exploratory tasks that are stated in the last few sentences requires a very large number of tests. Thus it is both expensive and time intensive.

Thus, it is necessary to consider alternate methods of determining the constitutive equations without conducting tests. This is accomplished by the use of ab initio methods to obtain the constitutive relations and foundations for chemical reactions in structural energetic materials without conducting tests. This needs an exploration of the analysis beyond continuum. First, it is necessary to study the quantum many body problem to quantitatively determine the internal energy of the material when subjected to different strain conditions. The current state of the technology is such that it is not possible to obtain an exact solution to the needed quantum many body problem that is modeled by the Schrödinger's equations. It is possible to solve these equations approximately by the approximation of density functional theory and Kohn Sham approximate equations. This

however, yields only energies at the ground state or at absolute 0ºK. Thus it becomes necessary to add both the lattice thermal contributions due to phonons and electron thermal contribution. Then, resulting energy is used to bridge to the continuum level and obtain the constitutive equations. This is the procedure that is used in this work.

Specific objectives of this study are not to design such materials but to characterize these materials. The primary research issues are the determinations of the constitutive relations for finite deformation of these energetic structural materials that can be designed to withstand impact loads. The issues of the constitutive equations form the focus of this thesis.

More specifically, the scope of the thesis is further reduced to analyze the constitutive equations of specific mixtures of nickel, aluminum with PTFE or Teflon as the binder. The equations of state $p=P(\rho,T)$ of the individual elements (nickel and aluminum), from ab initio studies, are reported in the literature. It is to be noted that the equations of state forms only a part of the complete constitutive relationships. However, the equation of state of PTFE, the equations of state of the mixtures of nickel, aluminum and PTFE are not studied or reported in the literature. Similarly, the problem of determination of the complete constitutive equations of crystalline materials, from ab initio methods under conditions of finite deformations, is still an open research area. The published papers do not consider the satisfaction of the principle of objectivity, the material symmetry conditions and the polyconvexity of the resulting expressions for the strain energy. Thus this thesis presents solutions to the following problems.

(1). Determination of the thermodynamically complete equation of state of the binder and the energetic material PTFE or Teflon, from ab initio methods based on the density functional theory and Kohn Sham equations.

(2). Determination of the equations of state of the granular composite or the mixture of nickel, aluminum and PTFE from ab initio methods.

(3). Determination of the complete constitutive equation of aluminum, from ab initio methods, under conditions of finite deformations, with principle of objectivity, material symmetry conditions and polyconvexity of the strain energy.

All results are compared to test results whenever they are available.

CHAPTER 1

INTRODUCTION

Aerospace structural materials are usually classified for their strength characteristics and the beneficial strength to weight ratios. In aerospace structural design, the strength implies resistance to loads experienced during the service life of the aerospace structure. These loads include fatigue loads and extreme loads that are expected during maneuvers. These structural materials are also expected to resist environmental conditions that result in corrosion failure, stress failure and other environmentally induced damage conditions. Thus, such structural materials are expected to have a single function of resisting loads experienced during the service life of the structure. However, the research work of the past few years is directed to explore the potential of new materials that are capable of providing more than one basic function of strength. Very often the additional functions such as the functions of sensing and actuation are considered. The focus of this work is to explore the potential of the second function of energetic characteristics. Thus, the dual functional materials have both the structural characteristics and energetic characteristics. Sometimes these materials are cited in the literature as the reactive material structures or dual functional structural energetic materials. The dual functions of such materials are realized by a synthesis of granular composites of reactive materials, binders, structural reinforcements and voids. Specific reactive materials that are considered include thermite mixtures, intermetallic combinations and oxidizing metals. There are several techniques that are available to synthesize these structural energetic materials or reactive material structures. There are also several research programs to develop new techniques to

synthesize these materials to meet many new specifications. Some of the synthesis techniques that are available include methods such as the sol-gel processes; press and cure processes; and explosive consolidation processes.

The goals of this work, however, are not to explore new techniques of synthesis of the structural energetic materials or reactive material structures. The objectives are to discuss multiscale models that are used to characterize the constitutive relations of the granular composite materials with dual functions. The objective also includes reaction characteristics of these materials. Usually, the determination of both the constitutive relations with all the needed parameters and chemical reaction characteristics are by the use of experiments. In this work, however, the goals are to explore the potential of different structural energetic materials that are made from different combinations of reactive materials, different binders and voids. In such exploratory studies, it is necessary to consider different ratios of the basic ingredients. Because the dual functional energetic structural materials are used in applications where the resulting structure encounters high intensity impact loads, impact and penetration into selected targets and shock induced chemical reactions, it is also necessary to consider large or finite deformations of these materials. The experimental techniques that are used consist of techniques such as the gas gun tests and flyer plate impact tests. To accomplish the exploratory tasks that are stated in the last few sentences requires a very large number of tests. Thus it is both expensive and time intensive.

Thus, it is necessary to consider alternate methods of determining the constitutive equations and chemical reaction characteristics without conducting tests. This is accomplished by the use of ab initio methods to obtain the constitutive relations and

foundations for chemical reactions in structural energetic materials without conducting tests. This needs an exploration of the analysis beyond continuum. First, it is necessary to study the quantum many body problem to quantitatively determine the internal energy of the material when subjected to different strain conditions. The current state of the technology is such that it is not possible to obtain an exact solution to the needed quantum many body problem that is modeled by the Schrödinger's equations. It is possible to solve these equations approximately by the approximation of density functional theory and Kohn Sham approximate equations. This however, yields only energies at the ground state or at absolute 0ºK. Thus it becomes necessary to add both the lattice thermal contributions due to phonons and electron thermal contribution. Then, resulting energy is used to bridge to the continuum level and obtain the constitutive equations. This is the procedure that is used in this work.

1.1 Reactive Materials

There are many different reactive materials that form the foundations for structural energetic materials. They are usually classified into three types. These are as follows.

- Metal/metal oxide mixtures (thermites);
- Metal/metal mixtures (intermetallics); and
- Combustible metals (metal to metal oxide reaction).

To discuss the possible design of mixtures, some of the characteristics of a few selected thermite mixtures, intermetallics mixtures and combustible metals are listed. Then, the next step is to select a mixture to meet specified goals or requirements.

I. THERMITES:

Reactive Materials	**Mixture Density (g/cc)**	**Reaction Temperature (ºK)**	**Heat of Reaction (Calories/g)**
$1.3Mg + B_2O_3$	1.785	6,389/3,873	2,134
$2Al + Ni_2O_3$	4.045	5,031/3,187	1,292
$2Y + Ni_2O_3$	4.636	7,614/3,955	1,120
$2Al + Fe_2O_3$	4.175	4,382/3,135	945
$4Al + 3MnO_2$	4.014	4,829/2,918	1,159
$Al + KclO_4$	2.5		3,000

II. INTERMETALLIC MIXTURES

Reactive Materials	**Mixture Density (g/cc)**	**Reaction Temperature (ºK)**	**Heat of Reaction (Calories/g)**
2B + Ti	3.603	3,043	1,320
Mo + 2Si	4.582	3,498	207
2B + Hf	8.232	3,945/3,653	742
Al + Ni	5.165	2,362/1,910	330
Hf + C	9.084	4,441/4,222	315
Al + Ta	9.952	1,011	57
2C + Th	8.169	3,073	247
2B + Ta	10.36	2,666	

III. COMUSTIBLE METALS

Metal/Metal Oxide	**Metal Density (g/cc)**	**Reaction Temperature (^oK)**	**Heat of Reaction (Calories/g)**
Hf / HfO_2	11.4	2,495	1,491
Ta/Ta_2O_5	16.6	3,390	1,390
Al / Al_2O_3	2.7	933	7,422
Mg / MgO	1.5	923	6,241
Mn /Mn_3O_4	7.3	1,519	2,012
Mo / MoO_3	9.1	2,896	1,856
Nb /Nb_2O_5	8.57	2,750	2,443
Ti /TiO_2	4.5	1,693	4,714
Y /Y_2O_3	4.47	1,799	2,819
W /WO_2	19.3	3,695	767

The thermite mixtures have the potential to yield a very high enthalpic energy. However, the density of the energetic structural material that results from the mixture is very low. For example a mixture of magnesium and boron has the potential to releases 2134 calories per gram. However the density of the mixture is only 1.785 g/cc. Similarly the strength is also low. The intermetallic mixtures do have high densities. For example, the intermetallic mixture of hafnium and carbon has a density of 9.085 g/cc. Similarly, the intermetallic mixture of aluminum and tantalum has a density of nearly 10 g/cc. These densities are much higher than the conventional structural material such as the steel. However the potential energy that can be released from these high density

intermetallic mixtures are very low, as is seen in the table. The combustible metals do have the potential to release high enthalpic energy. Even here the low density metal such as the aluminum has the potential to release a large amount of energy. However combustible metals require a high reaction initiation temperature. This suggests that another reaction must precede the initiation of the combustible metal to metal oxide reaction. Thus to realize energetic structural materials of high density and high enthalpic energy that can be released upon the initiated chemical reaction, it becomes necessary to create hybrid mixtures of reactive materials.

1.2 Thesis Outline

Goals of this study are not to design such materials but to characterize these materials. The primary research issues are the determinations of the constitutive relations for finite deformation of these energetic structural materials that can be designed to withstand impact loads. The second issue is the chemical reaction process. This takes the form of failure criteria if the structure is operating under conditions where only strength is desired. The chemical reaction process is a needed criterion when the energetic structural material is operated to release the enthalpic energy by an external stimulus and a sequence that takes place. The issues of the constitutive equations form the focus of this thesis. More specifically, the scope of the thesis is further reduced to analyze the constitutive equations of a specific mixture of nickel, aluminum and PTFE or Teflon as the binder. The equations of state $p=P(\rho,T)$ of the individual elements (nickel and aluminum), from ab initio studies, are reported in the literature. It is to be noted that the equations of state forms only a part of the complete constitutive relationships. However, the equation of state of PTFE, the equations of state of the mixtures of nickel, aluminum

and PTFE are not studied or reported in the literature. Similarly, the problem of determination of the complete constitutive equations of crystalline materials, from ab initio methods under conditions of finite deformations, is still an open research area. The published papers do not consider the satisfaction of the principle of objectivity, the material symmetry conditions and the polyconvexity of the resulting expressions for the strain energy. Thus this thesis follows the following outline.

(1). Determination of the thermodynamically complete equation of state of the binder and the energetic material PTFE or Teflon, from ab initio methods based on the density functional theory and Kohn Sham equations

(2). Determination of the equations of state of the granular composite or the mixture of nickel, aluminum and PTFE from ab initio methods.

(3). Determination of the complete constitutive equation of aluminum, from ab initio methods, under conditions of finite deformations, with principle of objectivity, material symmetry conditions, and polyconvexity of the strain energy.

All results are compared to test results whenever they are available.

CHAPTER 2

BACKGROUND

The mechanical response of materials is usually described using models based on experimentally observed results. In the last thirty years, the physical properties of materials such as the constitutive relations, including the equation of state are being studied by using first-principle methods that are based on the study of multi-body problems and the foundation of quantum mechanics. As explained in subsequent paragraph, foundation for use of a quantum mechanics approach to obtain the mechanical or thermomechanical response of solids is based on the fact that a solid is a collection of relatively heavy positively charged nuclei (particles) and very light negatively charged electrons. Thus many-body problem is formulated by Schröndinger, as Schröndinger equation. If the Schröndinger equation is solved to obtain the energy of the solid, the calculated energy with thermal contribution is useful in obtaining the constitutive equations. However, it is currently not possible to solve the Schröndinger equation. Thus there are levels of approximation. The first level of approximation is the Born-Oppenheimer approximation. The second level of approximation is the density functional theory. The ground state energy is calculated through the density functional theory. This ground state energy, together with lattice thermal energy, and electron thermal energy, is useful in calculating the Helmholtz free energy, which in turn, is used to obtain the constitutive equations.

Density functional theory is a powerful theoretical tool to gain quantitative understanding of complex molecules. It is the firm and rigorous foundation for a

relatively simple approach to the quantum mechanical treatment taking the full account of electron-electron interaction. The basis for this theory is the proof by Hohenberg and Kohn[2] that the electronic structure and ground state energy are determined completely by the electron density. A brief review of the literature in the key areas of using density functional theory is given here.

2.1 Schröndinger Equation and Born-Oppenheimer Approximation

A solid consist both heavy positively charged particles and very light negatively charged particles or electrons. If there are N nuclei, the number of particles is N+ZN interacting particles. The exact Hamiltonian of a quantum mechanical system is written as follows. Considering a system of N nuclei described by coordinates $R_1, \ldots, R_N \equiv R$, momentum $P_1, \ldots, P_N \equiv P$ and masses $M_1, \ldots, M_N$, and N_e *(ZN)* electrons described by coordinates $r_1, \ldots, r_{Ne} \equiv r$, momentum $p_1, \ldots, p_{Ne} \equiv p$ and spin variables $s_1, \ldots, s_{Ne} \equiv s$. Nuclear spin is ignored in the present discussion. The non-relativistic Hamiltonian of the system is given by

$$H = \sum_{I=1}^{N} \frac{\vec{P}_I^2}{2M_I} + \sum_{i=1}^{N_e} \frac{\vec{p}_i^2}{2m} + \sum_{i>j} \frac{e^2}{\left|\vec{r}_i - \vec{r}_j\right|} + \sum_{I>J} \frac{Z_I Z_J e^2}{\left|\vec{R}_I - \vec{R}_J\right|} - \sum_{i,I} \frac{Z_I e^2}{\left|\vec{R}_I - \vec{r}_i\right|}$$

$$\equiv T_N + T_e + V_{ee}(\vec{r}) + V_{NN}(\vec{R}) + V_{eN}(\vec{r}, \vec{R}) \qquad (2\text{-}1)$$

where m is the mass of the electron and Z_{Ie} is the charge on the Ith nucleus. In the second line, T_N, T_e, V_{ee}, V_{NN} and V_{eN} represent the nuclear and electron kinetic energy operators and electron–electron, nuclear–nuclear and electron–nuclear interaction potential operators, respectively. The solution of the time-independent Schrödinger equation

$$[T_N + T_e + V_{ee}(r) + V_{NN}(R) + V_{eN}(r,R)]\Phi(x,R) = E\,\Phi(x,R) \qquad (2\text{-}2)$$

yields the eigenfunctions and eigenvalues. In this equation, E is the energy. $x \equiv (r, s)$ denotes the full collection of electron position and spin variables, and $\Phi(x,R)$ is an eigenfunction of the non-relativistic Hamiltonian H with eigenvalue E. Clearly, an exact solution of equation (2-2) is not possible and approximations must be made. Currently technique to solve the complete Schröndinger equation for a solid is not available. The first kind of approximation to the Schröndinger Equation is the Born–Oppenheimer approximation that assumes a quasi-separable form in equation (2-2) and makes use of the fact that nuclei motion is small compare to the motion of light electrons. Then, the eigenfunction $\Phi(x,R)$ can be written as:

$$\Phi(x,R) = \Psi(x,R)\chi(R) \tag{2-3}$$

where $\chi(R)$ is a nuclear wavefunction and $\Psi(x,R)$ is an electronic wavefunction that depends parametrically on the nuclear positions. Substituting equation (2-3) into equation (2-2), the Schröndinger equations for the coupled system are reduced to a system of decoupled ion system and electron system.

$$\begin{cases} [T_e + V_{ee}(\vec{r}) + V_{Ne}(\vec{r},\vec{R})]\Psi_n(x,\vec{R}) = e_n(\vec{R})\Psi_n(x,\vec{R}) \\ [T_N + V_{NN}(\vec{R}) + e(\vec{R})]\chi(\vec{R}) = \varepsilon\chi(\vec{R}) \end{cases} \tag{2-4}$$

In many cases, non-adiabatic effects can be neglected, and we may consider motion only on the ground electronic surface. The total energy of the system is then split into the contribution from the ions and the contribution from the electrons on the ground-state surface.

$$E_0(\vec{R}) = e_0(\vec{R}) + V_{NN}(\vec{R}) \tag{2-5}$$

Equations (2-4) are a strong nonlinear system. The exact solutions of equation (2-4) can not be obtained within the range of current techniques. Two major techniques to

approximate the solutions are the Hartree-Fock method and the Density Functional Theory (DFT). In the HF technique, the wave function for the electron systems is assumed in a form of Slater determinant to characterize the interchange properties of electrons. Slater determinant is an antisymmetrized product of N one-electron wave functions. Then the electron system in the equation (2-4a) is reduced to a one wave equation. In the following section, we will give an introduction to the density functional theory.

2.2 Density Functional Theory (Kohn & Sham, 1965)

DFT is based on a Hohenberg and Kohn Theorem, which states

1. The ground-state energy of a many body system is a unique functional of the electron density

$$E_0 = E[n(\vec{r})] \tag{2-6}$$

2. The functional has its minimum at the equilibrium density $n_0(\vec{r})$

$$E_0 = E[n_0(\vec{r})] = \min_{n \to n_0}\{E[n(\vec{r})]\} \tag{2-7}$$

The electron density is defined as the probability of finding any of the N electrons within the volume element $d\vec{r}_1$.

$$n(\vec{r}) = N_e \int ... \int \left|\Psi(x)\right|^2 ds_1 d\vec{r}_2 ... d\vec{r}_{Ne} \tag{2-8}$$

The energy functional of the electron system is defined as

$$E[n] = T_e[n] + E_{ee}[n] + \int V_{Ne}(\vec{r}) n(\vec{r}) d^3 r \tag{2-9}$$

Therefore, the solution approach of the equation (2-4a) becomes a variation problem, which is to find the density $n_0(\vec{r})$ to minimize the energy functional in the equation (2-9). This variation problem is presented in the equation (2-7).

Although the formulation of this variation is very elegant, the forms for the kinetic energy $T_e[n]$, the electron-electron repulsion energy $E_{ee}[n]$ and the nuclei-electron interaction potential $\int V_{Ne}(\vec{r})n(\vec{r})d^3r$ are unknown for a general many electron system. In this, some techniques start from a known reference system. Based on the selected reference system, we can approximate the general system by adding corrections to the reference system. One of these techniques is the Kohn-Sham theory, which selects a system of non-interacting gas of electrons as the reference system (non-interacting means electrons do not interact via Coulomb repulsion). This reference system is chosen to have the same electron density as the many electron system. That is,

$$n^{ks}(\vec{r}) = n_0(\vec{r}) \tag{2-10}$$

For the non-interacting gas system, we have

$$n^{ks}(\vec{r}) = \sum_i |\phi_i(\vec{r})|^2 \tag{2-11}$$

where $\phi_i(\vec{r})$ is the one wave functions, called Kohn-Sham orbitals. The energy for the non-interacting gas system is given by

$$E^{ks}[n^{ks}] = T_e^{ks}[n^{ks}] + E_{ee}^{ks}[n^{ks}(\vec{r})] + \int n^{ks}(\vec{r})V_{Ne}[n^{ks}(\vec{r})]d^3r \tag{2-12}$$

The forms for the functionals in the equation (2-12) are known. They are

$$T_e^{ks}[n^{ks}] = \sum_i \int \phi_i^*(\vec{r})\left(-\frac{\hbar^2}{2m}\nabla^2\right)\phi_i(\vec{r})d^3r, \quad E_{ee}^{ks}[n^{ks}] = \frac{1}{2}\int \frac{n^{ks}(\vec{r})n^{ks}(\vec{r}')}{|\vec{r}-\vec{r}'|}d^3rd^3r' \tag{2-13}$$

For the interacting electron system, the electron density is $n_0(\vec{r})$. The energy for the interacting electron system is

$$E[n_0] = T_e[n_0] + E_{ee}[n_0] + \int V_{Ne}(\vec{r}) n_0(\vec{r}) d^3 r \tag{2-14}$$

As stated, the forms for the functionals in the equation (2-14) are unknown. An exchange-correlation functional is introduced to accommodate the difference between these two systems. This exchange-correlation functional describes the interactions between the electrons, which are not included in the non-interacting electron system.

$$E^{xc}[n_0] = E[n_0] - E^{ks}[n^{ks}] = E[n^{ks}] - E^{ks}[n^{ks}] \tag{2-15}$$

Therefore, the energy of the interacting system can be rewritten as follows.

$$E_0 = E[n_0] = E^{xc}[n^{ks}] + E^{ks}[n^{ks}] \tag{2-16}$$

The variation problem, which is to find an electron density of the interacting system n_0 to minimize its energy, is reduced to another variation problem, which is to find an electron density of the non-interacting system n^{ks} to minimize the energy of the corrected non-interacting system. Take the variation with respect to the Kohn-Sham orbitals, we obtain

$$\left(-\frac{\hbar^2}{2m}\nabla^2 + e^2 \int \frac{n^{ks}(\vec{r}')}{|\vec{r} - \vec{r}'|} d^3 r + V_{Ne}(\vec{r}) + \mu^{xc}[n^{ks}] \right) \phi_i(\vec{r}) = \varepsilon_i \phi_i(\vec{r}) \tag{2-17}$$

where $\mu^{xc}[n^{ks}]$ is the exchange-correlation potential.

$$\mu^{xc}[n^{ks}] = \frac{\partial E^{xc}[n^{ks}]}{\partial n^{ks}} \tag{2-18}$$

The energy of the interacting electron system as described in the equation (2-17) is given by

$$E_0 = \sum_i \varepsilon_i - \frac{1}{2}\int\int \frac{n^{ks}(\vec{r})n^{ks}(\vec{r}')}{|\vec{r}-\vec{r}'|} d^3r d^3r' + \int n^{ks}(\vec{r})\{\varepsilon^{xc}[n^{ks}(\vec{r})] - \mu^{xc}[n^{ks}(\vec{r})]\} d^3r \qquad (2\text{-}19)$$

where ε_i are the eigenvalues of the problem in the equation (2-17). $\varepsilon^{xc}[n^{ks}]$ is the exchange-correlation energy of a homogenous electron gas system, which is known as the Fermi-Thomas exchange-correlation energy. Let us keep in mind that the exchange-correlation energy is not known for a general system.

To solve for the equation (2-17), which is still a very tremendous task and out of current computational capacity, we need various approximation techniques. These approximation techniques can be grouped into three categories. The first group is about the selection for the exchange-correlation functional. The second group is about choosing the basis functions to represent the Kohn-Sham orbitals. The third group is to try to reduce the degrees of freedom of the interacting system by introducing a frozen concept.

DFT results in the exact total energy if the exact $E^{XC}[n]$ is known. However, the exchange-correlation functional is unknown. Instead, various approximations to the unknown part of the potential are used. Although the exchange-correlation potential is fully non-local, the approximations to it are local or semilocal. The most commonly used approximate functional is called the ``local density approximation" (LDA)[3]. This is a local operator in which the exchange-correlation potential at a point is chosen to be the same as that felt by an electron in a uniform electron gas of the same density. The general consensus nowadays is that another class of functionals, so called ``generalized gradient approximations" (GGA), which depend not only on the density at a point but also on its spatial derivative are superior in most situations, but particularly for studying molecules. This empirical observation is supported by the fact that, of the conditions which the true functional is known to obey, more of them are satisfied (by construction) by some of the

more recent GGAs than the LDA. Among the most widely used GGAs are those of Becke (1988)[81], lee and Parr (1988)[82], Perdew and Wang (1992)[83], Perdew et. al. (1996)[84]and Cohen and Handy (2001, 2002)[85-87].

2.2.1 Local Density Approximation (LDA) and Generalized Gradient Approximation (GGA)

In LDA method, for an electron gas in which density does not change very strongly in space, one can break down the whole space into small volumes in such a way that the electron density within each volume is approximately uniform as shown in Figure 2.1.

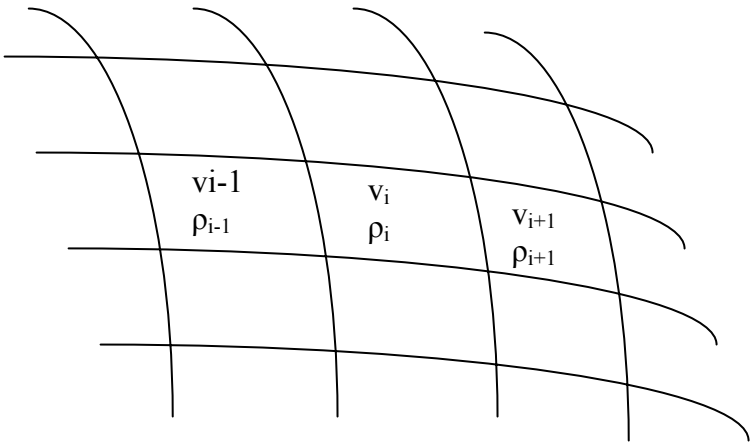

Figure 2.1 The volume of a system is broken into small volumes v_1, v_2, etc. with uniform electron densities n_1, n_2, etc. in each of them

If the number of electrons in each volume is n_1v_1, n_2v_2, etc, the exchange-correlation functional is taken to be the spatial integral over a local function that depends only on the density:

$$E_{XC}^{LDA}[n] \approx \sum_i n_i v_i \varepsilon_{XC}(n_i) = \int n(r)\varepsilon_{XC}(n(r))dr \tag{2-20}$$

where $\varepsilon_{XC}(n(r))$ is the exchange-correlation energy per particle of a uniform electron gas of density $n(r)$. This energy per particle is weighted with the probability $n(r)$ that there is in fact an electron at this position in space. E_{XC} written in this way defines the local density approximation (LDA). Exchange energy is a quantum correction to the Coulomb interaction between electrons. The correlation energy is due to the instantaneous interaction between the electrons, rather than just the average repulsion. It is the remaining correction due to the electron-electron interaction. $\varepsilon_{XC}(n(r))$ can be further split into exchange and correlation contributions,

$$\varepsilon_{XC}(n(r)) = \varepsilon_X(n(r)) + \varepsilon_C(n(r)) \tag{2-21}$$

where the first term, $\varepsilon_X(n(r))$, is the exact exchange energy of an electron gas of density *n* presented via the length parameter r_s defined as

$$\frac{4\pi}{3} r_s^3 n = 1 \tag{2-22}$$

Thus $\varepsilon_{XC}(n(r))$ can be expressed as:

$$\varepsilon_{XC}(n(r)) = -\frac{3}{4}\sqrt[3]{\frac{3n(r)}{\pi}} \tag{2-23}$$

The second term describes the correlation contribution. However, there is no known explicit expression for $\varepsilon_C(n(r))$. The most successful parameterization is the one

proposed by Perdew and Zunger[112]. $\varepsilon_C(n(r))$ is presented separately for the low ($r_s \geq 1$) and high ($r_s < 1$) densities of the electron gas:

$$\varepsilon_C(n(r)) = \frac{-0.1423}{1+1.0529\sqrt{r_s}+0.3334 r_s}, \; r_s \geq 1 \tag{2-24}$$

$$\varepsilon_C(n(r)) = -0.048 + (0.0311 + 0.002 r_s)\ln r_s - 0.0116 r_s, \; r_s < 1 \tag{2-25}$$

The assumption of the above equations is that electrons have identical electron densities when both spin "up" and "down", i.e. unpolarized electron gas. The correlation energy is significantly smaller than the exchange energy and the two energies change smoothly with the electron density. The exchange-correlation potential is obtained by varying the energy with respect to the density:

$$V_{XC}(r) = \frac{\delta E_{XC}(n)}{\delta n(r)} = \frac{\delta}{\delta n(r)} \int n(r')\varepsilon_{XC}(n(r'))dr' = \varepsilon_{XC}(n(r)) + n(r)\left(\frac{\partial \varepsilon_{XC}(n)}{\partial n}\right)_{n=n(r)} \tag{2-26}$$

The potential $V_{XC}^{LDA}(r)$ is local and depends only on the electron density.

The LDA is physically motivated by the notion that the interaction between the electrons and the nuclei creates only weak inhomogeneities in the electron density. Therefore, the form of $\varepsilon_{XC}(n(r))$ is obtained by evaluating the exact expressions for the exchange and correlation energies of a homogeneous electron gas of uniform density *n* at the inhomogeneous density *n(r)*. In general, the LDA underestimates the exchange energy by 10%, i.e. errors larger than the whole correlation energy. This is because that in LDA, uniform electron gas is assumed, which means that the density is assumed to be a slowly varying function. As a consequence, electron correlation and bond strengths are all overestimated.

Strictly speaking, the LDA is only applicable to system with slowly-varying densities. For instance, it cannot be justified for atoms, molecules or surfaces where the density away from the atoms, molecules or surfaces goes to zero resulting in a strong electron density gradient. However, over years of numerical application, the LDA has yields reasonably accurate results for semiconductors and metals.

Since in the LDA approximation spatial variations of the density are taken into account only approximately, the LDA breaks down in case where the electron density possesses sufficient inhomogeneities. Examples of such cases include dissociation or chemisorption of molecules on crystal surfaces, when energy differences associated with changes of bonding are concerned. In such cases, the LDA can be improved by adding an additional dependence on the lowest order gradients of the density, which is known as the *generalized gradient approximation* (GGA).

Typically, LDA is adjusted to reproduce some subset of the known properties satisfied by the exact exchange–correlation functional. One way to achieve this is to make the exchange and correlation energies dependent not only on the electron density, but also on derivatives of the density. In this way the dependence on the density becomes non-local and this type of approximation is called Gradient Corrected or Generalized Gradient Approximation[134] methods. The exchange-correlation functional is written as

$$E_{XC}^{GGA}[n_\alpha, n_\beta] = \int f\left(n_\alpha, n_\beta, \nabla n_\alpha, \nabla n_\beta\right) dr \tag{2-27}$$

E_{XC}^{GGA} can be split into two parts in practice[134], i.e.

$$E_{XC}^{GGA} = E_X^{GGA} + E_C^{GGA} \tag{2-28}$$

and the exchange and correlation terms are sought individually. The choice of the mathematical construction is dictated by the results obtained from them rather than the

physics. In other words, we usually can not get the physics these functional try to describe simply by the actual form of E_X^{GGA} and E_C^{GGA} [134].

$$E_X^{GGA} = E_X^{LDA} - \sum_\sigma \int F(s_\sigma) n_\sigma^{4/3}(r) dr \tag{2-29}$$

$$s_\sigma(r) = \frac{|\nabla n_\sigma(r)|}{n_\sigma^{4/3}(r)} \tag{2-30}$$

$s_\sigma(r)$ is known as a local inhomogeneity parameter. It assumes large values not only for large gradients, but also in regions of small densities, such as the exponential tails far from the nuclei. Similarly, small values of $s_\sigma(r)$ occur for small gradients, typically for bonding regions, and also for regions of large density.

Two different types of functions *F* have been put forward. The first one is based on a GGA exchange functional developed by Becke (1988)[113] and is written as

$$F^B = \frac{\beta s_\sigma^2}{1 + 6\beta s_\sigma \sinh^{-1} s_\sigma} \tag{2-31}$$

where β is an empirical parameter that was determined to 0.0042 by a least-squares fit to the exactly known exchange energies of the rare gas atoms He through Rn.

The second class of GGA exchange functionals use for *F* a rational function of the reduced density gradient. The *F* of exchange functional (Perdew[114]) is free of semiempirical parameters:

$$F^{P86} = \left(1 + 1.296\left(\frac{s_\sigma}{(24\pi^2)^{1/3}}\right)^2 + 14\left(\frac{s_\sigma}{(24\pi^2)^{1/3}}\right)^4 + 0.2\left(\frac{s_\sigma}{(24\pi^2)^{1/3}}\right)^6\right)^{1/15} \tag{2-32}$$

The corresponding electronic exchange energy as a functional of the density is[114]:

$$E_X = \int \rho_\sigma{}^{4/3} F^{P86}(s_\sigma) d^3 r \tag{2-33}$$

2.2.2 Basis Set and Cutoff Energy

In practical implementations of the Kohn-Sham methods, every KS-orbital is expanded into a set of basis function ϕ_i. This way, the KS-orbitals can be expressed as a function in the infinite coordinate system spanned by the complete basis set. However, we can only use finite basis set in the real computation. Then only the components of the KS-orbitals along those coordinate axes corresponding to the selected basis functions can be represented. Thus the smaller the basis set, the poorer the approximation.

To represent the Kohn-Sham orbital in a set of basis functions, there are several options: Slater or Gaussian orbitals, plane waves, linearized augmented plane wave, linear muffin time orbitals (LMTO), projector augmented waves (PAW)[100], etc. Plane wave and projector augmented wave are introduced here.

Plane wave basis set is a natural basis set for expanding the Kohn-Sham orbitals ϕ_i. The periodic boundary condition is the most commonly used boundary condition in calculations. In an infinite periodic system, the KS orbitals in equation (2-17) become Bloch functions of the form

$$\phi_{k+G}(\vec{r}) = \frac{1}{\sqrt{V}} e^{i(k+G)\vec{r}} \tag{2-34}$$

where $\vec{k}$ is a vector in the first Brillouin zone, while G is a reciprocal lattice vector. First Brillouin zone is a uniquely defined primitive cell of the reciprocal lattice. It is found by (1) Draw lines to connect a given lattice point to all nearby lattice points; (2) Draw new lines or planes at the midpoint and normal to these lines. The smallest volume enclosed in this way is the first Brillouin zone.

Since we cannot work with infinite basis set, the number of plane waves included in the computation needs to be specified. If all PWs with $|G| \le G_{\max}$ are included, as shown in Figure 2.2 , then it is clear that the total number of plane waves needed in the calculation will scale as the cube of G_{max}. Usually in practice, the cut-off energy $E_{cut} = \frac{\hbar^2 G_{\max}^2}{2m}$ is specified instead. This is the free electron energy corresponding to G_{max}.

In Figure 2.2, reciprocal lattice vectors G which are included for the given cut-off radius G_{max}. Two spheres of different cut-off radii $G_{\max}^1$ and $G_{\max}^2$ are shown. The vector G_1 is inside both of them, whereas G_2 will be included only if the larger cut-off, $G_{\max}^2$, is chosen. To include the plane wave with G_3 one has to choose a cut-off greater than $G_{\max}^2$

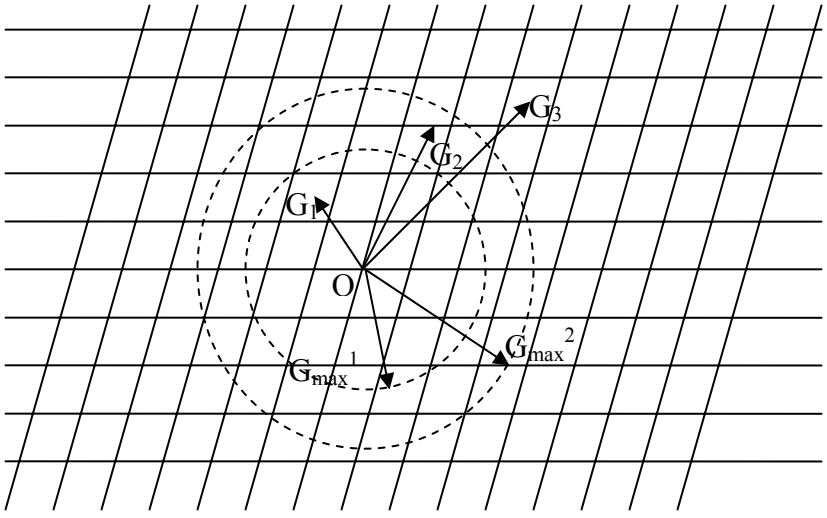

Figure 2.2 Reciprocal lattice vectors G and cut-off radius G_{max}

The advantage of plane waves includes the simplicity of the basis functions and the efficiency of forces calculation[135]. Since the calculations of various matrix elements can be done in the direct spaces, one can use the very efficient algorithms based on Fast Fourier Transforms (FFT)[136]. This comes from the fact that the kinetic energy and Hartree potential are easily calculated in reciprocal space. The electron-ion potential energy however is easily calculated in real space. Forward and inverse FFTs can be used to efficiently go back and forth between reciprocal space and real space. This method will reduce the scaling of the computation with respect to the number of PWs used.

The mainly disadvantage is the number of basis function needed to accurately represent the KS orbitals[135]. To reduce the number of PWs required in the atomic core regions, we need to ensure that the spin-orbitals which are expanded in PWs are sufficiently smooth in those regions. This is achieved by using various kinds of pseudopotential techniques[4].

Plane waves and its extended versions are used for solids, which have periodic structures and characteristics. Plane wave basis sets are good when describe the slowly varying delocalized electron densities, such as valence bands in the metal. When it comes to strongly localized core electrons around the nuclei, we need very large basis sets[4]. This type of basis set is therefore used in connection with pseudopotentials for modeling the effect of the core electron.

PAW is based on plane waves, however, by introducing the projector augmentation, the characteristics of the strong oscillations close to the nuclei region, which are smoothed out by representations of pure plane waves, are approximately reproduced[100]. The regions close to the nuclei are usually called core regions, or augmentation regions in

the PAW method. In the PAW method, the full valence electron function ϕ_v is split into three parts,

$$\phi_v = \tilde{\phi}_v + \chi_v - \tilde{\chi}_v \tag{2-35}$$

$\tilde{\phi}_v$ where $\tilde{\phi}_v$ is everywhere smooth and is exact outside the augmentation regions. The function χ_v incorporates all the necessary node structures of the exact ϕ_v and is exact inside the augmentation regions and smoothly tends to zero outside them. Finally, the function $\tilde{\chi}_v$ includes the net part, i.e. it is equal to $\tilde{\phi}_v$ inside the augmentation regions and is equal to χ_v outside them.

The advantages of the method is obvious since it allows an all-electron calculation from the beginning, it gives direct access to the full wavefunction, which is different from only valence pseudowavefunctions of the techniques based on pseudopotentials. Also, it has the computational benefits in that a very small number of PWs is required to expand the "smooth" part of the full wavefunction of every valence electron, i.e. $\tilde{\phi}_v$, whereas the functions $\tilde{\chi}_v$ and χ_v are highly localized in the augmentation regions.

2.2.3 Pseudopotential

Except for hydrogen atoms, a molecule or a solid has both core and valence electrons. The wavefunctions of the core electrons occupy a very small volume close to the nuclei since they are subject to the Coulomb potential of the nuclei. The wavefunctions of the valence electrons are more diffuse since they experience a much weaker Coulomb potential from the atomic nuclei. It is known that most physical properties of solids depend on the *valence* electrons to a much greater degree than that of the tightly bound *core* electrons[137,138]. Because their wavefunctions span only very small

regions around atomic nuclei, the core electrons are approximated to be *frozen* in their core configurations. Therefore, actual calculation of a given molecular system is simplified if only wavefunctions of the valence electrons are considered variationally, while the wavefunctions of the core electrons are assumed to be identical to those of the isolated atoms. This approximation considerably simplifies the task of solving the Kohn Sham equations, by eliminating all degrees of freedom related to the core orbitals. This is known as a frozen-core approximation[139]. The nuclear potential is replaced by a *weaker pseudopotential*, which takes into account the effects of the nucleus and the core electrons. Pseudopotential acts on a set of *pseudo "wavefunctions"* rather than the true valence "wavefunctions".

Various pseudopotentials are proposed. A so-called norm-conserving pseudopotential constrains the charge by pseudo wavefunctions, within a cut-off sphere around the nuclei, to be equal to the charge by the true wavefunctions. This pseudopotential requires large cut-off energy for the first-row and transition elements. Because the valence electrons are mainly responsible for the chemical bonding, it is essential to correctly determine the chemical bonding of the given material and thus ensure the correct description of most of its properties. The idea is to make the pseudofunction smooth inside the atomic core regions, i.e. essentially ignore its oscillations there. At the same time, the pseudofunction should be identical to the actual wavefunction outside the atomic core regions. Also, the pseudowavefunction has to be normalized to unity like the original wavefunction to ensure that other electrons and nuclei feel the correct Coulomb potential due to the pseudowavefunction. This is achieved simply by ensuring that the electron charge carried by each of the

wavefunctions in the core region is the same since the two functions are constructed to be identical outside the core region.

There is another pseudopotential called ultrasoft Vanderbilt pseudopotential[100] that relaxes the norm-conservation constraint and add augmentation charges inside the cut-off sphere to correct charge. These pseudopotentials are much softer potentials in the core region, so that they generate significantly *smoother pseudowavefunctions* and therefore result in a reduction of the size of the basis set and cut-off energies. PAW pseudopotentials decompose the wave functions or orbitals, charge densities, kinetic energy into three parts: pseudo, pseudo-onsite radial grids and exact onsite grids. Through a projector augmentation, the all-electron wave functions can be produced (Figure 2.3)

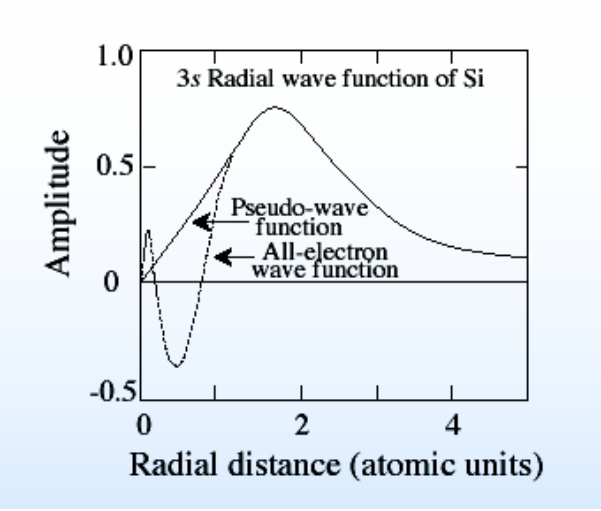

Figure 2.3 Plane waves and PAWs

The Kohn-Sham equation (2-17) are solved using iterative matrix diagonalization that was based on the minimization of the norm of the residual vector to each eigenstate[100] and optimized charge and spin mixing routines. Here solving means to find the coefficients c_p^i needed to express KS orbital ϕ_i in a given basis set ϕ_p^b.

$$\phi_i = \sum_{p=1}^{P} c_p^i \phi_p^b \tag{2-36}$$

The larger the P value, the better the approximation of the eigenfunction. However, larger P value will also require more time and computational power. In equation (2-17), μ_{xc} is the exchange-correlation energy for DFT. LDA or GGA are all approximation to this energy. A limited set of plane waves are used to express the KS orbitals. Then equation (2-17) is tackled as an eigenvalue problem. P eigenvalues results from the diagonalization of the Hamiltonian matrix. This diagonalization also results P sets of coefficients that express each of the P eigenfunctions in the given basis sets.

The calculations are implemented by a self-consistent cycle. First, an initial charge density function is obtained by guessing; then the one-electron Kohn-Sham's equations are solved to obtain a new charge density. The loop is repeated until the difference in two total energies reaches some convergence constraint.

2.3 Crystalline Solid

A perfect crystal is a periodic structure of unit cells. The primitive unit cell contains a minimum number of atoms. There are many ways of choosing the primitive axes and primitive cell for a given lattice. Wigner-Seitz primitive cell is one way to form the primitive cell. It is made by drawing planes normal and at the midpoint to the lines joining nearest lattice points to all nearby lattice point as is shown in Figure 2.4. The

smallest volume enclosed in this way is the Wigner-Seitz primitive cell. The Wigner-Seitz cell around a lattice point defines the locus of points in space which are closer to that lattice point than to any of the other lattice points. It can be shown mathematically that a Wigner-Seitz Cell is a primitive cell spanning the entire Bravais lattice without leaving any gaps or holes. First Brillouin zone is defined as the Wigner-Seitz cell in the reciprocal lattice.

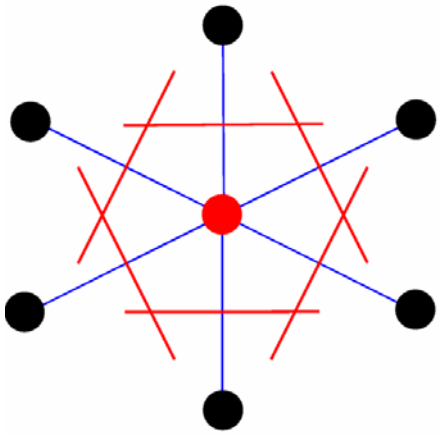

Figure 2.4 Wigner-Seitz primitive cell

Crystallography groups are composed of 32 classes of symmetry derived from observations of the external crystal form. From these 32 classes, 230 space groups are distinguishable using x-ray analysis.

The 32 point groups of crystal classes are obtained by consistent combinations of proper and improper rotation axes, i.e. 1, 2, 3, 4, 6, $\bar{1}$, $\bar{2}$, $\bar{3}$, $\bar{4}$, $\bar{6}$. Symbol 1 means that the principal symmetry axis is 1. Symbol 2 means that the principal axis is a diad axis of rotation. Symbol 3 signifies that the principal axis is a triad. Symbol 4 means that the principal axis is a tetrad. Symbol 6 means signifies that the principal axis is a hexad. For symbol $\bar{X}$, we perform the operation of rotation through $\frac{2}{n}$, where n = 1, 2, 3, 4, 6 for the appropriate class, and then invert through the centre to get the successive poles. The operation is continued until we come back to the initial point.

The combinations of these symmetries, in addition to mirror and glide symmetries, when repeated by plane lattice translations give 17 plane groups. Self-consistent combinations of these symmetries, plus screw axes and glide planes, and their repetitions by the space lattice translations, give the 230 space groups.

In the following, we give several examples of common space groups for metals[140,141]. A face-centered cubic crystal is at the space group 225, possessing a symmetry of Fm $\bar{3}$m. A primitive unit cell of a face-centered cubic contains four atoms at the corners (Figure 2.6). A body centered cubic is at the space group 229, possessing a symmetry of Im $\bar{3}$m. A primitive unit cell of a body-centered cubic contains only one atom at the center (Figure 2.7).

The crystal lattice can be described by three lattice vectors. Or by (a, b, c) and (α, β, γ)[141].

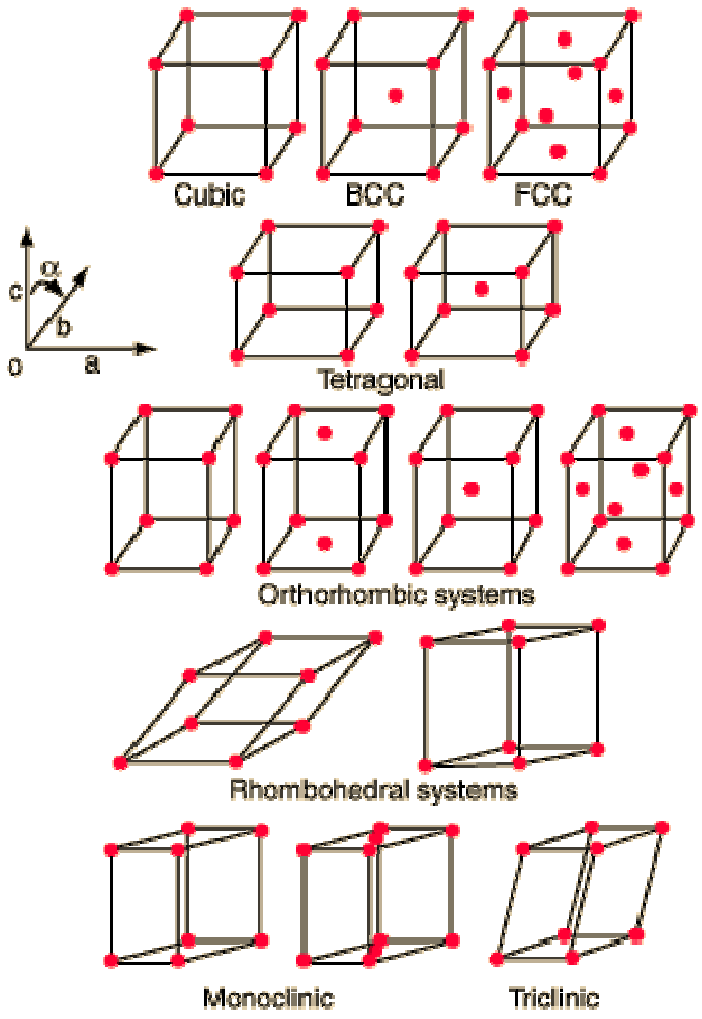

Figure 2.5 The 14 Bravais lattices

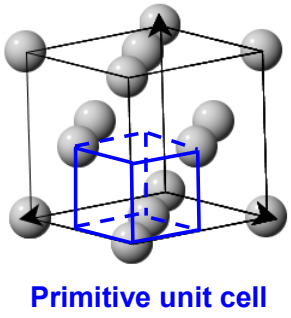

Figure 2.6 Face-centered cubic

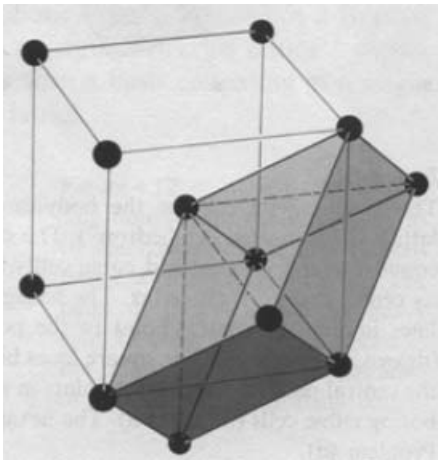

Figure 2.7 Body-centered cubic

A material's mechanical equation of state P=P(ρ, T) is a kind of constitutive relation, which describe how the material is constituted mechanically. A significant amount of literature is available in the research area concerning the first principles calculations of EOS for solids including semiconductor silicon and some metals. Among these materials, various approximation techniques have been used based on the characteristic electronic band structure and the associated lattice, electrical and magnetic properties.

The EOS is constructed from ab initio methods and bridged to the continuum scale by differentiating free energy $A(v,T)$ with respect to the volume v.

$$P(v,T) = -\frac{\partial A(v,T)}{\partial v} \tag{2-37}$$

where $A(v,T)$ is the associated Helmholtz free energy and is calculated from the internal energy.

In Swift (2001)[42], the internal energy of crystalline system is obtained from ab initio calculations as the sum of electron ground state energy and thermal energy. The internal energy $e(v,T)$ is split into the cold curve $e_c(v,T)$ and the thermal contributions from the ions $e_l(v,T)$ and electrons $e_e(v,T)$.

$$e(v,T) = e_c(v,T) + e_l(v,T) + e_e(v,T) \tag{2-38}$$

To calculate the electron ground state and thermal excitations, Swift[42] used ab initio quantum-mechanical methods based on the pseudopotential plane-wave method. The Helmholtz free energy A was calculated from its definition

$$A = e - Ts \tag{2-39}$$

where s is the specific entropy and is obtained by

$$s(T) = \int_0^T \frac{dT'}{T'} \frac{\partial e}{\partial T'} \tag{2-40}$$

For example, Godwal (1989)[44] also calculated the first principles equation of state of gold using the linear muffin-tin orbitals (LMTO) technique with approximate corrections for lattice vibrational and electronic contributions to the pressure. Comparisons with the static compression, shock Hugoniot, and ultrasonic measurements are also given. The result also showed that the electronic contribution to the high temperature equation of state is negligibly small.

The muffin-tin approximation is a shape approximation of the potential field in an atomistic environment. The potential varies continuously throughout the whole crystal, but still two crude regions can be perceived. The muffin-tin approximation uses these two regions to give a simple description of the crystal potential.

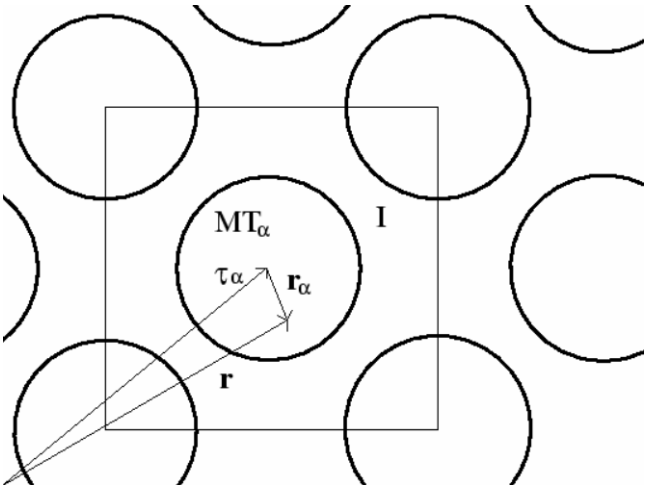

Figure 2.8 The muffin-tin potential approximation, used in the augmentation of the planewaves

The muffin-tin (MT) region consists of non-overlapping spheres with almost spherically symmetric potentials, one centered around each atomic site. All surrounding space constitute the second, interstitial (I) region with a fairly flat potential. The MT-approximation to the crystal potential is thus,

$$V_{MT}(r) = \begin{cases} cons\tan t & r \in I \\ V(r_\alpha) & r \in MT_\alpha \end{cases} \tag{2-41}$$

MT_α is the αth MT-sphere with its center at τ_α. The spherical coordinate r_α is the magnitude of the vector $r_\alpha = r - \tau_\alpha$. The radius r_α of the muffin-tin is an adjustable parameter. The potential in the outer region (this interstitial region is often called the muffin-pan) is flat and constant $V(r_\alpha)$. This shape of potential is called the muffin-tin potential.

Cohen (2001)[31] studied the static and thermal equation of state of Ta from first principles calculations. An electronic topological phase transition is found around 200

GPa and three different forms of thermal equation of state are provided. Boettger and Wallace (1997)[71] present an extensive study of the metastability and dynamics of the α-ε transition in iron. The wave evolution following planar impacts is calculated. Steinle-Meumann, Stixrude and Cohen (1999)[72] computed the elastic constant tensors for the hcp phased of three transition metals (Co, Re, and Fe). These tensors are calculated as functions of pressure using the linearized augmented plane wave method with both the local density and generalized gradient approximations. Nellis, et. al. (1988)[74] give the self consistent description of the thermodynamic states of metals at ultrahigh pressures. They combined the first principles theory and equation of state data with shock compression data for Al, Cu, and Pb in the pressure range 0.3-1 TPa. Sikka and Vijayakumar (1988)[75] computed the zero degree isothermal equation of state for Re using first principle methods. They employed a linear muffin-tin orbital electron-band theory technique. The computed isotherm is in reasonable agreement with those from empirical equation of states based on aero pressure parameters.

Also, there is a significant amount of literature on the first principle studies of metal oxides. Akber-Knutson, et. al. (2002)[77] determined the equation of state and structure of CaSiO3 perovskite at high pressures using the density functional based variationally induced breathing method. Ouyan and Ching (2001)[78] optimized the geometry of the crystal structures of several complex oxides including $MgAl_2O_4$, α-Al_2O_3, θ-Al_2O_3, r-Al_2O_3, Y_2O_3, $Y_3Al_5O_{12}$, and $YAlO_3$ by means of first principles total energy calculations with relaxation of all internal parameters. The bulk moduli and the pressure coefficients fro these crystals are calculated from fitting the energy vs volume data to the equation of state. Milman and Warren (2001)[79] studied the elastic properties, electronic structure

and equation of state of titanium diboride and magnesium diboride using a first principles pseudopotential method. Kushwah and Sharker (1998)[80] evaluated the pressure-volume-temperature relationship, isothermal bulk modulus K_T and pressure derivative of K_T for MgO in the temperature range 300-2000K and down to a compression of $V/V_0 = 0.6$. They used six different phenomenological forms for the isothermal equation of state. The results are discussed and compared with the values for MgO obtained by ab initio methods.

2.3.1 First Principle Study of Aluminum

Aluminum as a benchmark high-pressure material has been investigated via first principle method since 1970s. The earliest studies of aluminum EOS were involved in the development of DFT. Ross and Johnson (1970)[102] showed the results of self-consistent calculation on aluminum of the total energy, bulk modulus and band structure at zero Kelvin by the augmented plane wave method. Friedli and Ashcroft (1975)[101] calculated the cold curve of aluminum. Godwal (1979)[32] computed the shock Hugoniot equation of state for aluminum using the pseudopotential method. The nuclear Grüneisen parameters were derived from phonon frequencies. The electronic Grüneisen parameters are also calculated. Although the computed electronic Grüneisen parameter values depart considerable from 0.5, which is the value used often in analyzing shock-compression experiments, the P-V curve is in good agreement with the experiment results. This result showed that the thermal excitations of electrons can be omitted when calculating the total internal energy. We observed the exploration on better approximation of exchange and correlation potentials, selection of basis set and Muffin-tin approximation. These studies

also showed preliminary interests in the contribution of nuclei and electron thermal effects and possible phase transition to the EOS of aluminum.

In 1980s, Lam and Cohen[103] investigated the phonon frequencies of aluminum with the use of atomic number and the atomic mass The phonon frequencies are determined by calculated the total energy of the perfect crystal and that of the crystal distorted by a frozen-phonon mode. Consider a crystal with only one atom per lattice site, with harmonic approximation, the atomic positions of a phonon mode are given by

$$\vec{R}_i = \vec{R}_i^0 + \vec{u}_0 \cos\left(\vec{q}\cdot\vec{R}_i^0\right)\cos\left(\omega_q t\right) \tag{2-42}$$

where $\{\vec{R}_i^0\}$ are the equilibrium atomic positions. Then for this phonon mode, the kinetic energy T and the potential energy V per atom is

$$T = \frac{1}{N}\sum_i \frac{1}{2} M \left|\frac{d\vec{R}_i}{dt}\right|^2 = \frac{1}{2} M\omega_q^2 \left[\frac{1}{N}\left|\vec{u}^0\right|^2 \sum_i \cos^2\left(\vec{q}\cdot\vec{R}_i^0\right)\right]\sin^2\left(\omega_q t\right) \tag{2-43}$$

$$V = \frac{1}{N}\sum_i \frac{1}{2} M\omega_q^2 \left|\vec{R}_i - \vec{R}_i^0\right|^2 = \frac{1}{2} M\omega_q^2 \left[\frac{1}{N}\left|\vec{u}^0\right|^2 \sum_i \cos^2\left(\vec{q}\cdot\vec{R}_i^0\right)\right]\cos^2\left(\omega_q t\right) \tag{2-44}$$

where M is the ion mass and N is the total number of atoms. The summation of T and V is the phonon energy per atom E_{ph}. E_{ph} is time independent, and in particular, equals to the potential energy V when $t=0$:

$$E_{ph} = \frac{1}{2} M\omega_q^2 \left[\frac{1}{N}\left|\vec{u}^0\right|^2 \sum_i \cos^2\left(\vec{q}\cdot\vec{R}_i^0\right)\right] = \frac{1}{2} M\omega_q^2 \left\langle u^2\right\rangle \tag{2-45}$$

where the mean square distortion u^2 is defined as

$$\left\langle u^2\right\rangle = \frac{1}{N}\left|\vec{u}^0\right|^2 \sum_i \cos^2\left(\vec{q}\cdot\vec{R}_i^0\right) \tag{2-46}$$

For a $\vec{q}$ at the zone boundary, which means, $\vec{q} = \vec{G}/2$,

$$\left\langle u^2 \right\rangle = \left| \vec{u}^0 \right|^2 \tag{2-47}$$

Consider crystal distorted by a frozen lattice wave

$$\vec{R}_i = \vec{R}_i^0 + \vec{u}_0 \cos\left(\vec{q} \cdot \vec{R}_i^0\right) \tag{2-48}$$

E_{ph} is determined by calculated the total energy of a perfect crystal. Follow equation (2-45), the phonon frequency is obtained. This is the general formalism of frozen-phonon method.

Boettger and Trickey (1996)[70] determined the static lattice equation of state and crystalline phase stability of Al to 1 TPa by LDA calculation. Reasonable agreement with room temperature data up to 220 GPa is obtained by adding phonon effects to the static lattice EOS. The static–lattice phase transition for Al is predicted at 205±20 GPa and 565±60 GPa. The phase change sequence is fcc→hcp→bcc. Greene, Luo, and Ruoff (1994)[73] measured the static equation of state of Al to 220 GPa, corresponding to a compression of $V/V_0 = 0.5$. The ultrasonic, static, and shock equations of state of Al are reconciled and compared to theoretical predictions.

Chisolm, Crockett and Wallace (2003)[104] investigated the equation of state of Al that includes the possible liquid phase above the melting curve. The results were based on a previous calculation by using linear muffin-tin orbitals (LMTO). It indicated an error of 10% of overestimation about the density due to overbinding in the LMTO approximation.

2.3.2 First Principle Study of Nickel

Nickel as a ferromagnetic transition metal has obtained special interest. In early studies, the choice of basis functions mainly focus on local basis functions like Gaussian orbital[107] and linear muffin-tin-orbitals[105], [106] due to the consideration of

computational efforts. Comparing to aluminum, nickel is a transition metal and has 8 to 9 3d electrons. These 3d electrons have dual characters as atomic like and as itinerant like. The interplay of these two characters indicates a strongly correlated system.

Various methods have been proposed to improve the conventional band theory to accommodate for the strongly correlated electron interaction. GW approach[108], [111] and Hubbard Hamiltonian[109] have been used to perturb the expansion in the electron interaction; while dynamical mean-field theory[110], [111] has been used to include the fluctuations of electron occupation around LDA mean-field solution. In these studies, the electron spectra properties and magnetic moments were investigated to justify the methods. Xie, et. al. (2000)[76] calculated the thermodynamic, electronic and magnetic properties of Ni at high pressures using the ab initio pseudopotential plane wave method and density functional theory. The equation of state is obtained from the Helmholtz free energy of the crystal in the quasiharmonic approximation. In 1987, Levy et al.[105] preliminarily used both Thomas-Fermi model and linear-muffin-tin orbitals to calculate the electronic contribution to the EOS of Ni.

2.4 Equation of State for Alloys and Steels

Steel is a common alloy with many components and have metallic properties. The methods to analyze disordered alloys include mean field approach and direct sampling method.

The general idea of the mean field approach is to replace the random distribution of the atoms by their average occupation of lattice sites. The limitation of the mean field approach is that the effect of the local environments around the atoms is not considered. The reason is that this method uses only the average. However, certain characteristics

such as the interaction and the charge transfer are closely related with the local environments. Mikkelsen and Boyce[90] observed such effects in their experiment. To represent the average occupations of lattice sites occupied by all atoms, the weighted combination of individual average occupations of A atoms and B atoms in a substitutional disordered binary system $A_{1-x}B_x$ is used by Gyorffy (1972)[52], Mookerjee (1993)[53], Razee (1990~1993)[54-60], and Johnson (1987)[61].

Another method to analyze disordered alloys is direct sampling method, Muller (2001)[62, 63], Ozolins (1998)[64, 65], Wolverton (1995)[66], Silverman (1995)[67]. In this method, a statistical ensemble over all the possible configurations or simplified ensembles over a simplified set of representations of the structure is used to analyze disordered alloys.

Thermomechanical properties are important for projectile materials. These properties include equation of state (EOS), phase transition, melting, plastic effects, and dislocation evolution. In recent years, the first-principles are successfully applied to study the phase stability of simple crystal structures and their superstructures. However, theoretical predictions for steel alloys that are used as projectile materials are rather under developed. Even for simple crystal structures, phase stability[92, 93, 94] is still an active research area. On the other hand, there are very few published papers on the effect of pressure on the thermodynamic properties and the phase diagram[95-97]. The theoretical methods that are currently used for EOS of steel prediction include mixing model, generalized mixing model, and SQS (Special quasirandom structures) method.

2.4.1 Mixing Model

To study stiffness of materials, mixing model is a prevalent approximated model used to calculate EOS. It is also known as volume-addition model[46, 47]. The limitation of this mixing model is that the structure dependence of these quantities is ignored. The reason is that thermodynamic quantities are assumed to be the arithmetic average of each constituent in mixing model. The basic assumption is that the volume of alloys under the pressure P is given by the summation of equilibrium volume of each constituent under the same pressure P, i.e.

$$V(P) = \sum_i n_i v_i(P) \tag{2-49}$$

where n_i is the concentration and v_i(P) is the equilibrium volume of the i^{th} component at the pressure P. The total internal energy is then given by

$$E(P) = \sum_i n_i \varepsilon_i(P) \tag{2-50}$$

and the enthalpy is

$$H = \sum_i n_i(\varepsilon_i(v_i) + Pv_i) = \sum_i n_i H_i(v_i) \tag{2-51}$$

2.4.2 Generalized Mixing Model on the Cluster Expansion (CE) Method

Geng[48] proposed a more general EOS model based on the cluster expansion (CE) method that does not have the constraints of the mixing model. In the generalized mixing model, the convergence can be guaranteed under the assumption of the short range interaction. Without using the arithmetic average of each constituent, he suggested that the cluster expansion method (CEM) is a natural choice for the mixing model corresponding to the point approximation of CEM. EOS of Ni-Al alloys is investigated

by using this generalized mixing model and density functional calculations at the ground state. It is one of the few works on the investigation in EOS of alloys and the results agree with experiment reasonably well. The GGA approximation and LDA method are used in the calculations.

Neglecting the effects of temperature and compression on ionization, the internal energy and pressure are separately written as $E=E_x+E_v+E_e$ and $P=P_x+P_v+P_e$, where x corresponds to the cold curve energy, v corresponds to the thermal contribution from the lattice vibrations, and e corresponds to the thermal contribution from the electrons. With the cluster expansion methods, the cold curve free energy is expressed by means of correlation functions as[49]

$$E_x(V) = \sum_n v_n(V)\xi_n \tag{2-52}$$

The free energy of thermal vibrations[98] is written as

$$F_v(V,T) = \sum_n w_n(V,T)\xi_n \tag{2-53}$$

where ξ is the cluster correlation function as defined in the above equation[99]. The thermal contribution of the electrons is represented by an integration involving the configurational electronic density of state $n_\sigma(E)$:

$$F_e(\sigma,T) = \int_0^{\mu(T)} n_\sigma(E)\left[Ef(E) + k_B T\left[f(E)\ln f(E) + (1-f(E))\ln(1-f(E))\right]\right]dE \tag{2-54}$$

where E is the energy level, *f*(E) is the Fermi-Dirac distribution. Therefore, for any configuration,

$$F_e(V,T) = \sum_n \lambda_n(V,T)\xi_n \tag{2-55}$$

can be obtained by using CEM. V_n, w_n and λ_n can be provided from either ab initio calculations or fitting to experimental data. The thermodynamic properties and

equilibrium state can be calculated by using the cluster variation method[91]. With the above expressions and known values, pressure can be obtained by

$$P_x = -\frac{\partial E_x}{\partial V} \tag{2-56}$$

$$P_T = -\left(\frac{\partial F_T}{\partial V}\right)_T \tag{2-57}$$

The generalized EOS model can be constructed as follow

$$P_x(V) = -\sum_n \frac{\partial v_n(V)}{\partial V}\xi_n \tag{2-58}$$

$$P_v(V,T) = -\sum_n \frac{\partial w_n(V,T)}{\partial V}\xi_n \tag{2-59}$$

$$P_e(V) = -\sum_n \frac{\partial \lambda_n(V,T)}{\partial V}\xi_n \tag{2-60}$$

2.4.3 Supercell Based on SQS Method

A method known as the special quasirandom (SQS) method is proposed by Wei & Zunger[69]. This method is generated to circumvent the limitation of the current computational power. Martensson (1978)[68], Wei and Zunger (1990)[69] find a way to analyze a substitutional disordered structure of the $A_{1-x}B_x$ alloy by construct a large supercell, and the A and B atom are randomly placed. This approach would require huge supercells to adequately simulate the statistics of the random alloy. Obviously, density functional method is very difficult to use in this approach because it is always constrained by the number of atoms in the unit cell.

SQS method is to construct supercells of varying sizes that can be reasonably handled by available ab initio method and current computational power. The supercell is

designed to mimic the statistical characteristics of random alloys to a controllable accuracy. In other words, the correlation functions of the constructed SQS supercells can match the correlation functions of a random alloy with a selected error control.

Therefore, this reduced size of system represented by SQS structure can then be used in the first principle calculations to obtain EOS. A virtual periodic structure is constructed by using the supercell. This means that an alloy can be treated as a crystalline structure with SQS supercell as its unit cell. Then, the physical properties of alloys can be predicted based on this virtual crystalline structure.

2.5 Mixture

EOS of mixture is obtained once the EOS for each species is obtained. There are two mixture theories in continuum mechanics corresponding to two limiting cases. Homobaric mixture theory is equivalent to a series combination of the components. Uniformly blended mixture theory is equivalent to a parallel combination of the components. Tomar (2006)[50] developed an interatomic potential for carrying out MD simulations of mechanical deformation in the fcc Al+α-Fe_2O_3 material system. This material system has a combination of metallic, covalent, and ionic bonds. The potential can be used in MD simulations of fcc Al, bcc Fe, α-Fe_2O_3, and α-Al_2O_3 as well as for a system consisting of a combination of these crystalline components. Mizuno (2003)[51] performed first-principles electronic structure calculations for the constitutional defects in CoAl and CoTi. The difference in the bonding character induces the difference in the energetic and structural relaxations for the defects between CoAl and CoTi. The compositional dependence curves of the formation energy are obtained from the calculations employing supercells of various sizes. Fu, Ye and Yoo (1993)[88]

investigated the equilibrium point defects and their relation to the contrasting mechanical behavior in intermetallics with NiAl and FeAl. Bester, Meyer, and Fähnle (1999)[89] investigated the atomic defects in an ideal model of a homogeneous thermodynamically stable ordered compound B2-Co_xAl_{1-x}calculated the effective formation energies of vacancies and antistructure atoms on both sublattices. The method used combined ab initio electron theory and statistical mechanics.

2.6 Polymer EOS

First-principle (or ab initio) methods is a relatively new technique and have been used widely during the past three decades to obtain the electronic structure and EOS of metals. This progress is indebted partially to the powerful computer simulation tool. However, the application of ab initio methods in the structural characterization of complex polymeric materials is just beginning. Miao, Camp, et. al. (1996) [25] calculated the structural and electronic properties of PTFE systems with several different dihedral angles. They used two different local density approximations and optimized the geometrical parameters. The dihedral angle corresponding to the minimum torsional potential is also showed. Hageman, Meier, et. al. (1997) [26] calculated the Young's modulus for crystalline polyethylene using ab initio molecular dynamics based on density functional theory in the local density approximation. For the first time the modulus is evaluated ab initio with no bias from experimental data. Bartha, Bagar, et. al. (2000)[27] calculated the force constants and elastic properties of some polymers with density functional theory. Calculations are carried out on single helical chains of polyethylene, PTFE, polyglycine and nylon-3. It showed that some degrees of freedom of the polymer can be omitted from such a theoretical calculation without a considerable loss of

precision. Miao, Zhang and Doren (2001) [28] calculated the structure of crystalline polyethylene under high pressures with density function theory. The geometry, elastic moduli and band structures of the crystalline polyethylene are studied by a pseudopotential plane wave method as a function of applied pressure. D'Amore, Talarico and Barone (2006) [29] reported the main results of a successful attempt to predict some macroscopic properties of PTFE both in regular and disordered forms by using first principle quantum mechanical approaches at microscopic level. A statistical approach was applied to obtain the thermal concentration of defects and to reproduce the thermal behavior of PTFE. However, EOS of PTFE is not obtained on the basis of ab initio studies.

Several attempts have been made to measure the equation of state and lattice vibration property of PTFE. Morris and Fritz (1984) [10] measured the Hugoniot equation of state of PTFE. Shock-recovery experiments were performed to investigate the high-pressure equation of state. Bourne and Gray (2003) [23] measured five different production PTFE materials, two of which were produced in pedigree form, one as-received product, and two from previous in-depth literature studies. The equation of state of these variants were quantified by conducting a series of shock impact experiments in which both pressure-particle velocity and shock velocity-particle velocity dependencies were measured. Piseri and Powell (1972)[24] studied the normal modes of vibration propagating along the unique c axis of stretch-oriented PTFE at different temperatures by means of coherent neutron inelastic scattering methods. However, model for describing all the available data has not been established.

CHAPTER 3

EQUATION OF STATE FOR POLYTETRAFLUOROETHYLENE

The objective of this chapter is to determine the equation of state P=P(ρ, T) of Polytetrafluoroethylene(PTFE), commercially known as Teflon. PTFE is used as a binder and an energetic material in the structural energetic materials that are made from reactive material mixtures. Thus the equation of state of the individual components of the mixture are needed to determine the equation of state of the combined structural energetic material.

Specifically, the equation of state is a part of the constitutive relationship of the material. Usually the equation of state are determined from tests. The specific tests include gas gun tests or flyer plate tests. The objective of this chapter, however, is to determine the equation of state of PTFE without conducting tests. This is accomplished by using procedures that are based on quantum many body problem and the methods to approximately solve the problem. In particular, density functional theory based procedures are used.

3.1 Constitutive Relationships

Theoretically constitutive relationships are obtained based on the Helmholtz free energy of the system. First the discussion of the problem is under the assumption of small deformation. The first law of thermodynamic states that

$$\dot{K} + \dot{E} = \dot{Q} + \dot{W} \tag{3-1}$$

where the potential energy K is

$$K = \frac{1}{2}\int_{vol} \rho v_i v_i d(vol) \tag{3-2}$$

the internal energy E is

$$E = \frac{1}{2}\int_{vol} \rho e d(vol) \tag{3-3}$$

where e is the internal energy per unit mass and v_i is the velocity. The rate of heat added is

$$\dot{Q} = -\int_S h_i v_i dS = \int_{vol} h_{j,j} d(vol) \tag{3-4}$$

where h_i is the heat flux and v_i is normal to the surface S. Similarly the rate of work done is

$$\dot{W} = \int_{vol} F_i v_i d(vol) + \int_S \sigma_{ij} v_i v_j dS \tag{3-5}$$

or

$$\dot{W} = \int_{vol} \left(F_i v_i + \sigma_{ij,j} v_i + \sigma_{ij} v_{i,j}\right) d(vol) \tag{3-6}$$

Then from equation (3-1),

$$\frac{1}{2}\rho \frac{D}{Dt}(v^2) + \frac{v^2}{2}\frac{D\rho}{Dt} + \frac{v^2}{2}\rho div\vec{v} + \rho\frac{De}{Dt} + e\frac{D\rho}{Dt} + e\rho div\vec{v}$$

$$= -h_{j,j} + F_i v_i + \sigma_{ij,j} v_i + \sigma_{ij} v_{i,j} \tag{3-7}$$

By using the equations of conservation of mass and conservation of momentum

$$\frac{D\rho}{Dt} + \rho div\vec{v} = 0 \tag{3-8}$$

$$\rho\frac{Dv_i}{Dt} = F_i + \sigma_{ij,j} \tag{3-9}$$

the equation (3-7) simplifies to

$$\rho \frac{De}{Dt} = -\frac{\partial h_j}{\partial x_j} + \sigma_{ij} V_{ij}, \text{ where } V_{ij} = \frac{1}{2}\left(\frac{\partial v_i}{\partial x_j} + \frac{\partial v_j}{\partial x_i} \right) \tag{3-10}$$

or

$$\rho de = dQ + \sigma_{ij} d\varepsilon_{ij} \tag{3-11}$$

or

$$de = Tds + \frac{1}{\rho} \sigma_{ij} d\varepsilon_{ij} \tag{3-12}$$

The Helmholtz free energy is defined by

$$F = e - Ts \tag{3-13}$$

and

$$dF = de - Tds - sdT = -sdT + \frac{1}{\rho} \sigma_{ij} d\varepsilon_{ij} \tag{3-14}$$

Then

$$\rho \frac{\partial F}{\partial \varepsilon_{ij}} = \sigma_{ij}, \frac{\partial F}{\partial T} = -s \tag{3-15}$$

which are the constitutive equations for the material.

Not the procedure to obtain the constitutive equations without conducting tests is to determine the Helmholtz free energy F from the results of quantum many body problem, phonon thermal energy contribution, and electron thermal energy contributions.

3.2 Finite Deformation

In the small deformation analysis, the equation (3-14) used the strain energy density U as

$$dU = \sigma_{ij} d\varepsilon_{ij} \text{ or } U = U(\varepsilon_{ij}) \tag{3-16}$$

In finite deformations, this equation is replaced by

$$U = U(F_{iR}) = U([F]) \tag{3-17}$$

where F_{iR} or [F] is the deformation gradient tensor

$$F_{iR} = \frac{\partial x_i}{\partial X_R} \tag{3-18}$$

where X_R is the undeformed Cartesian system and x_i is the deformed system with

$$x_i = x_i(X_R),\ u_i = x_i - X_i \tag{3-19}$$

It is possible to show that[142]

$$\frac{D}{Dt}(F_{iR}) = \frac{\partial v_i}{\partial x_j}\frac{\partial x_j}{\partial X_R} \tag{3-20}$$

If the internal energy

$$e = \frac{U}{\rho_0} \tag{3-21}$$

Then[142]

$$\sigma_{ij}\frac{\partial v_i}{\partial x_j} = \frac{\rho}{\rho_0}\frac{DU}{Dt} = \frac{\rho}{\rho_0}\frac{\partial U}{\partial F_{iR}}\frac{DF_{iR}}{Dt} = \frac{\rho}{\rho_0}\frac{\partial U}{\partial F_{iR}}\frac{\partial x_j}{\partial X_R}\frac{\partial v_i}{\partial x_j} \tag{3-22}$$

or

$$\sigma_{ij} = \frac{\rho}{\rho_0}F_{jR}\frac{\partial U}{\partial F_{iR}} \tag{3-23}$$

However, U must satisfy simultaneously the principle of objectivity and the material symmetry. The material symmetry need not be included only in isotropic materials. In anisotropic materials, material symmetry should be included to obtain additional elastic constants than is obtained for isotropic materials.

In formulating the internal energy function, it is necessary to consider simultaneously the constraints of objectivity and material symmetry. In addition to these constraints, it is also necessary to consider poly convexity of these functions. These are discussed in chapter 4 where the complete constitutive equation of the fcc aluminum crystal is considered for large deformations. In further discussion of this chapter, it is assumed that only work done will be due to volume change under a pressure of $p=(\sigma_{11}+\sigma_{22}+\sigma_{33})/3$. Then the internal energy is given by

$$\rho de = \rho T ds - pdV \tag{3-24}$$

and the Helmholtz free energy is

$$dF = -sdT - \frac{1}{\rho} pdV \tag{3-25}$$

3.3 Procedures to Find the Internal Energy and EOS from Quantum Mechanics

The internal energy of crystalline system is obtained from ab initio calculations as the sum of electron ground state energy and thermal energy. The internal energy $e(v,T)$ is split into the cold curve $e_c(v,T)$ and the thermal contributions from the ions $e_l(v,T)$ and electrons $e_e(v,T)$.

$$e(v,T) = e_c(v,T) + e_l(v,T) + e_e(v,T) \tag{3-26}$$

In the above equation:

(1) The electron ground state energy $e_c(v,T)$ is the energy of the system with electrons in the ground state and ions in their crystallographic sites associated with some specific volume. It is obtained from quantum mechanical calculations as the zero-point

energy of the system for a given lattice parameter (a measure of the specific volume of the system). The configuration of the lattice is held unchanged and only the scale varies.

(2) The lattice thermal energies $e_l(v,T)$ are the contribution of thermal excitation of ions, which are calculated from phonon modes of the lattice. Phonons represent the internal motions of a lattice about its center of mass by perturbations of the ion positions from their ground states.

The phonon modes are then obtained from the eigenvalue problem of the structure defined by a given set of lattice parameters with the squared phonon frequencies representing the eigenvalues of the stiffness matrix. Ab initio elements of the stiffness matrix D_{ij} are obtained by calculating forces on the j^{th} atom when the i^{th} atom is perturbed from equilibrium by a finite displacement u_i.

$$D_{ij} = \frac{\partial^2 \Phi}{\partial \vec{u}_i \partial \vec{u}_j} \approx \frac{\partial \Phi(\vec{u}_i)}{\partial \vec{u}_j} \frac{1}{\left|\vec{u}_i\right|} \tag{3-27}$$

The electron ground-state energy is denoted by Φ. This approach of calculating the restoring forces directly avoids the need to assume explicit forms of inter-atomic potentials. The phonon eigen-problem is solved for each set of wave vectors of a structure for a given set of lattice parameters to obtain $g(\omega)$, the density of phonon states. The variation of lattice thermal energy $E_l(T)$ with temperature at a given density is then found by populating the phonon modes according to the Boltzmann statistics. This approach is employed for each set of lattice parameters (for each specific volume). $e_l(v,T)$ is then found from $E_l(T)$ by normalizing to three modes per atom and using a suitable interpolation scheme.

$$E_l(T) = \int_0^\infty \hbar\omega g(\omega) f_b(\omega, T) d\omega \text{ where } f_b(\omega, T) = \frac{1}{e^{\hbar\omega/kT} - 1} + \frac{1}{2} \quad (3\text{-}28)$$

where $f_b(\omega, T)$ is the probability of the occupation of a Boltzmann state of energy $\hbar\omega$ at temperature T.

(3) The electron thermal energies $e_e(v, T)$ are the contribution of thermal excitation of electrons from their ground states. The electron thermal contribution is calculated from the electron band structure by populating the calculated states according to the Fermi-Dirac statistics.

In the assumptions of the pseudopotential approach, the band structure refers to the valence electrons only and the core electrons are assumed to be occupied at all temperatures. The energy levels are used directly in estimating $e_e(v,T)$ or are collected into a numerical distribution function $n(\varepsilon)$. Given the density of levels $n(\varepsilon)$, the chemical potential μ is found as a function of temperature T by constraining the total number of valence electrons N.

$$\int_{-\infty}^{\infty} f_F(\varepsilon, T) n(\varepsilon) d\varepsilon = N \quad \text{and} \quad f_F(\varepsilon, T) = \frac{1}{e^{(\varepsilon - \mu)/kT} + 1} \quad (3\text{-}29)$$

where $f_F(\varepsilon, T)$ is the probability of occupation of a fermions state of energy ε at temperature T. This relation is not readily invertible to find the variation of μ with T. The quantity μ, i.e., chemical potential, is the solution to the equation (3-29). It is found by an iterative inversion algorithm[42]. At T = 0, μ is equal to E_F (i.e. Fermi level). As $T \rightarrow \infty$, $\mu \rightarrow 0$. Since the values of μ lie between 0 and E_F, the relation can be solved robustly by bisection. Once $\mu(T)$ is obtained, the expectation value of the electronic energy is obtained as

$$e_e(v,T) = \langle \varepsilon \rangle = \int_{-\infty}^{\infty} \varepsilon f_F(\varepsilon,T) n(\varepsilon) d\varepsilon \tag{3-30}$$

Thermal contributions due to electrons are usually small and therefore not included in the calculations.

Once the internal energy is obtained, Helmholtz free energy (specific) is obtained as

$$F(v,T) = e(v,T) - Ts(v,T) \tag{3-31}$$

where s is the specific entropy and is obtained by integration of the second law of thermodynamics (*de = Tds-pdv*, where *v* is specific volume and *s* is specific entropy)[42]

$$s(T) = \int_0^T \frac{dT'}{T'} \frac{\partial e}{\partial T'} \tag{3-32}$$

The thermodynamically complete EOS can be constructed by differentiating A with respect to the specific volume v,

$$P(v,T) = -\frac{\partial F(v,T)}{\partial v} \tag{3-33}$$

The equation of state is then constructed as is shown in equation (3-33)

3.4 Cold Curve Energy of an Ion-Electronic System

The theoretical background is given in detail in chapter 2. Here we give a brief review of the necessary knowledge.

As explained in chapter 2, the cold curve energy e_c in equation (3-26) of the interacting electron system is obtained by solving the Kohn-Sham equation:

$$\left\{ -\frac{\hbar^2}{2m}\nabla^2 + V_{Ne}(\vec{r}) + e^2 \int \frac{n^{ks}(\vec{r}')}{|\vec{r}-\vec{r}'|} d^3r + \mu^{XC}\left[n^{ks}(\vec{r})\right] \right\} \phi_i(\vec{r}) = \varepsilon_i \phi_i(\vec{r}) \tag{3-34}$$

where $\vec{r}$ describes the electrons coordinates, e is the charge of electron, $n^{ks}(\vec{r}')$ determines the probability of finding any of the N electrons within the volume element

dr. $V_{Ne}(\vec{r})$ is the nuclei-electron attraction functional, ∇^2 is the Laplace operator, $\phi_i(\vec{r})$ is the KS orbitals, $\mu^{XC}\left[n^{ks}(\vec{r})\right]$ is the exchange-correlation potential:

$$\mu^{XC}\left[n^{ks}(\vec{r})\right]=\frac{\delta E^{XC}\left[n^{ks}(\vec{r})\right]}{\delta n^{ks}(\vec{r})}=\frac{\delta\left\{n^{ks}(\vec{r})\varepsilon^{XC}\left[n(\vec{r})\right]\right\}}{\delta n^{ks}(\vec{r})} \tag{3-35}$$

After solving the Kohn-Sham equation, we can obtain the energy of the interacting electron system as given in the equation below

$$E_0=\sum_i\varepsilon_i-\frac{1}{2}\int\int\frac{n^{ks}(\vec{r})n^{ks}(\vec{r}')}{|\vec{r}-\vec{r}'|}d^3rd^3r'+\int n^{ks}(\vec{r})\left\{\varepsilon^{xc}[n^{ks}(\vec{r})]-\mu^{xc}[n^{ks}(\vec{r})]\right\}d^3r \tag{3-36}$$

Substituting the electron energy into the decoupled Schrödinger equation with Born-Oppenheimer approximation, which reduced the system to decoupled ion system and electron system

$$\begin{cases}[T_e+V_{ee}(\vec{r})+V_{Ne}(\vec{r},\vec{R})]\Psi_n(x,\vec{R})=e_n(\vec{R})\Psi_n(x,\vec{R})\\ [T_N+V_{NN}(\vec{R})+e(\vec{R})]\chi(\vec{R})=\varepsilon\chi(\vec{R})\end{cases} \tag{3-37}$$

We can solve the equation above to obtain the energy of the ion system. Therefore, the total energy for a coupled ion-electron system can be obtained from the equation

$$E(\vec{R})=e_0(\vec{R})+\varepsilon(\vec{R}) \tag{3-38}$$

As known, given nuclei positions $\vec{R}$, we can obtain the total energy of the system $E(\vec{R})$.

3.4.1 Solving the KS Equations

In order to solve the KS equations, a set of trial vectors (wavefunctions) representing all occupied and a few empty eigenstates: $\left\{\phi_n\middle|n=1,\ldots,N_{bands}\right\}$ are used. Then each wavefunction is improved by adding a fraction of the residual vector $\left|R(\phi_n)\right\rangle$,

$$\left|R(\phi_n)\right\rangle=\left(H-\varepsilon_n^{app}\right)\left|\phi_n\right\rangle,\ \varepsilon_n^{app}=\left\langle\phi_n\middle|H\middle|\phi_n\right\rangle \tag{3-39}$$

When all the states have been updated, we perform subspace diagonalization and calculate new charge density n_{out}. Then by mixing old n_{in} and n_{out}, the optimal new input-charge density can be determined. These steps are iterated until selfconsistency. The procedure is as listed in detail as follows:

From Kohn-Sham theory,

$$E[n(\vec{r})] = \int n(\vec{r})V(\vec{r})d^3r + \frac{e^2}{2}\iint \frac{n(\vec{r})n(\vec{r}')}{|\vec{r}-\vec{r}'|}d^3rd^3r' + T[n(\vec{r})] + E^{XC}[n(\vec{r})] \tag{3-40}$$

(1). Start with a density. For the 1st iteration, superposition of atomic densities is typically used. The density is the superposition of a set of one-electron orbitals representing a non-interacting reference system.

$$n(\vec{r}) = \sum_i |\phi_i(\vec{r})|^2 \tag{3-41}$$

(2). Calculate non-interacting kinetic energy in terms of the $\phi_i(\vec{r})$'s.

$$T_0[n] = \sum_i \int \phi_i^*(\vec{r})\left(-\frac{\hbar^2}{2m}\nabla^2\right)\phi_i(\vec{r})d^3r \tag{3-42}$$

(3). Establish the exchange correlation potential. With local density approximation,

$$E^{XC}[n(\vec{r})] = \int n(\vec{r})\varepsilon_{XC}[n(\vec{r})]d^3r \tag{3-43}$$

where $\varepsilon_{XC}[n(\vec{r})]$ is the exchange correlation energy of a homogeneous electron gas with the local density $n(\vec{r})$. For the exchange part, a Hartree-Fock calculation for a homogeneous electron gas with the density *n* leads to

$$\varepsilon_X[n(\vec{r})] = -\frac{3e^2}{4\pi}(3\pi^2 n(\vec{r}))^{1/3} \tag{3-44}$$

(4). Determine the optimal one-electron orbitals using the variational condition under the orthonormality constraint $\langle \phi_i | \phi_j \rangle = \delta_{ij}$

$$\delta\left\{ E[n(\vec{r})] - \sum_{i,j} \varepsilon_{ij} \left(\langle \phi_i | \phi_j \rangle - \delta_{ij} \right) \right\} = 0 \tag{3-45}$$

After diagonalizing ε_{ij}, the KS equations becomes

$$\left\{ -\frac{\hbar}{2m}\nabla^2 + V(\vec{r}) + e^2 \int \frac{n(\vec{r}')}{|\vec{r} - \vec{r}'|} d^3r + \mu_{XC}[n(\vec{r})] \right\} \phi_i(\vec{r}) = \varepsilon_i \phi_i(\vec{r}) \tag{3-46}$$

with the exchange-correlation potential $\mu_{XC}[n(\vec{r})] = \frac{\delta E_{XC}[n(\vec{r})]}{\delta n(\vec{r})}$. The total energy is

$$E = \sum_i \varepsilon_i - \frac{1}{2} \iint \frac{n(\vec{r}) n(\vec{r}')}{|\vec{r} - \vec{r}'|} d^3r d^3r' + \int n(\vec{r}) \{ \varepsilon_{XC}[n(\vec{r})] - \mu_{XC}[n(\vec{r})] \} d^3r \tag{3-47}$$

where the first term is the sum of one-electron energies and the remaining the terms are the double-counting corrections.

The variational conditions are

(4a). Total energy *E[n]*

$$\left. \frac{\delta E[n(\vec{r})]}{\delta n(\vec{r})} \right|_{n(\vec{r}) n_0(\vec{r})} = 0 \tag{3-48}$$

(4b). KS eigenvalues ε_i

$$\delta\left\{ \langle \phi_i | H^{KS} | \phi_i \rangle \right\} = 0 \text{ with } \langle \phi_i | \phi_j \rangle = 0, \ \forall \varepsilon_i < \varepsilon_j \tag{3-49}$$

(4c). Norm of residual vector $|R_i\rangle$

$$|R(\phi_i)\rangle = (H^{KS} - \varepsilon_i^{app}) |\phi_i\rangle, \ \varepsilon_i^{app} = \langle \phi_i | H^{KS} | \phi_i \rangle, \ \delta\left\{ \langle R(\phi_i) | R(\phi_i) \rangle \right\} = 0 \tag{3-50}$$

(5). From KS theory, the total energy is a nonlinear functional of the density

$\frac{\delta E[n(\vec{r})]}{\delta n_i(\vec{r})} = \varepsilon_i$ and the new density is $n(\vec{r}) = \phi_i^*(\vec{r})\phi_i(\vec{r})$ (3-51)

(6). If density or energy changed substantially, go to step (1).

(7). If Self Consistent Field (SCF) cycle converged and geometry optimization is not requested, go to step (10).

(8). Calculate derivatives of energy vs. atom coordinates, and update atom coordinates. This may require denser integration grids and recomputing of Coulomb and exchange-correlation potential.

(9). If gradients are still large, or positions of nuclei moved appreciably, go to step (1).

(10). Calculate properties and print results.

3.4.2 Approximation of KS Equations

To solve for the equation (3-34), which is still a very tremendous task and out of current computational capacity, we need various approximation techniques. These approximation techniques can be grouped into three categories. The first group is about the selection for the exchange-correlation functional. The second group is about choosing the basis functions to represent the Kohn-Sham orbitals. The third group is to try to reduce the degrees of freedom of the interacting system by introducing a frozen concept.

1). Approximation of Exchange-Correlation Functionals

About the exchange-correlation functional, several current techniques are available. The most commonly used one is called the local density approximation (LDA). In which, the Fermi-Thomas exchange-correlation functional $\varepsilon^{xc}[n^{ks}]$ is used to replace $\mu^{xc}[n^{ks}]$ in the equation (3-34). For a spin-polarized system, $n^{ks}(\vec{r}) = n^{ks}(\vec{r},\uparrow) + n^{ks}(\vec{r},\downarrow)$. The LDA

is extended to the local spin density approximation (LDSA) to include the spin effects. The exchange part is given by

$$\varepsilon^x(\vec{r}) = -\frac{3e^2}{4\pi}(3\pi^2)^{1/3}\left(\frac{n^{ks}(\vec{r},\uparrow)^{4/3} + n^{ks}(\vec{r},\downarrow)^{4/3}}{n^{ks}(\vec{r})}\right) \tag{3-52}$$

The correlation functional $\varepsilon^c(\vec{r})$ is fitted to the ground-state energy of a homogenous electron gas calculated using quantum Monte Carlo simulations.

There is a consideration about the effects of the gradient of electron density to the exchange-correlation energy. Therefore

$$E^{xc}[n(\vec{r},\uparrow), n(\vec{r},\downarrow)] = \int f[n(\vec{r},\uparrow), n(\vec{r},\downarrow), \nabla n(\vec{r},\uparrow), \nabla n(\vec{r},\downarrow)]d^3r \tag{3-53}$$

Current strategy is to adjust f such that it satisfies all known properties of the exchange-correlation hole and energy of different variants: *Perdew-Wang (PW), Becke-Perdew (BP), Lee-Yang-Parr(LYP), Perdew-Burke-Ernzernhof (PBE)*.

2). Frozen-Core Approximation

Most physical properties of solids are dependent on the *valence* electrons to a much greater degree than that of the tightly bound *core* electrons. Therefore, the core electrons can be approximated to be *frozen* in their core configurations. This approximation considerably simplifies the task of solving the Kohn Sham equations, by eliminating all the degrees of freedom related to the core orbitals. Then, the nuclear potential is replaced by a *weaker pseudopotential*, which takes into account the effects of the nucleus and the core electrons. Pseudopotential acts on a set of *pseudo "wavefunctions"* rather than the true valence "wavefunctions".

$$\left\{-\frac{\hbar^2}{2m}\nabla^2 + V(\vec{r}) + e^2\int\frac{n(\vec{r}')}{|\vec{r}-\vec{r}'|}d^3r + \mu_{XC}[n(\vec{r})]\right\}\phi_i(\vec{r}) = \varepsilon_i\phi_i(\vec{r}) \qquad \text{i} = 1,\ldots, \text{N} \tag{3-54}$$

$$\left\{-\frac{\hbar^2}{2m}\nabla^2 + V_{pseudo}(\vec{r}) + e^2\int\frac{n(\vec{r}')}{|\vec{r}-\vec{r}'|}d^3r + \mu_{XC}[n(\vec{r})]\right\}\tilde{\phi}_i(\vec{r}) = \varepsilon_i\tilde{\phi}_i(\vec{r}) \quad \text{i} = 1,\ldots, N_{\text{valence}} \tag{3-55}$$

where $\tilde{\phi}_i(\vec{r})$ is the Pseudo valence wavefunctions. We can see that the number of DOFs reduces from the number of all the electrons to the number of only valence electrons. The space is divided into an interstitial region and a core region. The core region consists of spheres of a core radius r_c surrounding the nuclei. The rest of the space is the interstitial region. A pseudopotential is constructed such that it matches the true potential in the interstitial region. Similarly, each pseudowavefunction must match the corresponding true wavefunction in the interstitial region. The pseudopotential is constructed in such a way that there are no radial nodes in the pseudowavefunction $\tilde{\phi}_l$ in the core region (i.e. the strong oscillations of the valence orbitals ϕ_l are smoothed out). Usually, to replace the true wavefunction by a node-less pseudowavefunction requires that

$$\int_0^{r_c}\phi_l(r)\phi_l^*(r)4\pi r^2 dr = \int_0^{r_c}\tilde{\phi}_l(r)\tilde{\phi}_l^*(r)4\pi r^2 dr \tag{3-56}$$

$$\phi_l(r_c)^{(n)} = \tilde{\phi}_l(r_c)^{(n)}, \quad n = 0,\ 1,\ 2 \tag{3-57}$$

The condition in the equation (3-56) is to preserve the charge of pseudowavefunction inside the core region to be equal to the true charge. This condition is also called the norm conservation. The condition in the equation (3-57) requires that up to the second order derivative, the pseudowavefunction have the same derivatives as the true wavefunction.

In some cases for a hybrid *p* and *d* states, the norm conservation condition is relaxed. Augmentation charges inside the cut-off sphere can be added to correct the charge. This technique is called the ultrasoft pseudopotentials. It gives more freedom to pseudizing the

p and *d* states. This leads to a much softer potentials in the core region, then significantly smoother pseudowavefunctions, and reduces the size of the basis set required.

3). Basis Functions

As known, we can use a series expansion to represent some functions. Similarly, we can choose various sets of basis functions to represent the Kohn-Sham orbitals. The following lists the current commonly used basis sets.

Slater type or Gaussian type orbitals

Plane waves (PW): Plane waves are not localized. Large numbers of plane waves are needed to reproduce atomic cores → pseudopotential

Linearized *augmented plane waves* (LAPW): Add atomic-like states to the plane-wave basis --- Expand the valence part of molecular orbitals in plane waves, the core part in compact atomic basis function

Projector augmented waves (PAW): The wave function is a superposition of different terms: a plane wave part, the so-called pseudowavefunction, and expansions into atomic and pseudo atomic orbitals at each atom.

Up to this point, we have discussed various techniques to simplify the problem of an interacting electron system. We can solve equation (3-55) in stead of equation (3-34) with the current computational capacity within reasonable time.

3.4.3 K-point Sampling

Kohn-Sham equations are frequently used in conjunction with periodic boundary conditions. The system is considered as periodic in 3D. This model is natural for periodic crystals. For systems which do not have 3D periodicity or have only some partial periodicity, the 3D periodicity is enforced. A certain number of the k points are needed

to represent adequately the electronic density n(r). The choice of k points needed to represents n(r) is important in calculations of periodic systems and is known as the k-point sampling. It depends on the size of the unit cell used in the calculations and on the system point symmetry. Normally, the bigger the cell, the smaller number of k points is needed. This is because the BZ becomes smaller in the reciprocal space when a bigger unit cell is used so that k points appear closer to each other and fewer of them are needed. To find the equilibrium geometry, the absolute convergence of the calculation needs to be checked. This is done by increase the k point and cutoff energy gradually to find the convergence. For PTFE calculation, the detail is shown in the following section.

3.5 Lattice Thermal Energy

The phonon properties of crystals are needed to explain thermodynamical functions, in specific heat, elastic constants, transport properties, in infrared absorption, Raman scattering, neutron scattering, in phase stability and phase transitions. Ab initio methods are also used to calculate the crystal response to an external perturbation. In particular, the dynamical matrix is directly related to the second derivative of the total energy with respect to atomic positions. Since the total energy of the ground state is calculated by ab initio method here, its second-order derivative is a property of ground state and can be calculated using DFT.

The calculations of phonon frequencies are classified into two methods: the linear-response (see for example[11, 12, 13]) and the direct approach. The direct method, also called frozen-phonon approximation, is used to calculate the required force constant. In this method, the phonon dispersion relations are calculated by using lattice dynamics. This involves setting of force constants between atoms, constructing the dynamical

matrix and diagonalizing it. Traditionally, the force constant parameters are found in the process of fitting the phonon dispersion curves to variety of experimental data. In the ab initio method one optimizes first the crystal supercell by a full quantum mechanical electronic structure calculation. In such calculations one can make a series of small displacements of one atom at a time and calculate the so called Hellmann-Feynman forces exerted on all atoms[143]. From ab initio Hellmann-Feynman forces the force constants are then derived. This is the essence of the direct method. In this approach, the forces on atoms due to distortion of a supercell caused by displaced atoms from their ideal lattice positions are calculated.

3.5.1 Vibrational Properties of the Lattice

We can describe a propagating vibration of amplitude *u* along the x-direction of a continuum rod of material with Young's modulus *E* and density ρ with the wave equation:

$$\frac{\partial^2 u}{\partial t^2} = \frac{E}{\rho}\frac{\partial^2 u}{\partial x^2} \tag{3-58}$$

By comparison to the general form of the 1-D wave equation:

$$\frac{\partial^2 u}{\partial t^2} = v^2 \frac{\partial^2 u}{\partial x^2}, \text{ where } v = \sqrt{\frac{E}{\rho}} \tag{3-59}$$

The wave speed is independent of the wavelength for an elastic medium. We can define the dispersion relation by

$$\omega = 2\pi f = 2\pi \frac{v}{\lambda} = kv \tag{3-60}$$

where $\omega(k)$ is called the dispersion relation of the solid and $v_g = \sqrt{\frac{d\omega}{dk}}$ is the group velocity.

In contrast to the solid which are continuum, the real solid is not uniform at an atomic scale, and thus it exhibits dispersion. Consider a 1-D chain of atoms as shown in Figure 3.1.

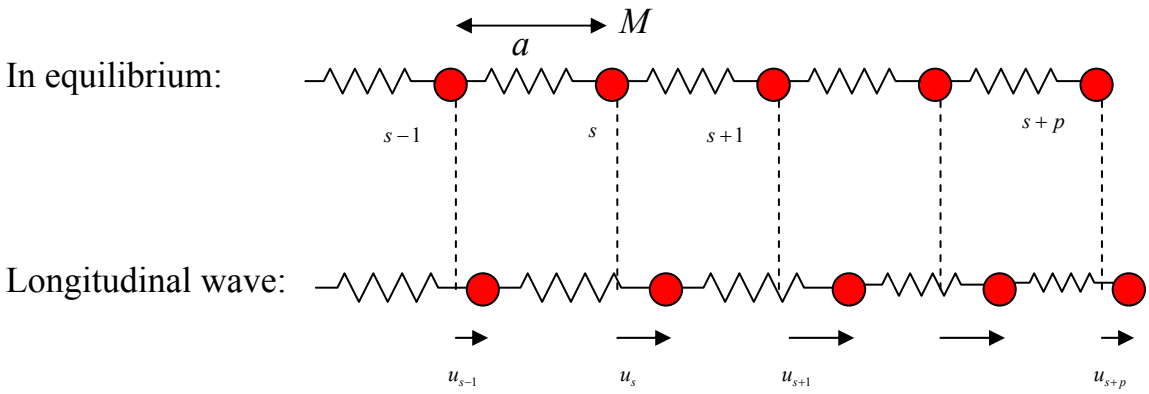

Figure 3.1 1_D monatomic lattice

For atom s,

$$F_s = \sum_p c_p \left(u_{s+p} - u_s\right) \tag{3-61}$$

where p is atom label, $p=\pm1$ mean the nearest neighbors, $p=\pm2$ means the next nearest neighbors and c_p is the force constant for atom p. Then, from Newton's second law,

$$F_s = M\frac{\partial^2 u_s}{\partial t^2} = \sum_p c_p\left(u_{s+p} - u_s\right) \tag{3-62}$$

For the expected harmonic traveling waves, we can write

$$u_s = ue^{i(kx_s-\omega t)},\ x_s = sa = \text{position of atom } s \tag{3-63}$$

$$Mu(-i\omega)^2 e^{i(ksa-\omega t)} = \sum_p c_p\left(ue^{i(k(s+p)a-\omega t)} - ue^{i(ksa-\omega t)}\right) \tag{3-64}$$

or

$$-M\omega^2 e^{i(ksa-\omega t)} = e^{i(ksa-\omega t)}\sum_p c_p\left(e^{ikpa}-1\right) \tag{3-65}$$

or

$$-M\omega^2 = \sum_p c_p\left(e^{ikpa}-1\right), \text{ since } c_{-p} = c_p \text{ by symmetry,} \tag{3-66}$$

or

$$-M\omega^2 = \sum_{p>0} c_p\left(e^{ikpa}+e^{-ikpa}-2\right) = \sum_{p>0} 2c_p\left(\cos(kpa)-1\right) \tag{3-67}$$

Then, the solution for a 1-D monatomic lattice is:

$$\omega^2 = \frac{2}{M}\sum_{p>0} c_p\left(1-\cos(kpa)\right) = \frac{4}{M}\sum_{p>0} c_p \sin^2\left(\frac{1}{2}kpa\right) \tag{3-68}$$

This is the dispersion relation of the monatomic 1-D lattice. It is reasonable to make the nearest-neighbor approximation (p=1), then

$$\omega^2 \cong \frac{4c_1}{M}\sin^2\left(\frac{1}{2}ka\right) \tag{3-69}$$

This result is periodic in k and the only unique solutions that are physically meaningful correspond to values in the range of $-\frac{\pi}{a} \le k \le \frac{\pi}{a}$. Figure 3.2 shows the curve for a = 1.

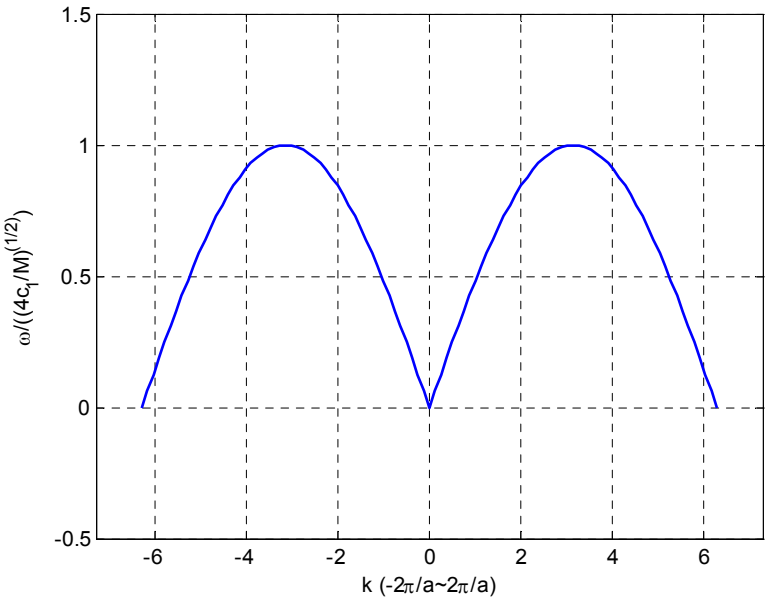

Figure 3.2 Dispersion relation of the monatomic 1-D lattice

The collective motion of atoms are expressed as the vibrational mode:

$$u_s(x,t) = ue^{i(kx_s - \omega t)} \tag{3-70}$$

with the quantum harmonic oscillator[144(p31)]:

$$E_n = n\hbar\omega \qquad \text{n} = 0, 1, 2, \ldots \tag{3-71}$$

The energy content of a vibrational mode of frequency ω is an integral number of energy quanta $\hbar\omega$. We call these quanta "phonons". A phonon is a quantized unit of vibrational (elastic) energy. Associated with each mode of frequency ω is a wavevector $\vec{k}$, which leads to the definition of a "crystal momentum": $\hbar\vec{k}$. Crystal momentum is analogous to but not equal to linear momentum. No net mass transport occurs in a propagating lattice vibration, so the linear momentum is actually zero. But for most practical purposes a phonon acts as if its momentum were $\hbar\vec{k}$. With the possible addition of a reciprocal lattice vector, the total wave vector of interacting waves is conserved in a periodic lattice. The crystal momentum of the whole system is conserved[141].

Lattice vibrations (phonons) of many different frequencies can interact in a solid. In all interactions involving phonons, energy must be conserved and crystal momentum must be conserved to within a reciprocal lattice vector. Figure 3.3 shows this schematically.

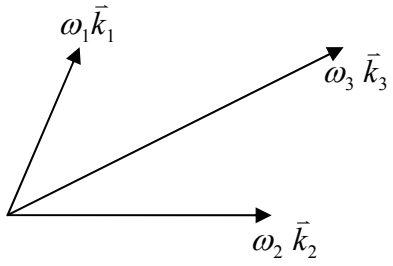

Figure 3.3 Phonons of many different frequencies interact in a solid

$$\hbar\omega_1 + \hbar\omega_2 = \hbar\omega_3 \tag{3-72}$$

$$\hbar\vec{k}_1 + \hbar\vec{k}_2 = \hbar\vec{k}_3 + \hbar\vec{G} \tag{3-73}$$

where $\vec{k}$ s are the photon wave vectors and $\vec{G}$ is the general translation vector of the reciprocal lattice.

The dispersion relation of the 1-D monatomic lattice, which repeats with period (in k-space) $2\pi/a$, is shown schematically in Figure 3.4 for a = 1. The 1st Brillouin zone is between [-π/a, π/a], the 2nd Brillouin zone is between [-2π/a, 2π/a], the 3rd Brillouin zone is between [-3π/a, 3π/a]. Each BZ contains identical information about the lattice.

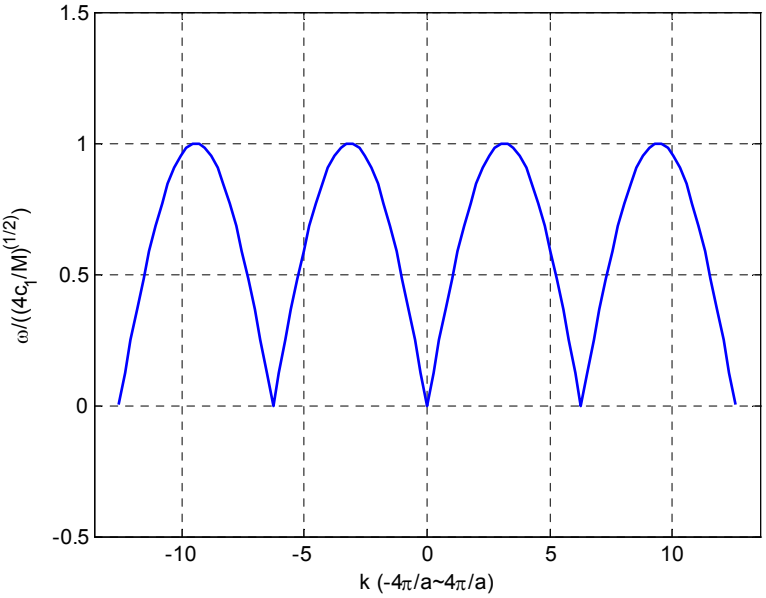

Figure 3.4 Dispersion relation of the 1-D monatomic lattice

The 1st Brillouin Zone (BZ) is the region in reciprocal space containing all information about the lattice vibrations of the solid. Only the $\vec{k}$ values in the 1st BZ correspond to unique vibrational modes. Any $\vec{k}$ outside this zone is mathematically equivalent to a value $\vec{k}_1$ inside the 1st BZ. This is expressed in terms of a general translation vector of the reciprocal lattice in Figure 3.5 with $\vec{k} = \vec{k}_1 + \vec{G}$.

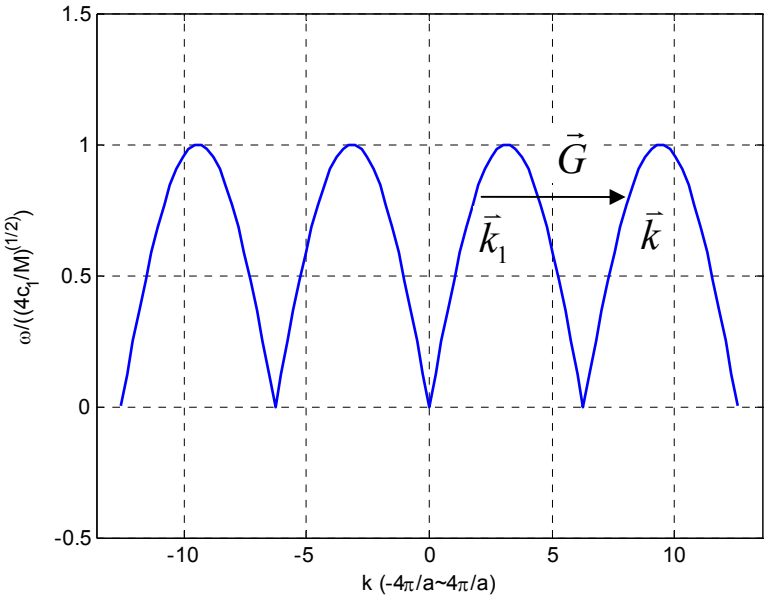

Figure 3.5 General translation vector of the reciprocal lattice

For 3-D lattices, the construction of the 1st Brillouin Zone leads to a polyhedron whose planes bisect the lines connecting a reciprocal lattice point to these neighboring points.

3.5.2 Basic Relationships of Direct Method[133]

Consider a crystal system, the corresponding dynamical matrix is given by

$$D(k;\mu,\nu) = \frac{1}{\sqrt{M_\mu M_\nu}} \sum_m \Phi(0,\mu;m,\nu) \exp\{-2\pi i k \cdot [R(0,\mu) - R(m,\nu)]\} \tag{3-74}$$

where n is the primitive unit cell index, μ is the atomic index, m runs over all atoms of the crystal, M_μ, M_ν are masses of atoms, and k is the wave vector. Eigenvalues of the dynamical matrix

$$\omega^2(k,j)e(k,j) = D(k)e(k,j) \tag{3-75}$$

give the phonon frequencies $\omega^2(k,j)$ and polarization vectors $e(k,j)$.

With small displacement assumption, we can expand the ground state energy E (at T = 0) as a function of atomic positions R(n, μ)

$$E(R(n,\mu),..R(m,\nu),..) = E_0 + \frac{1}{2} \sum_{n,\mu,m,\nu} \Phi(n,\mu,m,\nu)U(n,\mu)U(m,\nu) \tag{3-76}$$

where the force constant matrix

$$\Phi(n,\mu,m,\nu) = \left. \frac{\partial^2 E}{\partial R_i(n,\mu)\partial R_j(m,\nu)} \right|_0 \tag{3-77}$$

is defined at the extreme configuration $\left. \frac{\partial E}{\partial R_i(n,\mu)} \right|_0 = 0$ at which all first order derivatives vanish.

Consider a supercell and make a displacement to atom (m, ν) by U(m, ν). The force generated is $F(n,\mu) = -\partial E/\partial R(n,\mu)$ on all other atoms. Using expansion equation (3-76) one finds

$$F_i(n,\mu) = -\sum_{m,\nu,j} \Phi_{i,j}(n,\mu,m,\nu) U_j(m,\nu) \tag{3-78}$$

This relationship relates the generated forces with the force constant matrices and atomic displacements. The equations of the direct method are explained in the appendix.

3.6 PTFE Characterization

Polymer materials containing fluorine atoms have unique properties. Compared to the corresponding hydrocarbon analogues, they have:

i. very low surface tension and friction coefficient

ii. high chemical stability to strongly acidic or basic environments

iii. high thermal stability

iv. low refractive index

It is important to combine or enhance these basic characteristics of fluoropolymers in order to better use it. Thus, an atomistic understanding of the mechanical behavior is essential.

Teflon is the commercially trade name of polytetrafluoroethylene (PTFE). It is a linear chain polymer with structural repeat unit (-CF_2-CF_2-). It has lots of structural applications in the aerospace, defense and automotive industries. Since PTFE has the highest resistivity of any polymer under shock compression, it has been widely used in shock-wave experiments where an insulator of intermediate shock impedance is required. For this kind of application, the high pressure equation of state must be assessed.

PTFE at atmospheric pressure shows three crystalline phases as the temperature increases. Below 19°C, the repeat unit of the polymer chain consists of 13 CF_2 groups arranged in six complete turns of a helix. Chains in a 13/6 conformation are packed in a nearly hexagonal lattice with $a' = b' = 5.59\,\text{Å},\ c = 16.9\,\text{Å},\ \gamma' = 119.7°$. Between 19 and 30°C, the helical chains slight untwisting from 13/6 helix into 15/7 helix (15 CF_2 units in 7 turns). According to Piseri[24], the hexagonal arrangement of chain positions is maintained. The lattice parameters change to $a' = b' = 5.66\,\text{Å},\ c = 19.5\,\text{Å},\ \gamma' = 120°$.

The international notation of crystal space group symmetry of PTFE between 19 and 30°C is $P3_121$. P means primitive unit cell. The first symmetry in the space group symbol represents the symmetry along the unique axis c. In this case it is threefold screw axes along c direction. So 3_1 represents the symmetry along the unique axis *c*. In this case it is threefold screw axes along *c* direction. An axis 3_1 will repeat the CF_2 group at heights 1/3, 2/3, 3/3 in orientation at 120°, 240°and 360°. The second symmetry in the space group symbol represents the symmetry along the equivalent axes *a* and *b* and the third along the normal to a and b. Here, 2 is the symmetry along the equivalent axes *a* and *b*. Both are 2 fold rotation axis. Along the axis normal to *a* and *b*, 1 means no symmetry along the axes.

Above 30°C, the molecules untwist further and large amount of disorder appear. This property of displaying various helical configurations within different temperature range is of most interesting.

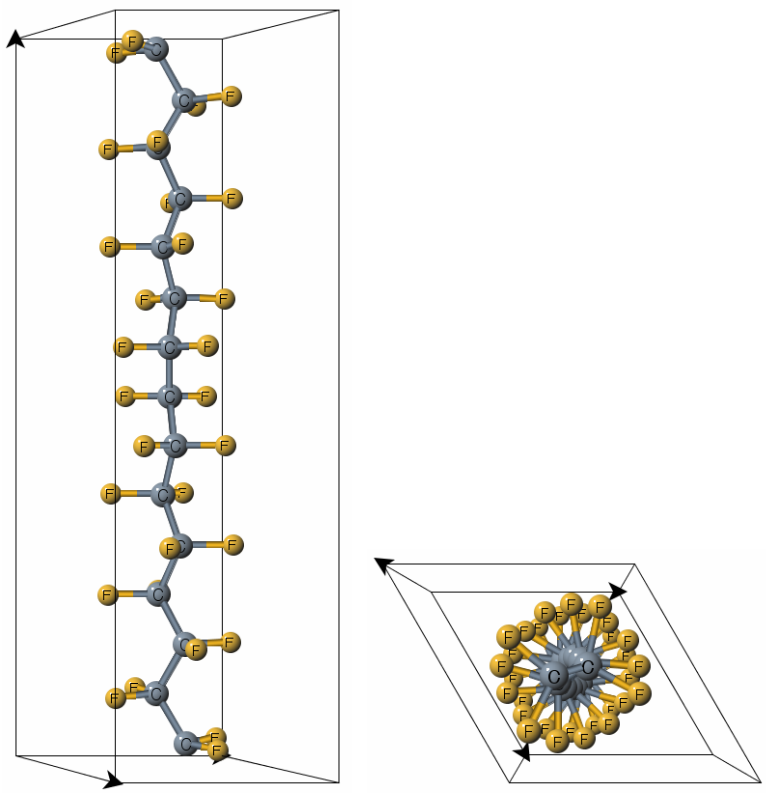

Figure 3.6 PTFE unit cell with 15_7 configuration

With evaluation of structural and energetic parameters, we can introduce them into statistic thermodynamic equations or numerical simulations, which lead to quantities that can be directly compared with experiments.

3.7 Cold Curve EOS for PTFE

3.7.1 Molecular Crystal Structure of PTFE in Tetragonal Unit Cell

The tetragonal unit cell shown in Figure 3.7 is used first. The input atom position is shown below:

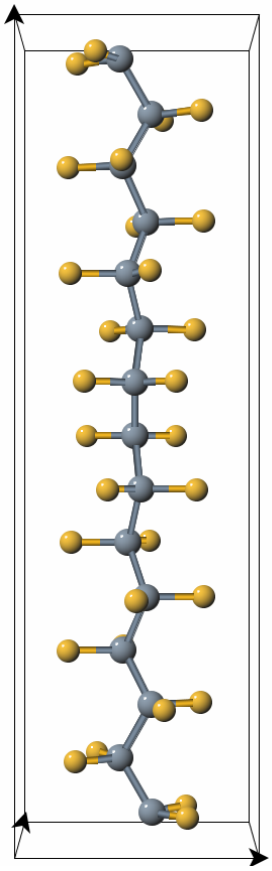

Figure 3.7 Tetragonal unit cell

The output atom position is then calculated while both the cell shape and volume are allowed to be changed. Since the remaining force is larger than 0.01ev/A, the output position of last calculation is used as input position for the calculation followed. This step is repeated 3 times, and the remaining force does not decrease. It is oscillating from last 3 repeated calculations. Then 2 cases are tried:

- use another algorithm
- use hexagonal unit cell

3.7.2 Molecular Crystal Structure of PTFE in Hexagonal Unit Cell

The Hexagonal unit cell is then used. The input atom position is shown below:

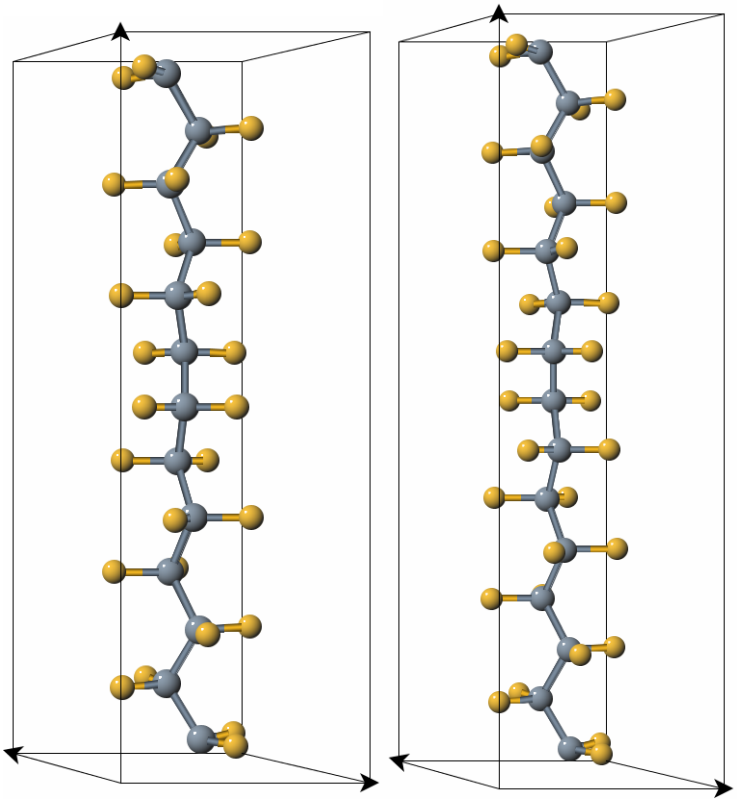

Figure 3.8 13_6 (left) and 15_7 (right) conformation of PTFE

PTFE at atmospheric pressure shows three crystalline phases as the temperature increases. Below 19°C, the repeat unit of the polymer chain consists of 13 CF_2 groups arranged in six complete turns of a helix, and the chains form a triclinic crystal structure with a=b=5.59Å, c=16.9Å, γ=119.3°. Between 19 and 30°C, the unit cell is trigonal with a=b=5.66Å, c=19.5Å. The 15 CF_2 groups are arranged in seven turns. Above 30°C, the molecules untwist further, and their conformation becomes irregular. Figure 3.9 showed the unit cell of the 13_6 (left) and 15_7 (right) conformation of PTFE.

To find the equilibrium geometry, the absolute convergence of PTFE calculation needs to be checked. There are two major sources of error

- Fundamental errors associated with the approximations used in the calculation such as the use of the local density approximation (LDA) (explained in section 3.4.2).
- Systematic errors associated with inaccuracies in the wavefunctions introduced by using a finite basis set and wavefunction sampling in reciprocal space

The latter of these must be reduced to a minimum. The calculation is repeated several times with increasing precision in the basis set and with various MP grid densities. Figure 3.9 below shows the total energy as a function of the basis set size and different K-Points for the 15_7 conformation.

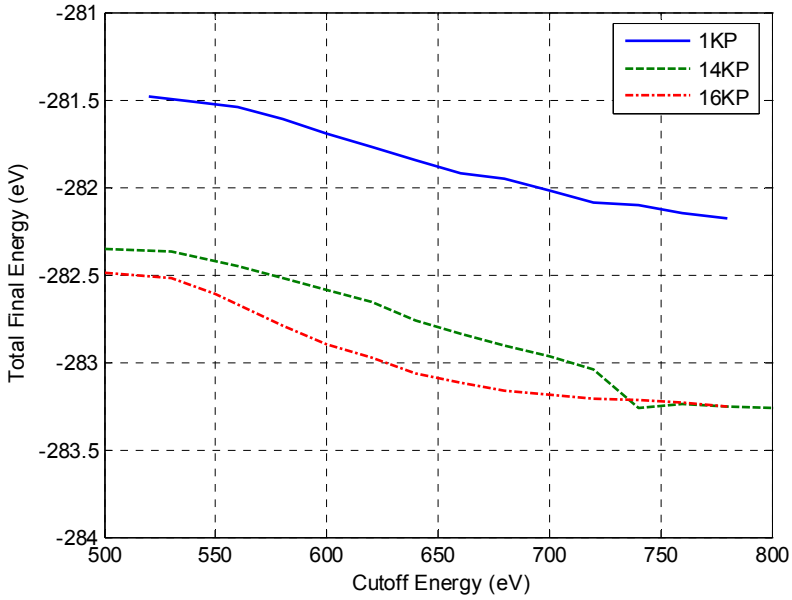

Figure 3.9 Total energy as a function of the basis set size and K-Points (15_7)

The cutoff energy (explained in section 2.2.2) is a variational parameter and as it is increased, the energy will converge asymptotically to the ground state from above. The key point about convergence with respect to the sampling grid density is that the difference in energy from one grid density to the next should be minimized. It is seen that increasing the MP grid density from 14 to 16 k-points has a negligible difference on the total final energy. Also, the total energy converges with respect to the cutoff energy about 750eV. In summary, the fully converged basis set parameters are 16 k-points in the reciprocal space sampling grid and a cutoff energy of 760 eV or higher.

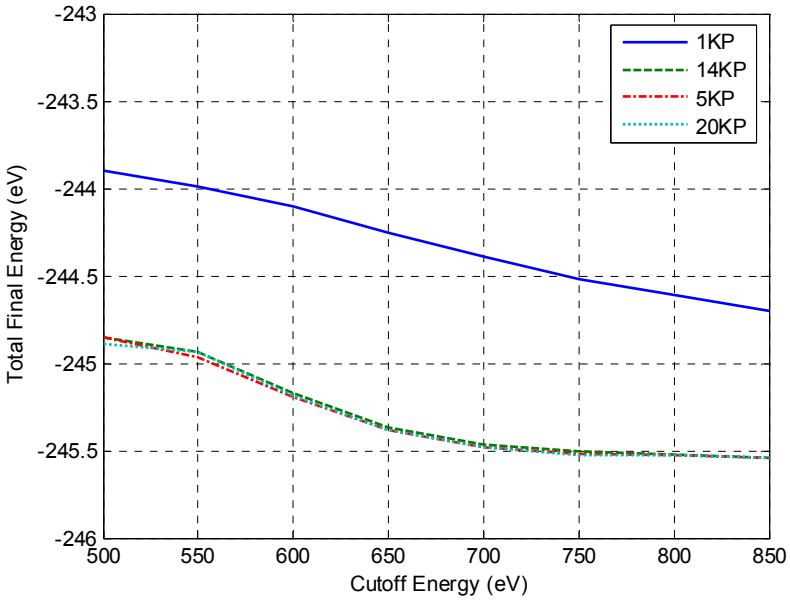

Figure 3.10 Total energy as a function of the basis set size and K-Points (13_6)

Figure 3.10 shows the total energy as a function of the basis set size and different K-Points for the 13_6 conformation. The fully converged basis set parameters are 20 k-points in the reciprocal space sampling grid and a cutoff energy of 850 eV or higher

3.7.3 Cold Curve EOS for PTFE

The cold curve of 15_7 conformation of PTFE is then calculated and shown on Figure 3.11 and Figure 3.12. We discrete the volume ratio v/v_0 from 0.5 to 0.7 at an interval of 0.02 and calculated the cold curve energy. Then the pressure is calculated as explained in section 3.3 without thermal contribution. Method 1 is calculated by relax only the position of ions. Method 2 relaxes both the ion position and the shape of the unit cell.

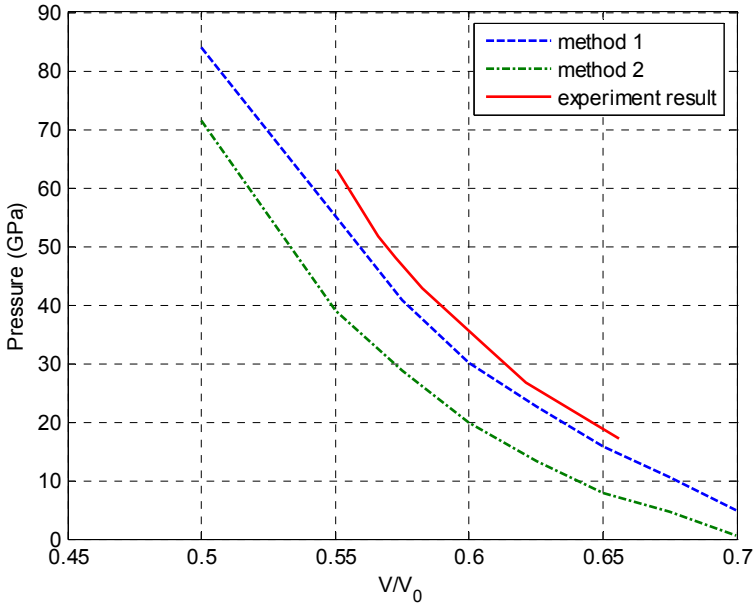

Figure 3.11 Cold curve EOS for 15_7 conformation

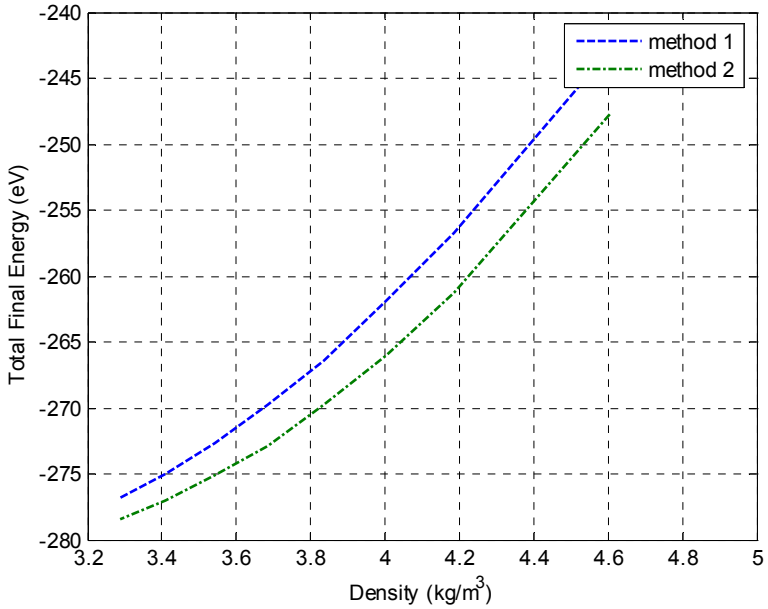

Figure 3.12 Cold curve energy for 15_7 conformation

The cold curve of 13_6 conformation of PTFE is then calculated with both LDA and GGA approximation. Figure 3.13 shows the results.

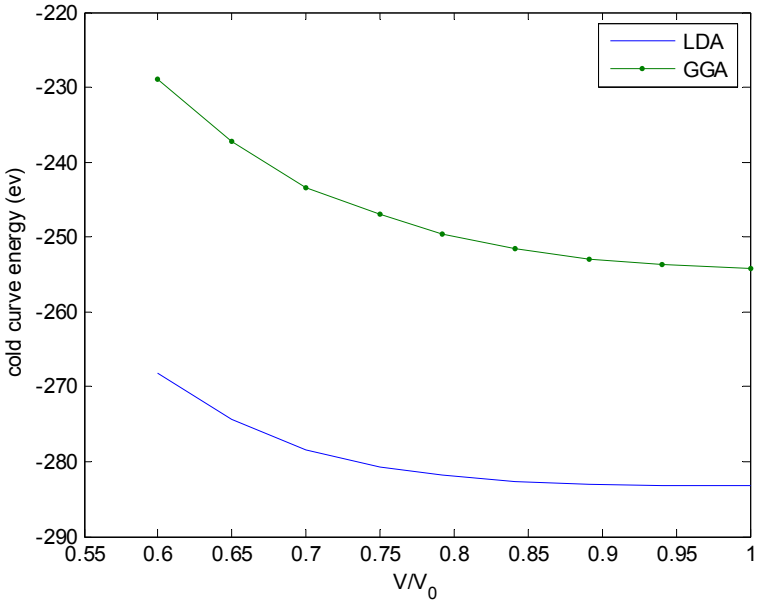

Figure 3.13 Cold curve energy with LDA and GGA approximation

It can be seen that the GGA approximation results in a higher energy. Section 2.2.1 explained the detail about GGA and the difference between LDA and GGA. Then the following calculation is done with LDA approximation and the cold curve equation of state is shown on Figure 3.14 and Figure 3.15.

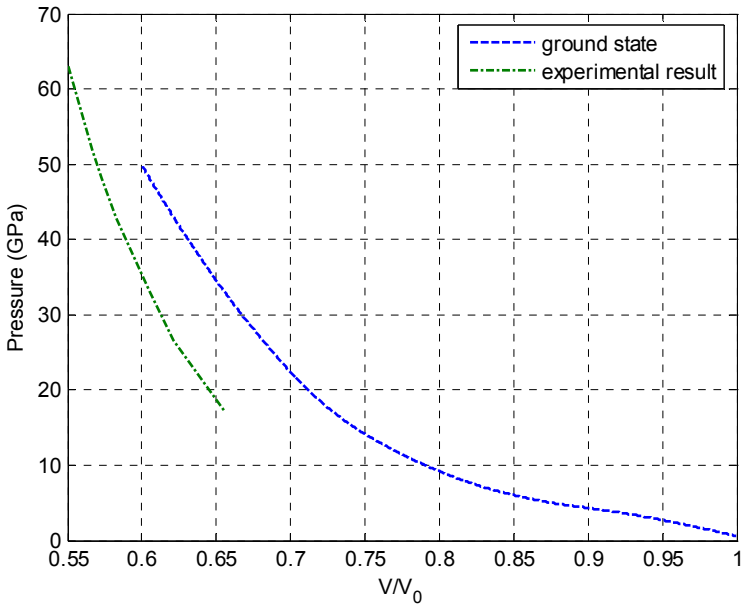

Figure 3.14 Cold curve EOS for 13_6 conformation

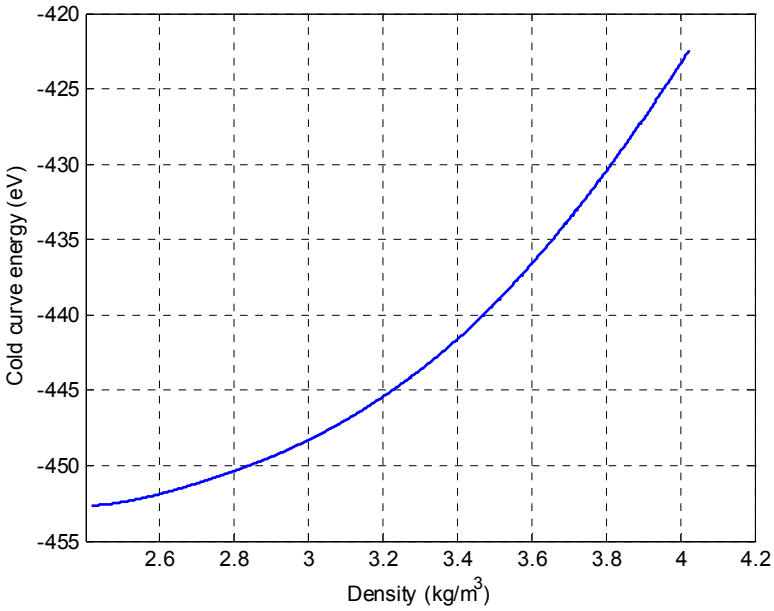

Figure 3.15 Cold curve energy for 13_6 conformation

3.8 Thermodynamically Complete EOS for PTFE

The thermodynamically complete equation of state of PTFE is shown on Figure 3.16.

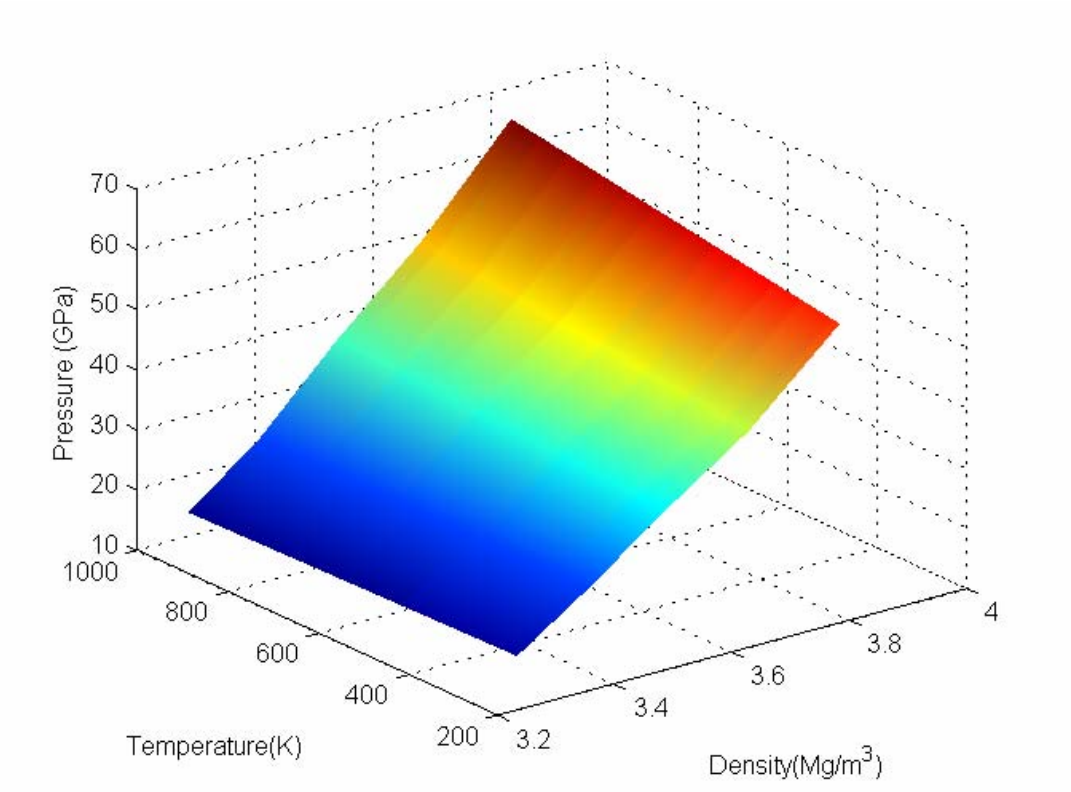

Figure 3.16 Equation of state for PTFE

Based on the 5 unit cell configurations that finished calculation, I use finite difference to calculate the derivative of the free energy, i.e. the pressure.

To compare with the experiment, the Figure 3.17 below is the curve above 19°C that generated. Both ion position and shape of the unit cell are relaxed. There are some differences between the curves generated from my calculation and that comes from experiment. This difference comes from the model. In this calculation, the PTFE was treated as perfect crystalline without defect and amorphous state. The real world polymer will always contain certain ratio of amorphous state. So the material will be stiffer under same pressure.

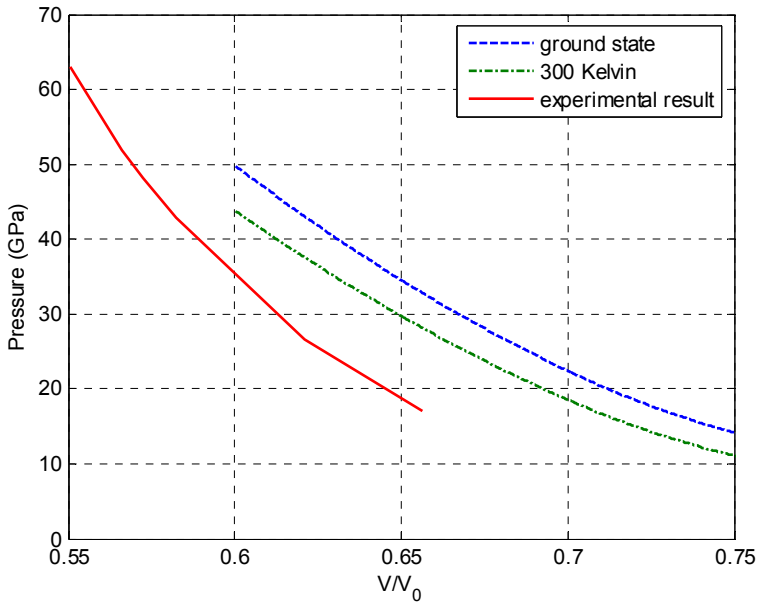

Figure 3.17 EOS for PTFE comparison with experimental result

CHAPTER 4

AB INITIO CALCULATION OF CONSTITUTIVE RELATIONS FOR AL AND PTFE

This chapter addresses the problem of obtaining the complete constitutive relationships for solids under conditions of finite deformations without experiment data. For small deformation case, the constitutive equations are theoretically determined if the Helmholtz free energy is known. For finite deformation case, it is necessary to modify the constitutive equations by considering the deformation gradient, the principle of objectivity, and first or second Piola-Kirchoff stress. Theoretically the free energy is obtained from the ground state energy that is obtained from solving the Kohn-Sham equations. Phonon thermal energy and electron thermal energy are added to determine the Helmholtz free energy. In this thesis, first principles by the use of the density functional theory and foundations of continuum mechanics of finite deformation elasticity are used. The generalized gradient approximation are used to represent the exchange correlation energy and projector augmented wave potentials are used as the basis function to solve Kohn-Sham equations. A polyconvex strain energy density function for hyperelastic materials with cubic anisotropy is used. The model response is investigated under finite deformations.

In the literature, to date, several papers covered the ab initio calculation of constitutive equation for materials under small deformation[127-132]. There are also published papers on ideal strength and finite deformation ab initio calculation[123-126]. However, in the published work, the foundations of finite deformation elasticity are not

considered. These include the invariance requirements concerning the crystal symmetry under specific rotations and objectivity. The principle of objectivity imposes the condition that the resulting constitutive equations are invariant under superimposed rigid body motions on the current configuration. This means if the deformed coordinates $x \rightarrow QF$ then $U(F) = U(QF)$ for every Q in the spatial orthogonal group. (The deformation gradient is denoted by F.) First, this implies that $U= U(C) =U(F^TF)$ where $C = F^TF$ is the Cauchy-Green deformation tensor. Next, the anisotropy or the crystal symmetry is characterized by the material crystal symmetry group G^M. Then $U(C) = U (QC)$ for all $Q \in G$. This then requires the use of structural tensors introduced by Boehler[117]. Thus, to satisfy the principle of objectivity the energy obtained from DFT should be expressed as functions of the invariants of the stretch tensor C and the structural tensors[118,119] applicable to the specific crystal symmetry group. Without such a representation the constitutive relationships are not correct and do not satisfy the requirements of finite deformation elasticity and the needed principle of objectivity. This is an important research issue that has not been considered before and is addressed in the thesis. Once U(C) is formulated, based on the foundations of finite deformation elasticity as discussed in this paragraph, the second Piola-Kirchhoff stress tensor $S = F^{-1}T = 2\partial U/\partial C$, where T is the first Piola-Kirchhoff stress tensor, is then calculated. The U is to be obtained from density functional theory.

The next step is to modify these techniques to obtain the finite deformation Helmholtz free energy and finite deformation constitutive relationships for solids without performing experiments. This is approached first by formulating expressions for free energy from the foundation of the finite strain elasticity. This provides guidelines to

straining the lattice for density functional theory calculations and finding elastic constants once the free energy is obtained from first principles or quantum mechanical foundations. This involves finding the ground state energy from density functional theory from selected strained lattices. This energy is at zero degrees Kelvin. Then, the relationships between the free energy and the constitutive relationships are obtained. To account for higher temperature it is necessary to add phonon thermal energy and the electron thermal energy. In the thesis only ground state energy is used.

In this work, we present a systematic way to obtain the constitutive equations for large deformation elasticity, including the equation of state of aluminum, using density function theory. In the next section, the theory and the framework of numerical procedure to calculate the large deformation constitutive equations, including the equation of state are introduced. The calculated result as well as the description of a simulation setup is in section 2. The results are discussed in section 3. Comparisons are also given where experimental results are available.

4.1 Elastic Constants under Finite Deformation

4.1.1 Elastic Models to Large Deformation

There are several general requirements on the strain-energy function. The fundamental issue is to guarantee the existence of solutions for a given constitutive model. The polyconvexity[120] condition addresses this concern. Another issue is that the deformation and consequently the strain energy density of a material point must not depend on the position of the observer who records the motion. This requirement is called objectivity. A strain energy density function is objective if and only if it can be expressed as a function of the right Cauchy-Green tensor $G=F^{T}F$.

Further constraints to the strain-energy density function arise from material symmetry. If the material response in some preferred directions is identical, the strain energy function is expected to reflect that property. Structure tensors impose the structural symmetry in constitutive relations. The material symmetries of an oriented continuum impose definite restrictions on the form of constitutive relations. The restrictions are taken into account in the representations for anisotropic tensor functions and specify the type and number of variables involved in a constitutive relation. Thus, in a properly written constitutive equation the material symmetries are automatically satisfied. To obtain a concise formulation, employing a minimal number of variables, it is necessary to develop irreducible representations. Zheng and Spencer[118,119] showed that the cubic system is characterized by the single fourth order structural tensor:

$$M = e_1^{(4)} + e_2^{(4)} + e_3^{(4)},\ e_i^{(4)} = e_i \otimes e_i \otimes e_i \otimes e_i \tag{4-1}$$

A polyconvex model for elastic materials with cubic anisotropy used in this work consists of a linear combination of polyconvex monomial functions[120,121,122].

$$U(V_0, \varepsilon_{ij}) = \alpha_1(-\log(I_3)) + \alpha_2 I_3 + \alpha_3 I_4 + \alpha_4 I_1 \tag{4-2}$$

$$I_1 = tr(G),\ I_2 = tr^2(G) - tr(G^2),\ I_3 = \det(G) \tag{4-3}$$

$$I_4 = G : M : G = \sum_{i=1}^{3}\left[F^T F : e_i^{(2)} \otimes e_i^{(2)} : F^T F\right] = \sum_{i=1}^{3}\left[F^T F : e_i \otimes e_i\right]^2 \tag{4-4}$$

where U is the strain energy density function, I_is are the invariants, and α_is are related to the elastic behavior. One way to determine the model parameters α_is is by enforcing that the 2nd PK stress S equal to zero under undeformed configuration as is shown in equation (4-5). This means that the material is free of stress in the reference configuration. This can be achieved by require that the tangent moduli in the undeformed configuration

match the anisotropic elastic constants of specific materials obtained from experiments. For the strain energy density in equation (4-2), the resulting conditions are:

$$S = 2\frac{\partial U}{\partial C},\ S(I) = 0$$

$$\alpha_1 = (C_{12} + 2C_{44})/4,\ \alpha_2 = C_{12}/4,\ \alpha_3 = (C_{11} - C_{12} - 2C_{44})/4, \tag{4-5}$$

$$\alpha_3 = (-C_{11} + C_{12} + 4C_{44})/8$$

If the deformation gradient is $F = \begin{bmatrix} F_{11} & F_{12} & F_{13} \\ F_{21} & F_{22} & F_{23} \\ F_{31} & F_{32} & F_{33} \end{bmatrix}$, then the Cauchy-Green deformation tensor $G = \begin{bmatrix} G_{11} & G_{12} & G_{13} \\ G_{21} & G_{22} & G_{23} \\ G_{31} & G_{32} & G_{33} \end{bmatrix}$, where $G_{ii} = F_{ii}^2$

$$I_1 = tr(G),\ I_3 = det(G),\ I_4 = G_{11}^2 + G_{22}^2 + G_{33}^2 \tag{4-6}$$

The author[120] pointed out that the non-negativity of the model parameters α_i, i=1,…,4 follows from the restriction on the anisotropic ratio $A = \frac{2C_{44}}{C_{11} - C_{12}}$ to between 0.5 and 1. Although the elastic constant of aluminum at 0º Kelvin does not satisfy this requirement, simulation results showed that the model give reasonable result for stretch smaller than 2.

To define the stress-strain relationship of materials under large deformation, the first step is to find the strain energy of the material. The elastic models of crystalline materials is determined from the properties of potential energy E of a unit cell. Therefore, the shape of the energy is first needed. This is calculated by ab initio prediction of the electron ground state and the lattice thermal energy.

4.1.2 Ab Initio Numerical Calculation

Schrödinger equation HΨ=EΨ define the exact many-body eigenstates Ψ and energies E. With variational principle, the ground state is defined as the minimum of $E = \langle \Psi | H | \Psi \rangle$ with respect to all allowed variations in Ψ. Nielsen[129,130] gives the ab initio variational formulation of the energy for a system under a rotation-free infinitesimal strain tensor $\varepsilon_{\alpha\beta}$.

$$H = \sum_i \frac{p_i^2}{2m_i} + V_{\text{int}} + V_{ext} \tag{4-7}$$

with infinitesimal strain[129], $\vec{r} \to (I+\varepsilon)\vec{r}$

$$\Psi_\varepsilon(\vec{r}) = \det(I+\varepsilon)^{-\frac{1}{2}} \Psi\left((I+\varepsilon)^{-1}\vec{r}\right), \text{ together with } (I+\varepsilon)^{-1} \approx I - \varepsilon \tag{4-8}$$

$$\langle \Psi_\varepsilon \mid H \mid \Psi_\varepsilon \rangle = \int \Psi^*(\vec{r}) \left[\sum_i \frac{1}{2m_i} \left[p_i^2 - 2\sum_{\alpha,\beta} \varepsilon_{\alpha\beta} p_{i\alpha} p_{i\beta} + \sum_{\alpha,\beta,\gamma} \varepsilon_{\alpha\beta}\varepsilon_{\alpha\gamma} p_{i\beta} p_{i\gamma} \right] \right] \Psi(\vec{r}) d\vec{r} \tag{4-9}$$

$$+ \int \Psi^*(\vec{r}) \left[V_{\text{int}}\left((I+\varepsilon)\vec{r}\right) + V_{ext}\left((I+\varepsilon)\vec{r}\right) \right] \Psi(\vec{r}) d\vec{r}$$

This equation is the fundamental equation to derive the stress for infinitesimal strain.

For finite deformation, similarly, $\vec{r} \to F\vec{r}$, where F is the deformation gradient tensor.

$$\Psi_\lambda(\vec{r}) = \det(F)^{-\frac{1}{2}} \Psi\left(F^{-1}\vec{r}\right) \tag{4-10}$$

$$\langle \Psi_\lambda \mid H \mid \Psi_\lambda \rangle = \int \Psi^*(\vec{r}) \left[\sum_i \frac{1}{2} m_i v_i^2 + V_{\text{int}}(F\vec{r}) + V_{ext}(F\vec{r}) \right] \Psi(\vec{r}) d\vec{r} \tag{4-11}$$

$$= \int \Psi^*(\vec{r}) \left[\sum_i \left(\frac{p_i^2}{2m_i} + \frac{1}{2} m_i \left\| (F-I)\dot{\vec{r}}_i \right\|_2^2 \right) + V_{\text{int}}(F\vec{r}) + V_{ext}(F\vec{r}) \right] \Psi(\vec{r}) d\vec{r}$$

This equation is the fundamental equation to derive the stress for finite strain.

The elastic stiffness matrix C is defined as

$$C = \frac{\partial S}{\partial F} = 4\frac{\partial^2 U}{\partial G^2}, \tag{4-12}$$

where G is the Cauchy-Green deformation tensor.

We want to investigate the pressure dependence of the elastic constants. The bulk modulus are obtained by

$$\mathrm{K(V_0)} = \frac{1}{3}(\mathrm{C_{11}} + 2\mathrm{C_{12}}) = \mathrm{V_0}\frac{\partial^2 \mathrm{E(V)}}{\partial \mathrm{V}^2}\bigg|_{\mathrm{V_0}} \tag{4-13}$$

For V/V_0 = 0.9, 0.8, 0.7, 0.6, 0.5, we calculated the elastic constants for the deformation shown below.

1. In the first deformation, the stretch is along x axis. λ varies from 1.6 to 0.6 at a interval of 0.05 for each case.

$$F = \begin{bmatrix} \lambda & 0 & 0 \\ 0 & 1 & 0 \\ 0 & 0 & 1 \end{bmatrix} \text{ is the deformation gradient tensor} \tag{4-14}$$

$$F_{ij} = \frac{\partial x_i}{\partial X_j} = \begin{cases} 1 + \dfrac{\partial u_i}{\partial X_i} \\ \dfrac{\partial u_i}{\partial X_j} \end{cases} = I + \left[\frac{\partial u_i}{\partial X_j}\right], \quad u_i = x_i - X_i, \tag{4-15}$$

where I is the identity matrix

$$G = F^T F \text{ is the right Cauchy-Green deformation tensor. } G = \begin{bmatrix} \lambda^2 & 0 & 0 \\ 0 & 1 & 0 \\ 0 & 0 & 1 \end{bmatrix} \tag{4-16}$$

This uniaxial deformation leads to a strain tensor $\gamma = \frac{1}{2}(G - I)$ is the Lagrangian strain tensor,

$$\gamma = \frac{1}{2}\begin{bmatrix} \lambda^2 - 1 & 0 & 0 \\ 0 & 0 & 0 \\ 0 & 0 & 0 \end{bmatrix} \tag{4-17}$$

Substituting the equation (4-16) into (4-12), we have

$$C_{11} = 4\frac{\partial^2 E}{\partial G_{11}{}^2}\bigg|_V \tag{4-18}$$

2. The second deformation involves performing volume-conservative tetragonal strains. λ varies from 1.6 to 0.6 at a interval of 0.05 for each case. The deformation gradient tensor F is

$$F = \begin{bmatrix} \lambda & 0 & 0 \\ 0 & \lambda & 0 \\ 0 & 0 & \lambda^{-2} \end{bmatrix}$$

$G = F^T F$ is the right Cauchy-Green deformation tensor. $G = \begin{bmatrix} \lambda^2 & 0 & 0 \\ 0 & \lambda^2 & 0 \\ 0 & 0 & \lambda^{-4} \end{bmatrix}$ (4-19)

The Lagrangian strain tensor is

$$\gamma = \begin{bmatrix} \frac{\lambda^2 - 1}{2} & 0 & 0 \\ 0 & \frac{\lambda^2 - 1}{2} & 0 \\ 0 & 0 & \frac{\lambda^{-4} - 1}{2} \end{bmatrix} \tag{4-20a}$$

Then we have

$$3(C_{11} - C_{12}) = \frac{\partial^2 E}{\partial G_{11}{}^2}\bigg|_V \tag{4-20b}$$

3. The remaining independent modulus, C_{44}, was found by shearing crystal with the monoclinic strain. λ varies from -0.25 to 0.25 at a interval of 0.05 for each case

$$F = \begin{bmatrix} 1 & 0 & \lambda \\ 0 & 1 & 0 \\ \lambda & 0 & 1 \end{bmatrix}, \; G = \begin{bmatrix} 1+\lambda^2 & 0 & 2\lambda \\ 0 & 1 & 0 \\ 2\lambda & 0 & 1+\lambda^2 \end{bmatrix} \tag{4-21a}$$

$$\gamma = \begin{bmatrix} \frac{1}{2}\lambda^2 & 0 & \lambda \\ 0 & 0 & 0 \\ \lambda & 0 & \frac{1}{2}\lambda^2 \end{bmatrix} \tag{4-21b}$$

Substituting the equation (4-21) into (4-12), we have

$$C_{44} = 4 \frac{\partial^2 E}{\partial G_{13}{}^2}\bigg|_V \tag{4-22}$$

Then from the equations (4-18), (4-20) and (4-22), we can solve for the three elastic constants C_{11}, C_{12} and C_{44}.

4.2 Constitutive Relations for Al under Finite Deformation

Once the system is optimized, the second derivative of the energy is calculated by changing the unit cell length in the chain direction. The total energy is obtained for each configuration of the unit cell by the method described above. Around the equilibrium configuration of the system, the response of the system to elongations by deforming the equilibrium geometry is calculated. The structure is optimized while keeping the nonequilibrium length unchanged. We calculated the total energy of each strain for a number of values of λ. These energies were then fitted to a polynomial in λ and the curvature of the energy versus ε curve was obtained.

Based on the methods described above, the elastic constant of aluminum is calculated.

Elastic constants at 0ºK from Kittel's book (GPa)

$C_{11} = 114.3$, $C_{12} = 61.9$, $C_{44} = 31.6$

Elastic constants at 0ºK from ab initio calculation (GPa) (no hydrostatic pressure)

$C_{11} = 112.0$, $C_{12} = 63.3$, $C_{44} = 30.7$

In ab initio calculation, strain changes are made by directly changes in the input cell data. In our calculation, the cut-off energy of the plane-wave basis set was 320 eV. The exchange-correlation energy was evaluated using the generalized-gradient approximation (GGA) with the parameterization of Perdew and Wang. We used conjugate gradient optimization of the wave functions, reciprocal-space projection, a 11×11×11 k mesh for the reciprocal-space integration with a Monkhorst-Pack scheme. The solution was considered to be self-consistent when the energy difference of two subsequent iterations was smaller than 0.1meV.

Figure 4.1 shows plots of the energy at the harmonic regime and Figure 4.2 shows the second piola-kichhoff stress components σ_{11} as a function of the Lagrangian strain tensor component γ_{11} with no hydrostatic pressure.

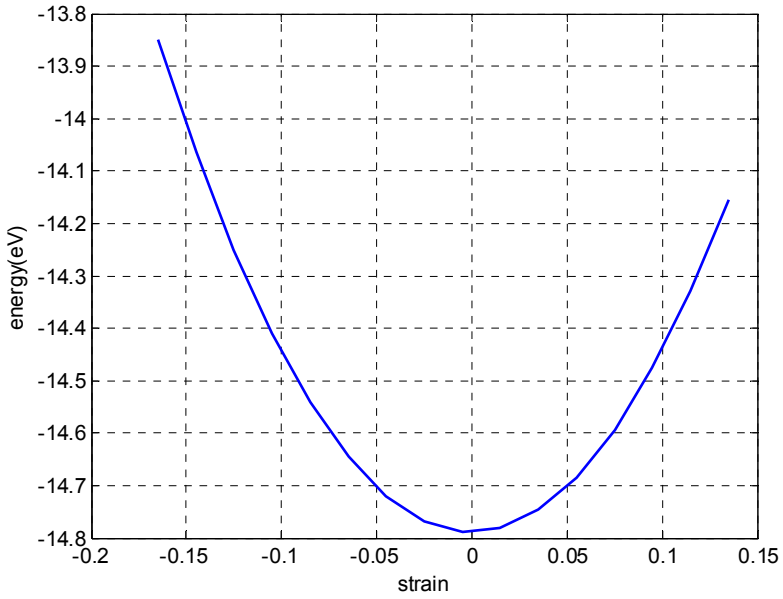

Figure 4.1 Energy vs. γ_{11} with no hydrostatic pressure at the harmonic regime

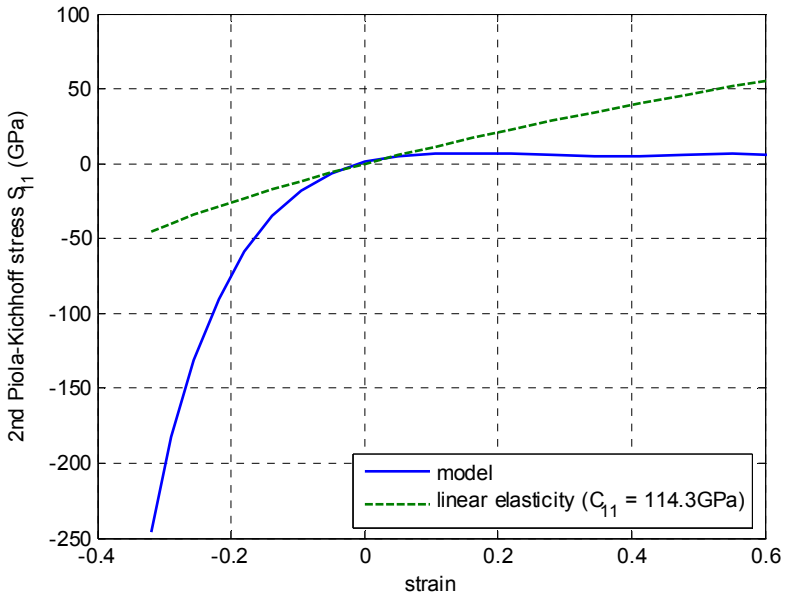

Figure 4.2 2nd pk stress components σ_{11} vs. γ_{11} with no hydrostatic pressure

Figure 4.3~4.5 shows plots of the energy, second piola-kichhoff stress components σ_{11} and elastic constant C_{11} as functions of the Lagrangian strain tensor component γ_{11} with different hydrostatic pressure.

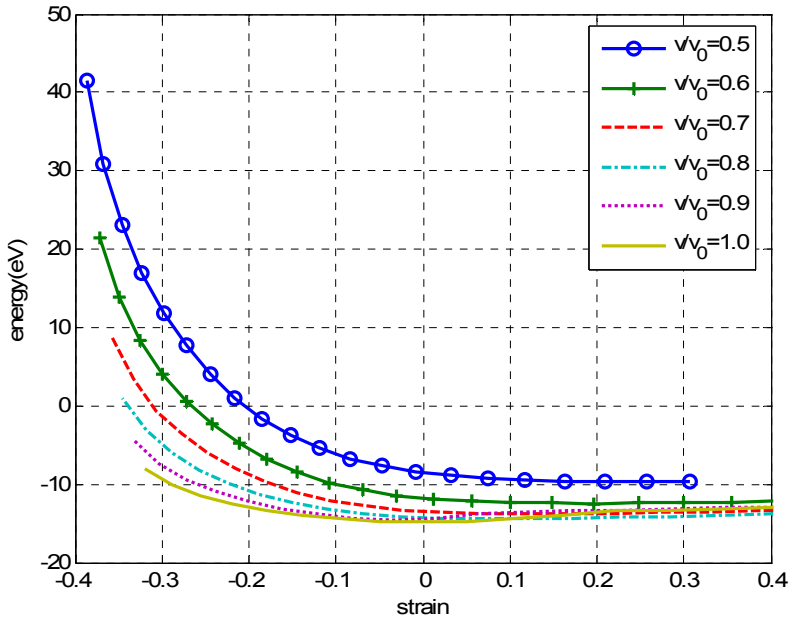

Figure 4.3 Energy vs. γ_{11} with hydrostatic pressure

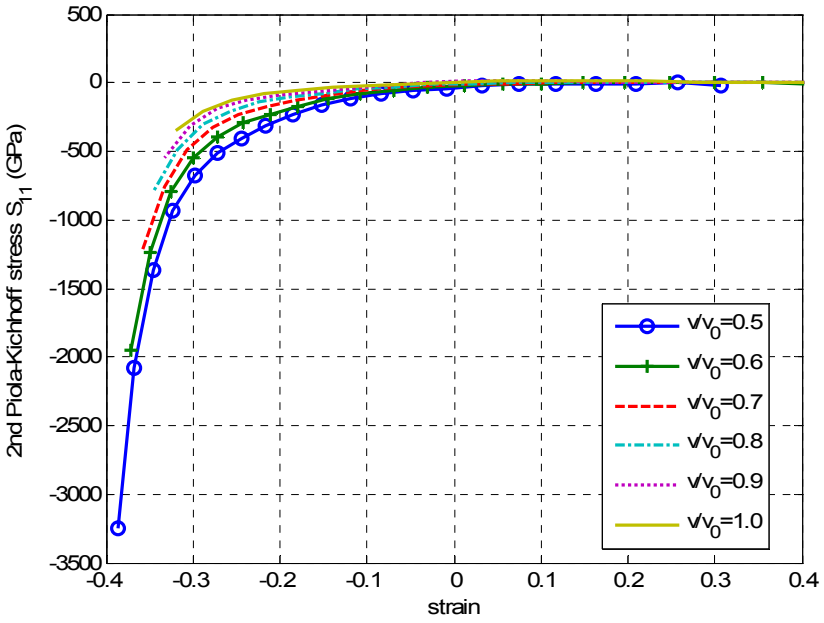

Figure 4.4 2nd pk stress components S_{11} vs. γ_{11} with hydrostatic pressure

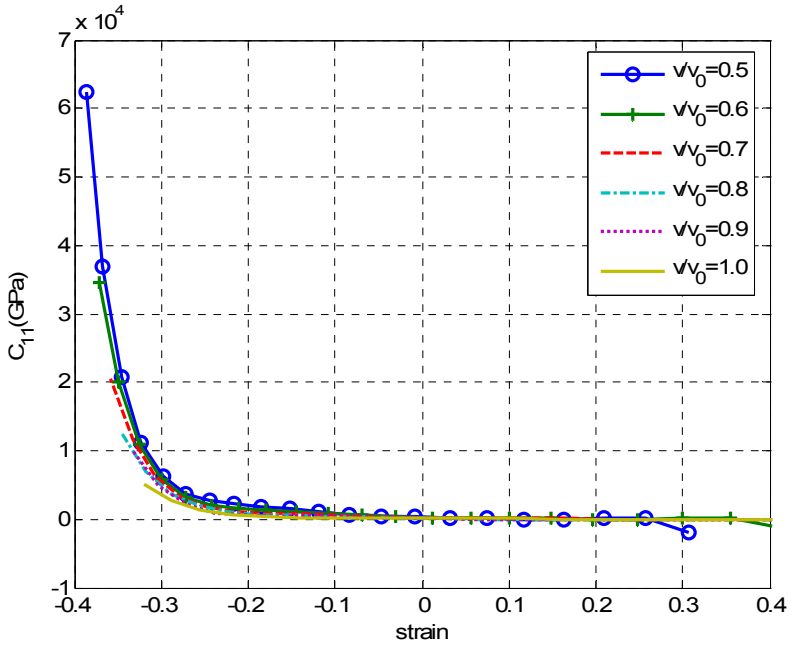

Figure 4.5 Elastic constant C_{11} vs. γ_{11} with hydrostatic pressure

Figure 4.6~4.8 shows plots of the energy, Cauchy stress components σ_{13} and elastic constant C_{44} as functions of the stretch λ.

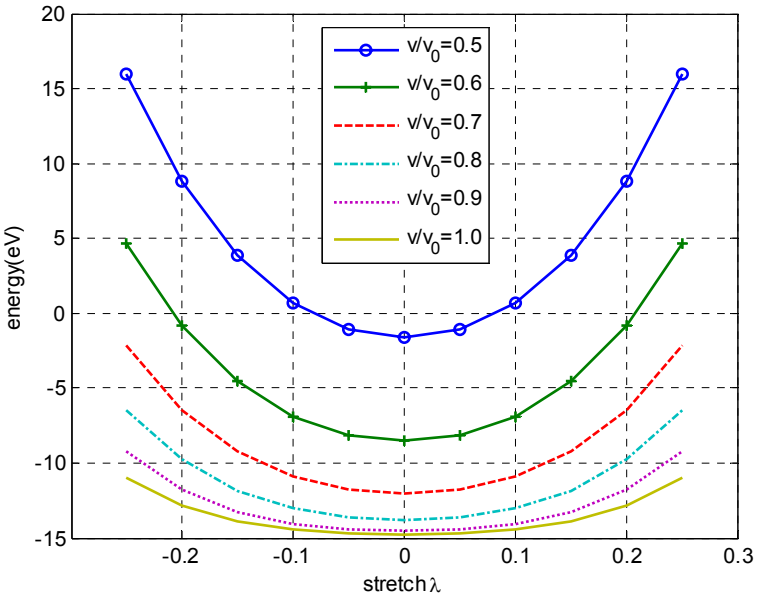

Figure 4.6 Energy vs. stretch with hydrostatic pressure

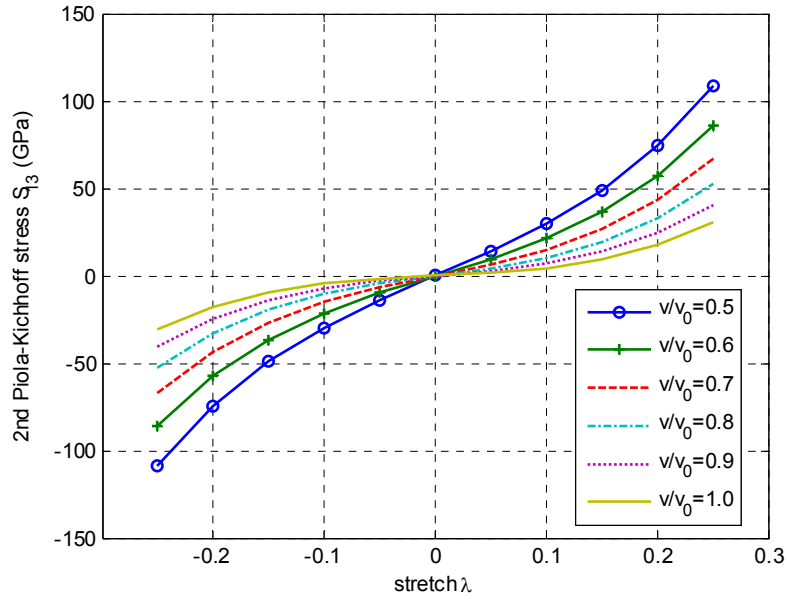

Figure 4.7 2nd pk stress components S_{13} vs. stretch with hydrostatic pressure

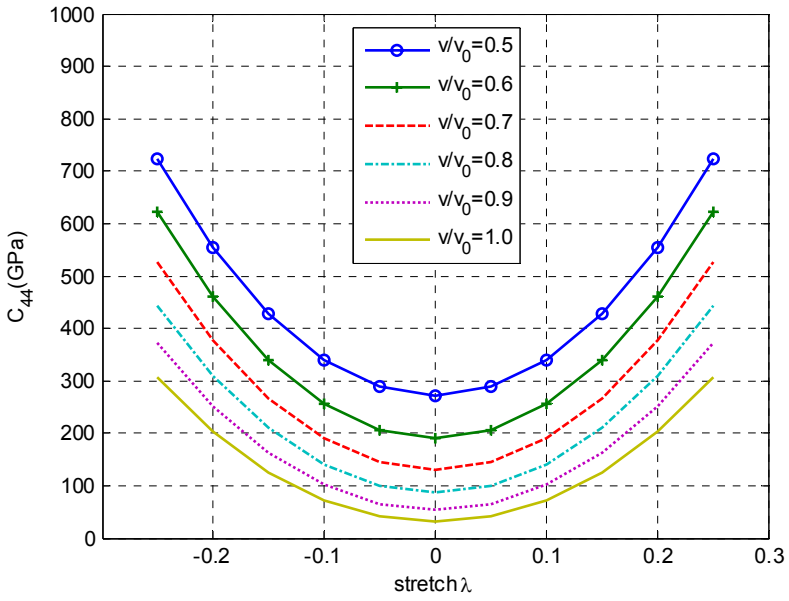

Figure 4.8 Elastic constant C_{44} vs. stretch with hydrostatic pressure

The elastic constant with addition of the hydrostatic pressure versus relative volume for FCC aluminum is obtained and are listed below:

Table 4.1 Elastic constants under hydrostatic pressure for fcc aluminum

V/V_0	$(C_{11}-C_{12})/2$ (GPa)	C_{44} (GPa)
1.0	27.3768	31.449
0.9	42.814	56.739
0.8	64.886	99.986
0.7	96.795	170.44
0.6	144.96	273.84
0.5	211.94	437.79

4.3 Ab Initio Calculation of Elastic Constant for PTFE under Small Deformation

As discussed in the first section, we can obtain the energy of a coupled ion-electron system for the given ion positions. A crystal is a special case of coupled ion-electron system and constructed by repeating unit cells. According to its space group, each unit cell has some constraints on the relevant positions of ion. From first principles calculations, we can obtain the energy E_0 for a crystal in its equilibrium state. By distorting the crystal, which corresponds to a strained state, we also can obtain the energy

E of the system. Let the volume of the unstrained crystal be V_0. We have a relation of E and E_0.

$$E(V_0, \varepsilon_{ij}) = E_0 + \frac{V_0}{2} C_{ijkl} \varepsilon_{ij} \varepsilon_{kl} \tag{4-23}$$

For a general solid, the linear elastic constitutive relations are given by

$$\sigma_{ij} = C_{ijkl} \varepsilon_{kl} \tag{4-24}$$

For a crystal, by its symmetric properties, the 81 constants of C_{ijkl} reduce to a much smaller number of independent constants. A cubic crystal has a=b=c and α=β=γ=90°, only has three independent elastic constants, C_{11}, C_{12}, C_{44} (in two-suffix notation).

$$C = \begin{bmatrix} C_{11} & C_{12} & C_{12} & & & \\ C_{12} & C_{11} & C_{12} & & & \\ C_{12} & C_{12} & C_{11} & & & \\ & & & C_{44} & & \\ & & & & C_{44} & \\ & & & & & C_{44} \end{bmatrix} \tag{4-25}$$

This means that three types of strain must be applied to the starting crystal. We can choose three highly symmetrical types of deformation.

(1) The first type involves calculating the bulk modulus (K), which is related to the elastic constants by $K = \frac{1}{3}(C_{11} + 2C_{12})$. For various values of V, the energy E(V) can be calculated. From the equation (4-23), we can obtain

$$K(V_0) = \frac{1}{3}(C_{11} + 2C_{12}) = V_0 \left. \frac{\partial^2 E(V)}{\partial V^2} \right|_{V_0} \tag{4-26}$$

(2) The second type involves performing volume-conservative tetragonal strains. We vary the ration c/a=(1+e), where e is selected small parameter. This leads to a strain tensor

$$\varepsilon = \begin{bmatrix} \varepsilon_1 & & \\ & \varepsilon_1 & \\ & & \dfrac{1}{(1+\varepsilon_1)^2} - 1 \end{bmatrix} \quad where\ \varepsilon_1 = \frac{1}{(1+e)^{1/3}} - 1 \tag{4-27}$$

Substituting the equation (4-27) into (4-23), we have

$$E(\varepsilon_1, V_0) = 3(C_{11} - C_{12})\varepsilon_1{}^2 V_0 + O(\varepsilon_1{}^3) \tag{4-28}$$

Then we have

$$6(C_{11} - C_{12})V_0 = \left.\frac{\partial^2 E}{\partial \varepsilon_1{}^2}\right|_{V_0} \tag{4-29}$$

(3) The last type of deformation we can choose a rhombohedral distortion. For that kind of strain, we vary the length of the great diagonal of the cubic cell. By selecting a primitive cubic lattice, the rhombohedral lattice is defined by its related hexagonal vectors, $\vec{a}_H$.

$$\begin{pmatrix} \vec{a}_H \\ \vec{b}_H \\ \vec{c}_H \end{pmatrix} = \begin{bmatrix} 1 & -1 & 0 \\ 0 & 1 & -1 \\ 1 & 1 & 1 \end{bmatrix} \begin{pmatrix} \vec{a}_r \\ \vec{b}_r \\ \vec{c}_r \end{pmatrix} \tag{4-30}$$

Then we vary $\vec{c}_H = (1+e)\vec{c}_{H0}$. For cubic lattice, the resulting strain tensor is

$$\varepsilon = \frac{e}{3}\begin{bmatrix} 1 & 1 & 1 \\ 1 & 1 & 1 \\ 1 & 1 & 1 \end{bmatrix} \tag{4-31}$$

Substituting the equation (4-31) into (4-23), we have

$$E(e, V_0) = \frac{e^2}{3}(C_{11} + 2C_{12} + 4C_{44})V_0 + O(e^3) \tag{4-32}$$

Then we have

$$\frac{2}{3}(C_{11}+2C_{12}+4C_{44})V_0=\left.\frac{\partial^2 E}{\partial e^2}\right|_{V_0} \tag{4-33}$$

Then from the equations (4-26), (4-29) and (4-33), we can solve for the three elastic constants C_{11}, C_{12} and C_{44}.

(4) Second derivatives calculation

Finite difference method is applied to calculate the 2nd derivative of the energy. The forward difference divided by *h* can be used to approximate the first order derivative when *h* is small.

$$f'(x)=\frac{f(x+h)-f(x)}{h}+O(h) \tag{4-34}$$

The central difference formula for the 2nd derivative of *f* at *x* is

$$f''(x)=\frac{f(x+h)-2f(x)+f(x-h)}{h^2}+O(h^2) \tag{4-35}$$

This formula is for the calculation of the second derivative of the energy.

To calculate the Young's modulus, the first step is to find the total energy of the polymer chain. The elastic modulus of crystalline polymers is determined from the properties of potential energy *E* of a unit cell at the equilibrium point. Therefore, the shape of the energy surface around the equilibrium geometry is first needed. This is calculated by ab initio prediction of the electron ground state and the lattice thermal energy. In "elongation-relaxation" method, the total energies of several unit cells with small length difference along the chain direction are found first.

The deformation of crystals under hydrostatic pressure is given by the Murnaghan equation of state.

$$E(V) = E_0 + \frac{B_0 V}{B_0'}\left(\frac{(V_0/V)^{B_0'}}{B_0' - 1} + 1\right) - \frac{B_0 V_0}{B_0' - 1} \tag{4-36}$$

where V is the volume, V_0 is the equilibrium volume, B is the bulk modulus, B_0 is the value of B when pressure is zero. When the cross section area is known, Young's modulus is expressed as a function of the second derivative of the total energy.

$$Y = \frac{L_0}{A} F \tag{4-37}$$

where A is the cross section area, L_0 is the length along the chain axis around the equilibrium configuration and F is the force constant.

$$F = \frac{d^2}{dL^2} E \bigg|_{L=L_0} \tag{4-38}$$

Young's modulus is an equilibrium property of the material. The second derivation of the energy must be obtained first to estimate the Young's modulus. For single chain infinite polymer, "elongation-relaxation" method[26,27,28] is extensively used to calculate the response of the system to elongation. The key point of this method is to deform the equilibrium geometry of the system around the lowest energy position. Certain amount of strain is set artificially and kept constant. Then the geometry of the system is optimized. Once the equilibrium geometry of several such points around the lowest energy geometry are known, numerical analysis method can be applied to get the Young's Modulus though the second derivative of the energy on the equilibrium position of the system.

Once the system is optimized, the second derivative of the energy is calculated by changing the unit cell length in the chain direction. The total energy is obtained for each configuration of the unit cell by the method described above. Around the equilibrium configuration of the system, the response of the system to elongations by deforming the

equilibrium geometry is calculated. The structure is optimized while keeping the nonequilibrium length unchanged. The Young's modulus is obtained from the second derivative around the minimum energy, resulting in 0.42GPa (7% harder than 0.393 GPa of ASTM D638).

In this research work, the Young's modulus and the thermal equation of state for PTFE are calculated from ab initio method. Without introducing the sample impurities and imperfection, needless to say, the property obtained with first principle method give the upper bound for these properties. Since it is relatively easy to prepare a perfect crystalline state PTFE sample, it is more reasonable to apply the theoretical evaluation to PTFE than to polymers without this property. Comparison with experiment value is difficult since real sample always contain imperfections. The comparison should be carried out on samples as perfect as possible. The proposed value at room temperature is 0.42GPa. The presented work is part of an attempt for calculating the thermodynamically complete equation of state of PTFE.

CHAPTER 5

EQUATION OF STATE FOR MIXTURE OF AL+NI+PTFE

Structural-energetic materials are synthesized from reactive materials with a binder. One of the profound binder materials is Teflon or PTFE because of the energetic characteristic of PTFE. Since structural-energetic materials are used in structures that are subject to impact, it is necessary to analyze such structure under impact conditions. During impact, the structural-energetic material is expected to withstand the impact without any failure and shock-induced chemical reaction. (The reactions are induced any where the energetic function of the structural-energetic material are needed)

Thus, to optimize the mixture ratio, it is necessary to characterize the material including the constitutive relations of the granular composite material that forms the structural-energetic material. As explained before, an important part of the constitutive relationship is the equation of state. Thus, in the section the equation of stat of a structural-energetic material consisting of Ni, Al and PTFE is determined from ab initio methods. In the past the ab initio methods are used to characterize the equation of state of crystalline materials like Al, Ni, Iron and some compound such as Fe_2O_3. The problem of characterizing the equation of state of alloys is still an active research area. However, the problem of finding the equation of state of mixtures (that are not alloys) is an open research area.

Thus, the procedure to obtain the thermodynamically complete equation of state $P=P(\rho,T)$ for an intermetallic mixture of nickel and aluminum with porosity and PTFE binding material is formulated in the thesis via first principle calculations for pressures.

Two approaches are used to calculate for the EOS of the mixture. The first is based on ab initio calculations of EOS for each component. Then, mixture theories are utilized to obtain the EOS for the mixture. The second approach fully based on ab initio methods and used a supercell that is constructed to represent proper mixture architecture with porosity. In the first approximate approach, two mixtures theories are used. They are homobaric and a uniformly blended mixture theory, which correspond to two limiting cases. We only calculated the cold curve equation of state with the supercell method and compare it with the results from the mixture theories. The nature of a real mixture is intermediate to those of the two idealized mixtures and hence can be modeled as a weighted combination of the two cases. The effects of the porosity on the EOS are introduced by considering the air as the third component in the mixture.

All the ab initio calculations for the static-lattice EOS are carried out in the framework of the density functional theory (DFT), using spin-generalized gradient approximations (GGA) or spin-GGA (sGGA), ultrasoft psuedopotentials and projector augmented wave (PAW) methods. The phonon modes are calculated by the density functional perturbation theory (DFPT). The lattice thermal contributions are obtained by populating the phonon modes according to the Boltzmann statistics. The electronic thermal contributions are obtained by populating the band structure according to the Fermi-Dirac statistics. For aluminum and nickel, we compared the predicted EOS with experimental data and listed the results in Appendix. We also compare the predicted EOS for mixture of nickel, aluminum and PTFE obtained by these two approaches.

5.1 Background

The objective of this chapter is to determine the equation of state (EOS) of an energetic mixture of nickel, aluminum and PTFE from quantum-mechanical methods. This type of intermetallic materials with binding materials possesses both high-energy content and high strength. Thus there is a great potential in the applications of debris-free explosions. The study of this type of materials in the shock physics includes the investigation of the shock-induced chemical reactions and the material synthesis techniques by using shock consolidation techniques. All these studies require a complete information on equation of state.

A thermodynamically complete EOS characterizes the material mechanical behavior under hydrostatic pressure and is expressed as the dependence of pressure on the specific volume and temperature. Traditionally, the complete EOS requires a large number of tests and measurements. However, the extreme difficulty of the temperature measurement in shocked systems unavoidably leads to an incomplete EOS. Especially at the design stage of new materials, the experimental determination of EOS involves a tremendous effort at high cost. Therefore, using first principles calculations to obtain EOS of new materials is very appealing. The most important part of such a procedure is that it provides a thermodynamically complete EOS.

There exist some literature on the use of first principles to calculate EOS of solids including semiconductor material silicon[42], metals[70,31,32,44,73,34,35,36,37], and even polymers. Among theses materials, various approximation techniques are used based on the characteristic electronic band structures and the associated lattice, electrical and

magnetic properties. Aluminum as a benchmark high-pressure material has been investigated using quantum mechanic principles since 1970s.

The earliest studies[102,7] of aluminum equation of state are used in the development of DFT. In 1980s, Lan and Cohen investigated the lattice structure, bulk modulus, phonon dispersion and phase transition by using DFT. In 1996, Boettger and Trickey used LDA approximation to obtain the cold curve EOS and phase transition and study the phonon effects. In 2003, Chisolim et al. investigated the EOS of Al which includes the possible liquid phase above the melting curve. Nickel as a ferromagnetic transition metal has obtained special interest. In early studies, the choice of basis functions mainly focus on local basis functions like Gaussian orbital[107] and linear muffin-tin-orbitals[105,106] due to the consideration of computational efforts. Comparing to aluminum, nickel is a transition metal and has 8 to 9 3d electrons. These 3d electrons have dual characters as atomic like and as itinerant like. The interplay of these two characters indicates a strongly correlated system.

Various methods have been proposed to improve the conventional band theory to accommodate for the strongly correlated electron interaction. GW approach[108,111] and Hubbard Hamiltonian[109] are used to perturb the expansion in the electron interaction; while dynamical mean-field theory[110,111] has been used to include the fluctuations of electron occupation around LDA mean-field solution. GW approximation was originally derived from a many-body perturbation theory as a first term in the expansion of the self-energy in the screened Coulomb potential W, rather than the bare Coulomb potential v. In these studies, the electron spectra properties and magnetic moments were investigated to

justify the methods. In 1987, Levy et al.[105] preliminarily used both Thomas-Fermi model and linear-muffin-tin orbitals to calculate the electronic contribution to the EOS of Ni.

For the energetic mixture like the Al-Ni-PTFE mixture, two approaches are used to obtain the EOS of the mixture by ab initio quantum mechanical calculations. In the first method, the EOS is obtained for each individual component from first-principle calculations. Then, the EOS of the mixture is approximated using mixture theories, namely homobaric mixture theory and uniformly blended mixture theory. Ab initio methods are based on the psuedopotential plane-wave methods. The generalized gradient approximations, ultrasoft psuedopotential and projector augmented wave method are also utilized. The prediction of the EOS consists of two parts: the static-lattice EOS and thermal effects. The range of pressure and temperature of consideration is up to 300 GPa and 1000K. As known, the melting temperatures of aluminum and nickel at the ambient pressures are about 933 K and 1,728 K, respectively. However, at high pressures, these melting temperatures are changed. For shock induced chemical reactions of intermetallic mixture of Al and Ni, the chemical reaction initiation temperatures are estimated in the range of 1000K. In this work, the possible polymorphic phase transitions are not considered. Chapter 3 covered the calculation of EOS for PTFE. The details for aluminum and nickel EOS calculation are given in the appendix. The details for EOS of the mixture are presented in the section below.

5.2 EOS by Using Mixture Theories

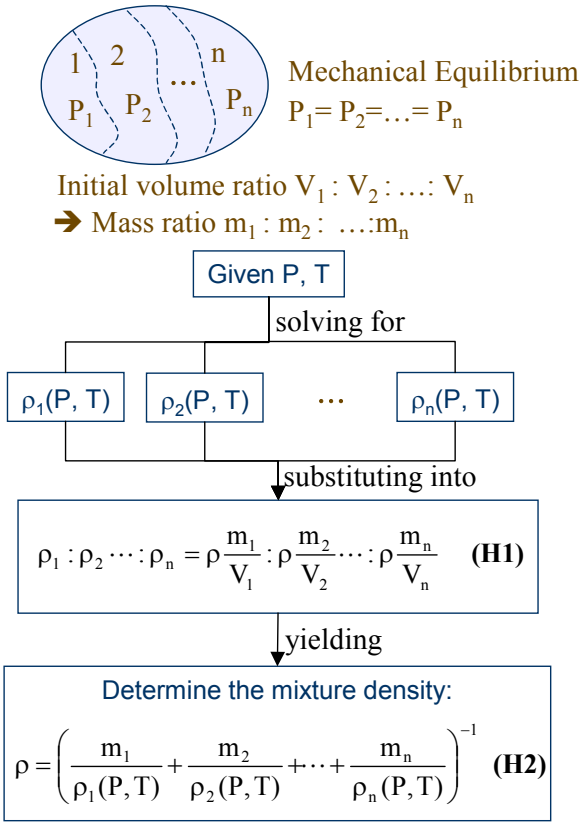

Figure 5.1 The procedure for the EOS of mixture with homobaric mixture theory

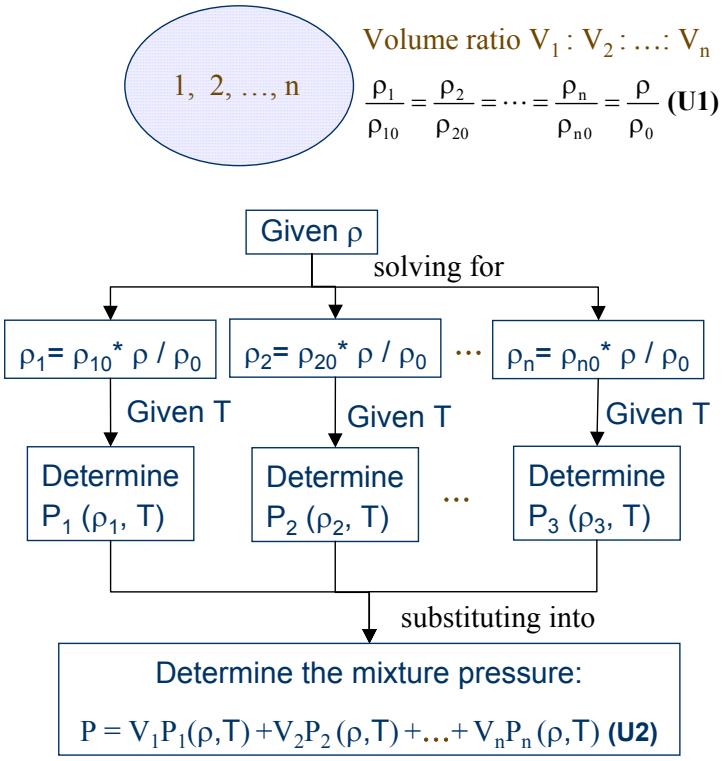

Figure 5.2 The procedure for the EOS of mixture with uniformly blended mixture theory

A mixture theory is used as a weighted combination of two limiting cases, one of which is equivalent to a series combination of the components (homobaric mixture theory) and the other is equivalent to a parallel combination of the components (uniformly blended mixture theory). In the first case (homobaric), the interface between components is assumed to be in mechanical equilibrium, and every component occupies its own fractions of volume and mass. The relations in equations (H1) (as shown in Figure 5.1) hold. While in the parallel case, different components deform at the same strain. It indicates the relations in equations (U1) as shown in Figure 5.2. The procedures

for constructing the EOS of mixture by these two mixture theories are shown in Figure 5.1 and Figure 5.2, respectively. Initially, the EOS of each component is known or obtained by the ab initio techniques. For the homobaric mixture theory, given P and T, every component of mixture experiences the same P and T. The density of every individual component $\rho_i(P,T)$ (i=1, 2, …, n) is obtained from its known EOS. Then we substitute ρ_i (P,T) into equation (H2) (as shown in Figure 5.1), which is obtained by solving equations (H1), to obtain the EOS of mixture. For the uniformly blended mixture theory, given the density of mixture ρ, we can solve for the corresponding density of every component ρ_i (i=1, 2, …, n) from equations (U1). From the EOS of component, we can determine the component pressure $P_i=P_i(\rho_i,T)$ (i=1, 2, …, n). The mixture pressure P is determined by the summation of component pressure weighted by its component volume fractions as shown in equation (U2) in Figure 5.2. In practice, it is not possible to obtain mixtures without any void content.

The currently available techniques and application do not permit the synthesis of intermetallic mixtures of full density without any voids. There is always some accompanying porosity. Usually, the materials synthesized in the laboratory leads to Ni+Al+PTFE mixtures with densities in the range of 75% - 88% of the material. Some researchers think of that the existence of porosity and its collapse-induced dissipation is necessary to provide the enough energy to overcome the energy barriers for chemical reactions to release the stored energy in the energetic mixture[145,146]. Therefore, the EOS of porous mixture is very important for the applications of these energetic materials. To construct the EOS of a porous mixture, we introduce the porosity (or air) as the fourth

component consisting of the mixture. The van der Waals EOS is used for air, which is suitable at relatively high pressures (for a gas).

$$\left(P + a\rho^2\right)\left(\frac{1}{\rho} - b\right) = RT \tag{5-1}$$

In this equation, the constant 'a' accounts for the repulsion between molecules and increases the forces between them. The constant 'b' accounts for the volume physically occupied by molecules and decreases the effective open volume. Numerical values of 'a' and 'b' can be calculated as follows.

$$a = \frac{27R^2T_{critical}^2}{64P_{critical}} \qquad b = \frac{RT_{critical}}{8P_{critical}} \tag{5-2}$$

For air, at 1 atm and 0ºC, the density of air is 1.29kg/m^3. The critical temperature $T_{critical}$ and pressure $P_{critical}$ of air, corresponding to the critical point for phase changes from liquid and gas, are $T_{critical}$=132.5K and $P_{critical}$=3.77 MPa. As discussed, the homobaric mixture is softer than the uniform mixture. Especially, when air is introduced as the third component, which has no stiffness compared to the other two solid components, the mixture is very soft at low pressures, which is indicated by the observation that the pore collapse occurs at very low pressures. Therefore, the homobaric assumption is more appropriate to model the porous mixture at low pressures.

The EOS is calculated for a mixture: 5Ni+5Al+PTFE (mass ratio 25%:12%:64%) with some porosity based on these two mixture theories. The results are shown in Figure 5.3 and Figure 5.4. As expected, the EOS from homobaric mixture theory is 'softer' than that from uniformly blended mixture theory. In reality, the nature of the actual mixture is intermediate to that of the two idealized mixtures and hence is modeled as a weighted combination of the two cases.

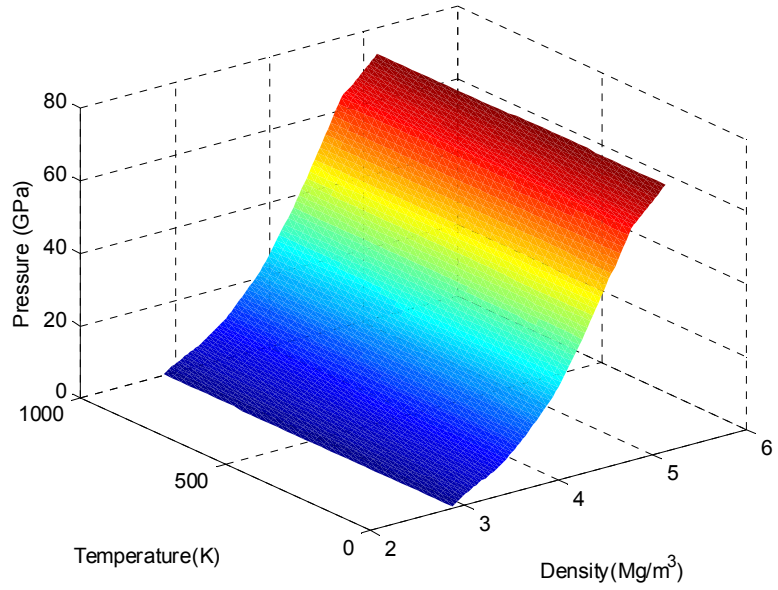

Figure 5.3 EOS of mixture by using uniformly blended mixture theory

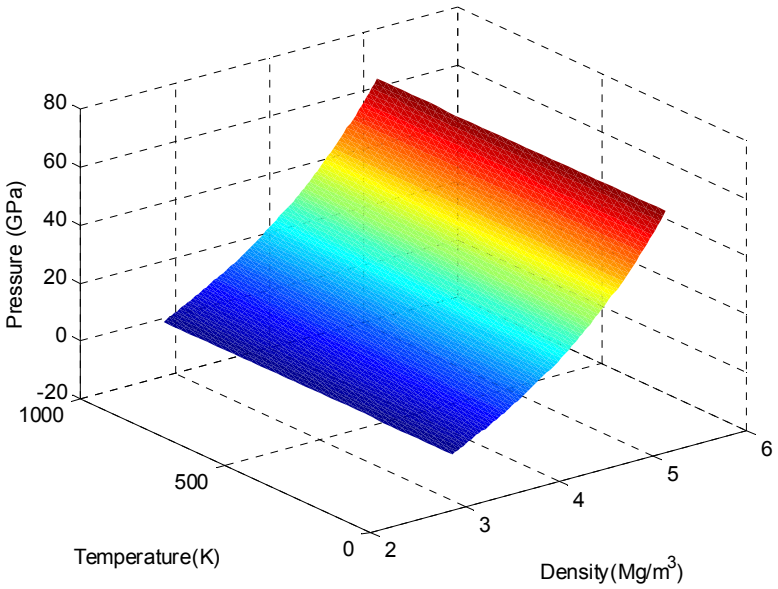

Figure 5.4 EOS of mixture by using homobaric blended mixture theory

5.3 Ab Initio Based Cold Curve EOS of Mixture by Using a Supercell Approach

Various supercells are constructed to simulate the mixture of aluminum, nickel, and PTFE with porosity. Considering various interfacial conditions between aluminum and nickel, supercells are built with various types of interfacial layers between 5 layers aluminum and nickel lattices at each side. All the layers are in the direction (1 1 1). Interfacial layers containing 2 layers aluminum and 2 layers nickel at each side are constructed through a constraint relaxation calculation. Vacuum spaces are introduced to the supercell to simulate the porosity. The constructed supercells are presented in Figure 5.5. In Figure 5.5, the entire aluminum and nickel lattice is stretched to match the PTFE lattice. A 2.8% vacuum was introduced. Because experimental results are not available, the cold-curve EOS for this supercell is compared with the cold-curve EOS obtained by using the two mixture theories. The results are shown in Figure 5.6. We can see that the comparison results coincide with our expectation. The two mixture theories correspond to two limiting cases. The supercell results lie in the between these limiting cases.

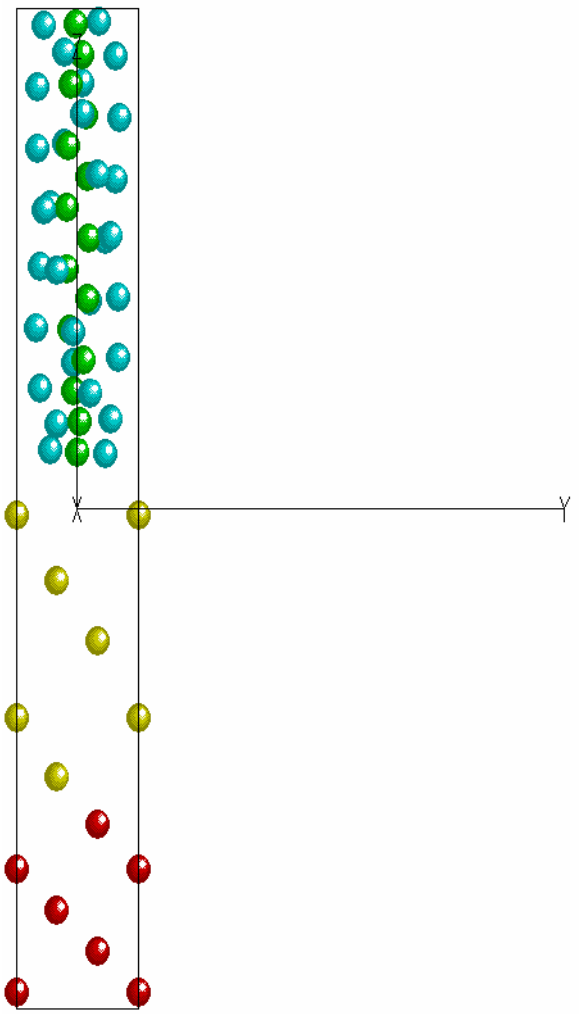

Figure 5.5 Supercell of mixture of 5Ni+5Al+PTFE

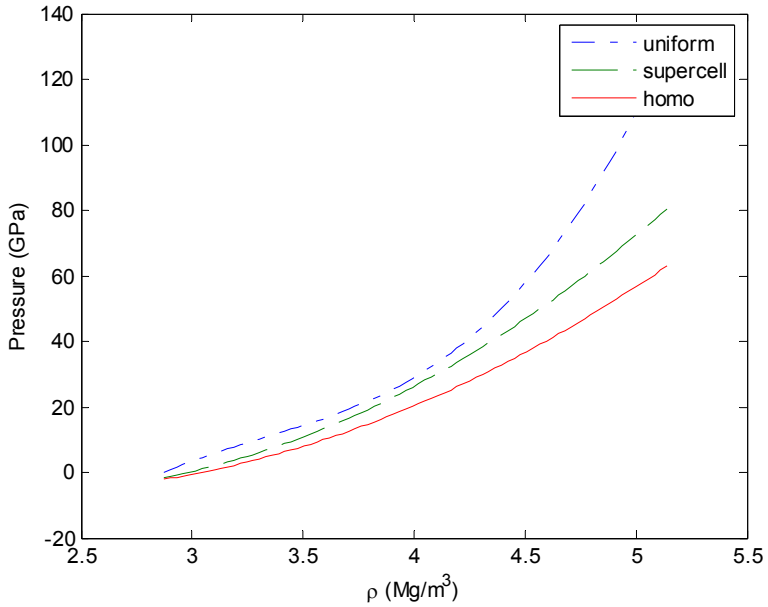

Figure 5.6 EOS of mixture by using blended mixture theories and by supercell approach

In this work, we have used the complete ab initio based supercell approach to obtain the cold curve EOS of a porous energetic inter-metallic mixture of nickel and aluminum. We have also used the two mixture theories to obtain the thermodynamically complete equation of state of the structural-energetic mixture. First, the EOS for each individual component consisting of the mixture is obtained from the thermodynamic relations and based on the first principle calculation of internal energy. Then, two different mixture theories as two limiting cases of reality are discussed and used to calculate the EOS of mixture. The cold curve EOS of porous mixture is also constructed by introducing air as the other constructing component. Future work includes obtaining the thermodynamically

complete EOS of a porous energetic inter-metallic mixture of nickel, aluminum and PTFE with complete ab initio based supercell approach.

CHAPTER 6

CONCLUSION & FUTURE WORK

6.1 Conclusions

In this work, we discussed multiscale models that are used to characterize the constitutive relations of the granular composite materials with dual functions. Because the dual functional energetic structural materials are used in applications where the resulting structure encounters high intensity impact loads, impact and penetration into selected targets and shock induced chemical reactions, the finite deformations of these materials are also considered. This is accomplished by the use of ab initio methods to obtain the constitutive relations and foundations for chemical reactions in structural energetic materials without conducting tests. Then, both the lattice thermal contributions due to phonons and electron thermal contribution are added. The resulting energy is used in numerical integration of conservation equations to bridge to the continuum level and obtain the constitutive equations.

This work focuses on the issues of the constitutive equations. More specifically, we analyzed the constitutive equations of a specific mixture of nickel, aluminum and PTFE or Teflon as the binder. The equations of state $p=P(\rho,T)$ of PTFE, from ab initio studies, are reported. The equations of state of the mixtures of nickel, aluminum and PTFE are studied. The complete large or finite constitutive equations of crystalline aluminum, from ab initio methods under conditions of finite deformations, are also studied. We considered the satisfaction of the principle of objectivity, the material symmetry conditions and the polyconvexity of the resulting expressions for the strain energy.

By using the procedure mentioned above, several problems are studied in this work:

(1). We determined the thermodynamically complete equation of state of the binder and the energetic material PTFE or Teflon, from ab initio methods based on the density functional theory and Kohn Sham equations.

(2). We also determined of the equations of state of the granular composite or the mixture of nickel, aluminum and PTFE from ab initio methods.

(3). The constitutive equation of aluminum, from ab initio methods, under conditions of finite deformations, with principle of objectivity, material symmetry conditions, and polyconvexity of the strain energy is also determined.

All results are compared to test results whenever they are available.

6.2 Future Work

To discuss the possible design of mixtures of dual-functional materials, we need to characterize the constitutive relationships and chemical reactions properties of the selected thermite mixtures, intermetallics mixtures and combustible metals. Then, the next step is to select a mixture to meet specified goals or requirements.

We can explore the potential of different structural energetic materials that are made from different combinations of reactive materials, different binders and voids. In such exploratory studies, it is necessary to consider different ratios of the basic ingredients. The future work also includes the reaction characteristics of these materials.

We can also characterize the constitutive relationships of polymer under hydrostatic pressure. With different crystalline symmetry, we can define the effect of hydrostatic pressure on different elastic constants with ab initio methods.

The future work should formulate the thermodynamically complete EOS for granular mixture of Ni + Al + PTFE + Structural reinforcement and voids. The thermal effect of ab initio supercell approach should be considered. The future work should also include investigation of the effect of different ratios of the materials in the mixture and different combination of materials. The ab initio methods should be developed as a design tool to develop future granular composite for other different applications. Such a procedure can be used to evaluate the different combination of dual functional structural energetic materials and make the design of such materials more efficient.

APPENDIX

A.1 EOS for aluminum and nickel[147]

By using ab initio methods, in the framework of projector augmented wave method, we study fcc phases of aluminum. First, we perform a ground state analysis. A ground-state EOS is then constructed as a function of the density. Then, we investigate the characteristics of phonon dispersions and obtain associated lattice free energy by using the phonon density of state and Boltzmann statistics. Thirdly, we calculate the electronic thermal contribution to the total free energy by using predicted electronic band structures and Fermi-Dirac statistics. After obtaining the total free energy from the three contributions: cold-curve energy, electronic and lattice thermal energy, we construct the total free energy as a function of density and temperature. The thermodynamically complete EOS for aluminum is then calculated.

The electron ground states were calculated using the density functional theory in the projector augmented plane-wave psuedopotential implementation using the Vienna ab-initio simulation packageVASP. The local density approximation or the generalized gradient approximation was chosen to model the exchange and correlation potentials depending on the characteristics of system. For GGA, a semi-local form PW91 exchange-correlation functional was chosen. The effects of core electrons were taken into account by the psuedopotentials, while the outer electrons were expanded in the framework of the projector augmented wave method. For an aluminum atom, with $3s^2 3p^1$ chosen as valence electrons and the others as core electrons, psuedopotential was generated with cutoff radius of 2.65 Å and 1.402 Å respectively, with nonlinear core corrections and a cutoff

radius of 2.974 Å for projector operators. A finite number of basis states were used, corresponding to a selected energy cutoff. The Kohn-Sham equations were solved using iterative matrix diagonalization that was based on the minimization of the norm of the residual vector to each eigenstate and optimized charge- and spin- mixing routines. In the ion relaxation loop, the total energy converged to 10^{-5} eV, while in each electron relaxation loop, the total energy converged to 10^{-6} eV. The electron wave functions of the valence electrons were expanded in a plane-wave basis set for which the amplitudes of each band were optimized to find the ground state. The electron wave functions are calculated explicitly on a discrete grid of locations in k space. Standard Monkhorst Pack grids or Gamma centered grids were generated in k space. The number of k points is determined to resolve the Fermi surface accurately. In this study, for ground state energy calculation 11×11×11 k-points are used. However, for calculations of electron density of state, a much larger number of k points (up to 64×64×64) were used to impose the accuracy of electron band structures.

The fcc aluminum crystal is in Space group Fm_3m, with a = b = c, $\alpha = \beta = \gamma = 90°$. For fcc aluminum, a conventional unit cell of 4 aluminum atoms was used for calculations. By using the conjugate-gradient algorithm to relax the cell shape, cell volume and ion positions at every ion relaxation step, the ground state equilibrium lattice parameter is determined to be 4.049 Å, corresponding to a volume of 66.38 $Å^3$ (or a specific volume of 0.621154844 $Å^3$/amu). A discrete scaling parameter ξ, was chosen to scale down on the lattice parameters a, b and c. For an equilibrium lattice, $\xi = 1$. Discrete values of ξ are selected from 0 to 1. Each ξ corresponds to a specific volume, which is equal to $0.62115\xi^3$ $Å^3$/amu. For the fcc aluminum calculation, discrete values of ξ from

0.6 to 0.9 were selected at an interval of 0.025, from 0.9 to 1 at an interval of 0.01. In the energy calculations, ion positions were relaxed under the constraints of cell shape and cell volume. By using either LDA or GGA, the cold curves and cold curve EOS for the fcc aluminum were predicted. The results for LDA and GGA are compared in Figure A.1. It is seen that LDA results in a harder property than GGA. In comparison to the experimental Hugoniot EOS in the low pressure range, GGA gives a better fit than does the LDA (Figure A.1b).

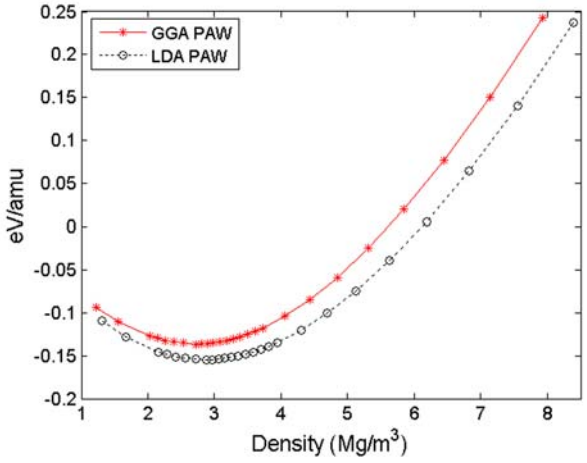

(a)

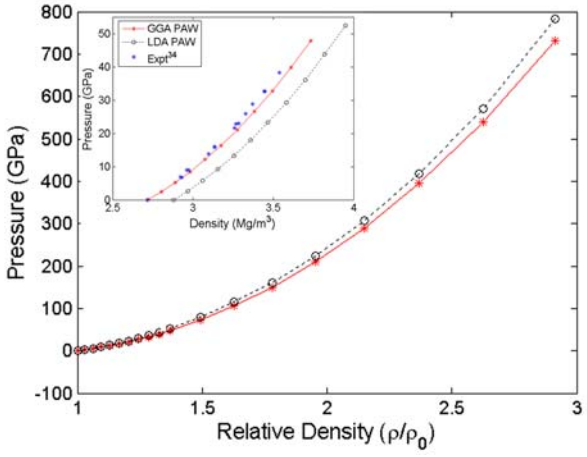

(b)

Figure A.1 Comparison of cold curve calculations for fcc Al by using LDA and GGA PAW methods: (a) Cold curve energy; (b) Cold curve EOS

Table A.1 Predictions of the cold-curve properties

Methods		Density (kg/m^3)	Bulk Modulus (GPa)
LDA PAW	fcc	2879.427296	83.33
	hcp	2852.916117	79.82
	bcc	2804.201313	73.37
GGA PAW	fcc	2721.262729	75.20
	hcp	2694.609913	71.87
	bcc	2641.805331	65.72
Expt.	fcc	2700	76
		2715	72.7

Similarly, discrete a, chosen for the fcc Ni, are from 2.7 to 3.5 at a interval 0.1 Å. Small interval 0.01 Å is chosen for the values between 3.4 and 3.52Å, which is the equilibrium lattice parameter. Following the procedure, we obtained the thermodynamically complete EOS for Al and Ni. They are presented in Figure A.6 and Figure A.7. To investigate the thermal effects on EOS, the isotherm EOS at three temperatures 0K, 1000K, 3000K are presented in Figure A.8 and Figure A.9. The ab initio 300K isotherm EOS for Al and Ni is compared with their shock Hugoniot data. The comparisons are shown in Figure 10a and b, respectively.

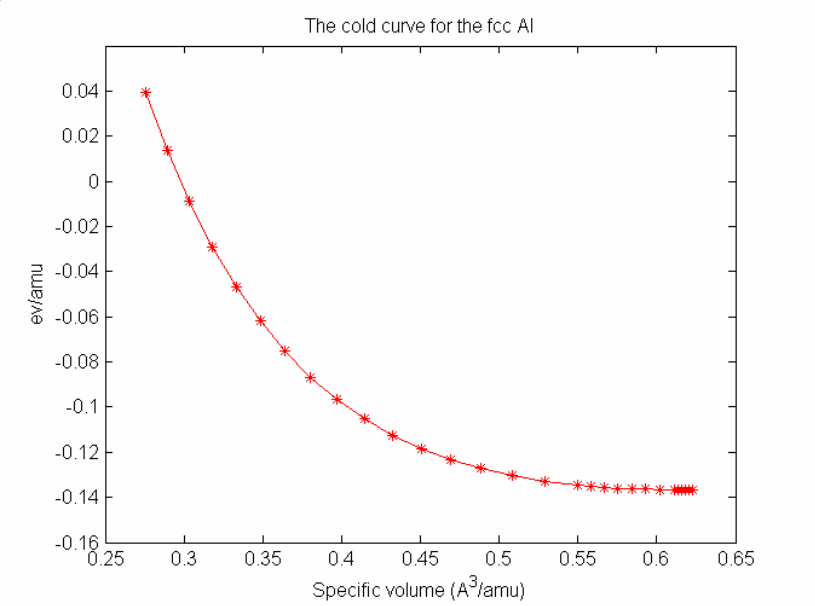

Figure A.2 The cold curve of Al

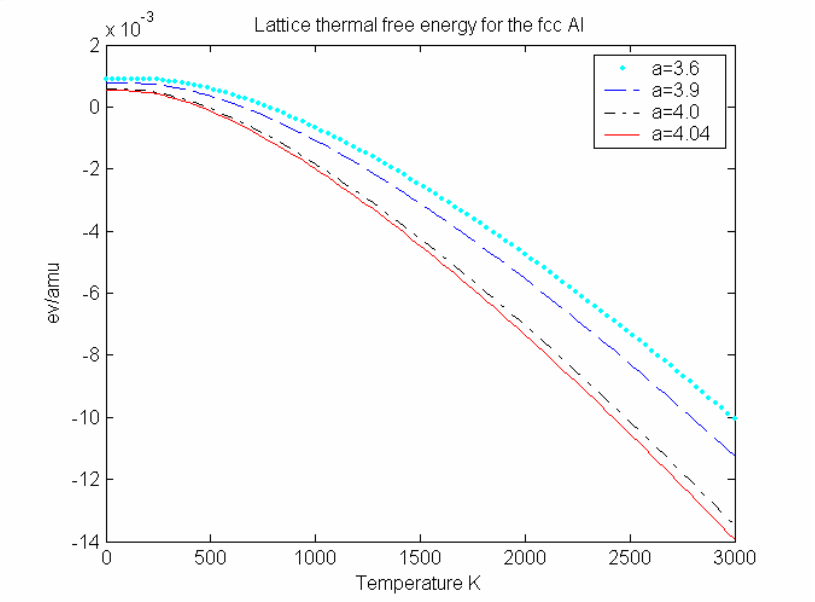

Figure A.3 The lattice thermal free energy of Al vs. the temperature at selected lattice parameters

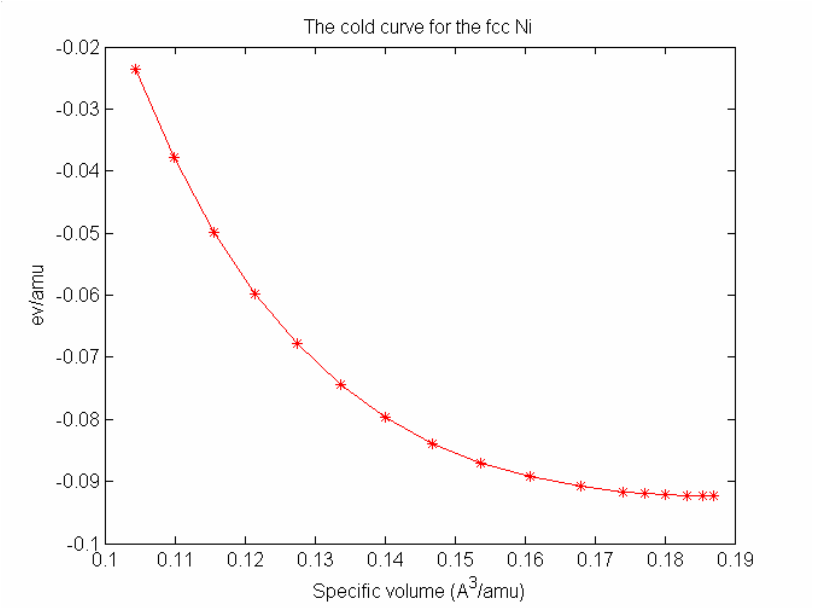

Figure A.4 The cold curve of Ni

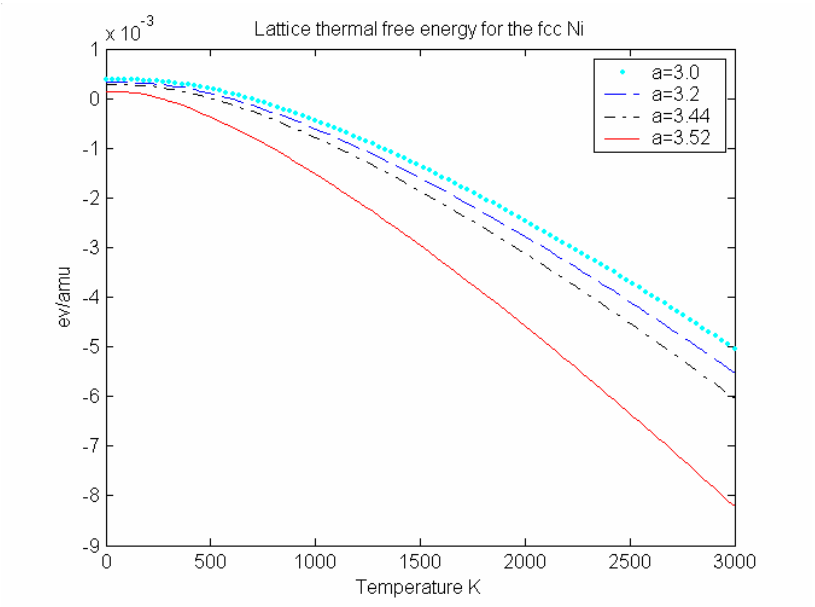

Figure A.5 The lattice thermal free energy of Ni vs. the temperature at selected lattice parameters

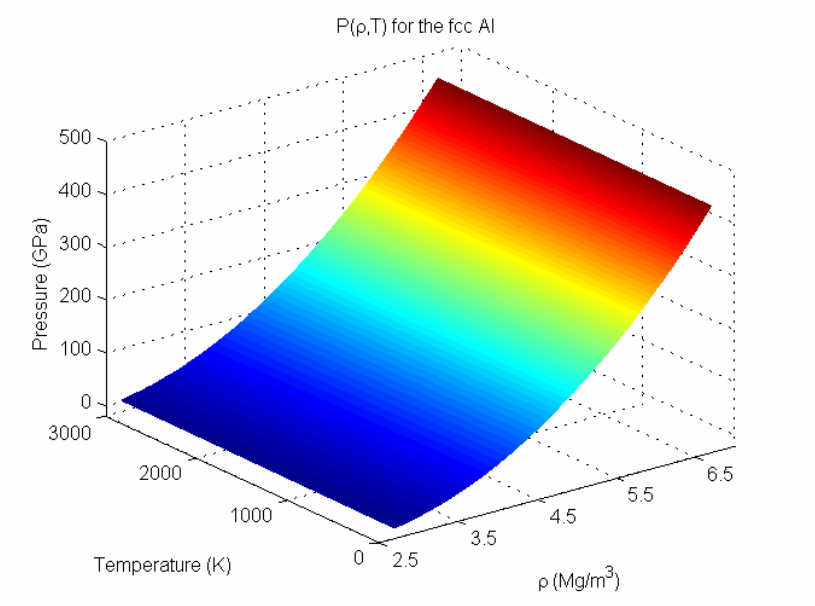

Figure A.6 The thermodynamically complete equation of state of Al

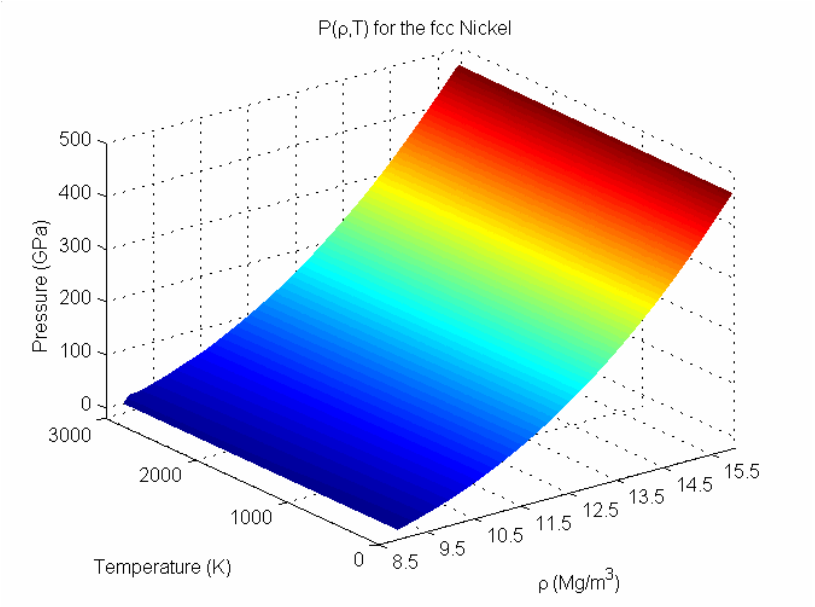

Figure A.7 The thermodynamically complete equation of state of Ni

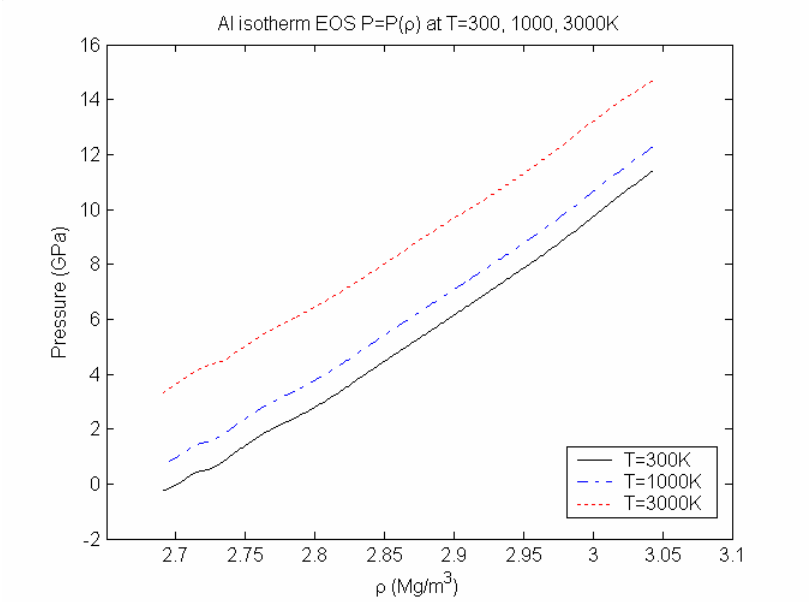

Figure A.8 Isotherm EOS for Al at T=0, 1000, 3000K

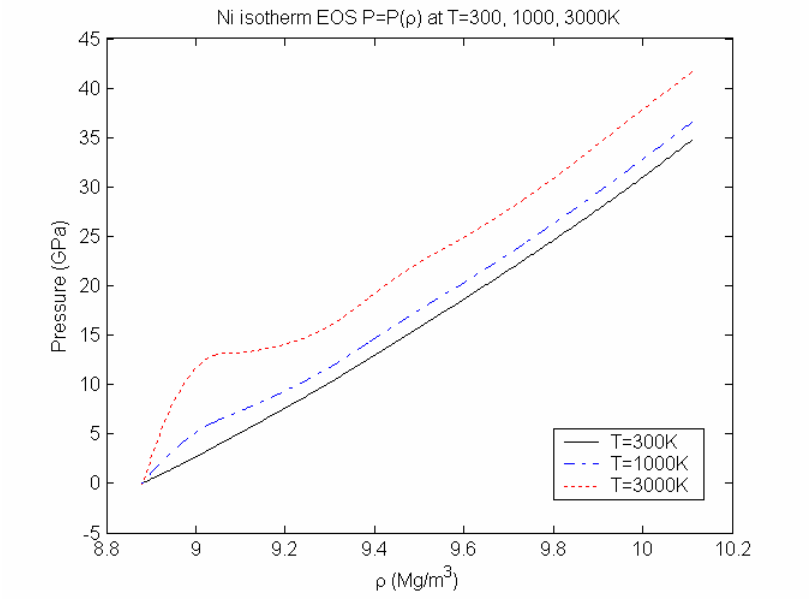

Figure A.9 Isotherm EOS for Al at T=0, 1000, 3000K

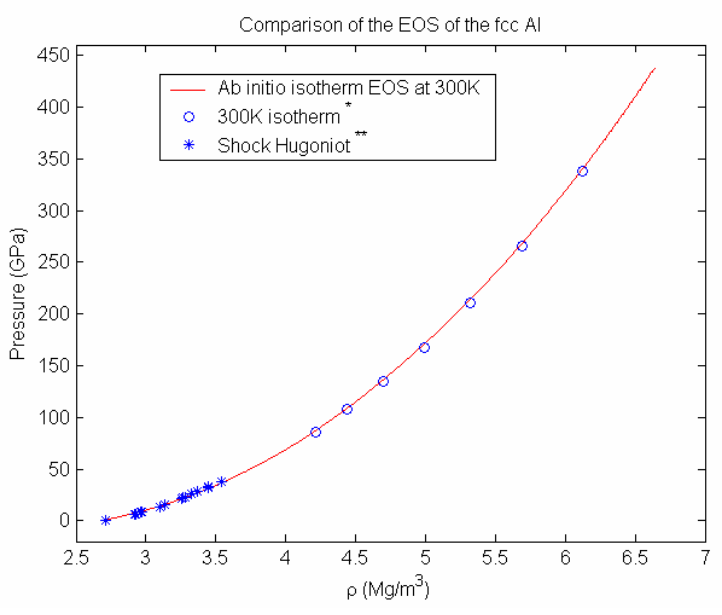

(a)

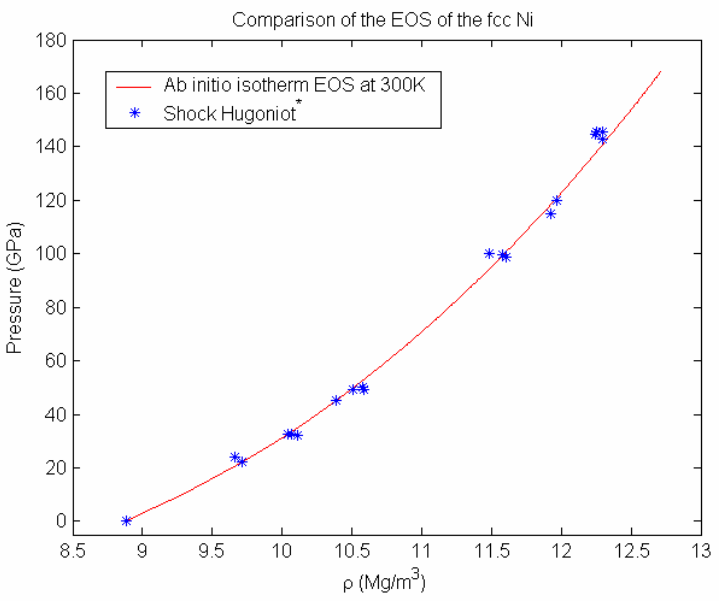

(b)

Figure A.10 Comparisons of EOS by ab initio isotherm EOS at 300K and shock Hugoniot. (a) Al, experimental data from Thadhani (low pressures) and Reference 35 (high pressures, with assumed ρ_0=2.67kg/m^3); (b) Ni, experimental data from Thadhani

A.2 Equations of the Direct Method[133]

If the force constant is written in the form of a vector, then it becomes

$$F(n,\mu) = -\sum_{(m,\nu)\in SC} U_{(3\times 9)}(m,\nu)\cdot \Phi^{(SC)}_{(9\times 1)}(n,\mu,m,\nu) \tag{A-1}$$

A force constant matrix $\Phi(n,\mu;m,\nu)$ represents a bond between two atoms (n, μ) and (m, ν) in one supercell. The displacement vector U = (U_x, U_y, U_z) has been converted to (3 × 9) matrix

$$U_{(3\times 9)} = \begin{pmatrix} U_x & U_y & U_z & 0 & 0 & 0 & 0 & 0 & 0 \\ 0 & 0 & 0 & U_x & U_y & U_z & 0 & 0 & 0 \\ 0 & 0 & 0 & 0 & 0 & 0 & U_x & U_y & U_z \end{pmatrix} \tag{A-2}$$

The supercell force constant can be represented by a nine-component vector and decoupled to the symmetry A and parameter $P^{(sc)}$ parts

$$\Phi^{(SC)}_{(9\times 1)}(n,\mu,m,\nu) = A_{(9\times p)}(n,\mu;m,\nu)\cdot P^{(SC)}_{(p\times 1)}(n,\mu;m,\nu) \tag{A-3}$$

Inserting it into equation (A-1), one finds

$$F(n,\mu) = -\sum_{(m,\nu)\in SC} U_{(3\times 9)}(m,\nu)\cdot A_{(9\times p)}(n,\mu;m,\nu)\cdot P^{(SC)}_{(p\times 1)}(n,\mu;m,\nu) \tag{A-4}$$

Denoting

$$C_{(3\times p)}(n,\mu;m,\nu) = -\sum_{(m,\nu)\in SC} U_{(3\times 9)}(m,\nu)\cdot A_{(9\times p)}(n,\mu;m,\nu) \tag{A-5}$$

equation (A-4) simplifies to

$$F(n,\mu) = C_{(3\times p)}(n,\mu;m,\nu)\cdot P^{(SC)}_{(p\times 1)}(n,\mu;m,\nu) \tag{A-6}$$

or in the global form

$$F = C\cdot P^{(SC)} \tag{A-7}$$

where F, C and $P^{(SC)}$ are matrices of dimensions (3ns×1), (3ns×p') and (p'×1). Here, n is the number of atoms in the supercell, s is the number of used displacements for which the Hellmann-Feynman forces were calculated, and p' is the total number of independent parameters. As a rule the number of forces 3ns is greater then the number of independent parameters i.e. 3ns > p', and the system of equation (A-7) is overdetermined. It may be solved by applying the singular value decomposition method[14] to matrix C, and expressing the parameter matrix in term of forces

$$P^{(SC)} = C^{-1} \cdot F \tag{A-8}$$

The C matrix is sparse, therefore, an algorithm for solving singular value decomposition for the sparse matrix could speed up the calculations. The direct method produces a solution, which is the best approximation in the least-square sense. Knowing parameters P^{SC} all supercell force constants can be found from equation (A-3). Equation (A-7) is the main equation of the direct method. It should be constructed with the aim of the supercell crystallite space group H, therefore, it depends on the selection of the supercell shape.

A.3 VASP Programming

The following four files are the central input files, and must exist in the work directory before VASP can be executed[5].

i. INCAR file

The INCAR file is the central input file of VASP. It determines 'what to do and how to do it'. It is a tagged format free-ASCII file: Each line consists of a tag (i.e. a string) the equation sign '=' and one or several values. Defaults are supplied for most parameters. A

default for the energy cutoff is for instance given in the POTCAR file, and therefore usually not required in the INCAR file.

ii. POSCAR

The POSCAR file contains the positions of the ions. The positions can be given in direct (fractional) or Cartesian coordinates. In the second case, positions will be scaled by the universal scaling factor supplied in the second line. The lattice vectors are always scaled by the universal scaling factor.

iii. KPOINTS

The KPOINTS files determines the k-points setting. The first line is a comment. If the second line equals zero, k-points are generated automatically using the Monkhorst-Pack's technique (first character in third line equals \M").

iv. POTCAR

The POTCAR file contains the pseudopotentials (for more then one species simply con-cat POTCAR files using the UNIX command cat). The POTCAR file also contains information about the atoms (i.e. their mass, their valence, the energy of the atomic reference configuration for which the pseudopotential was created etc.).

A.3.1 PTFE Input

a. INCAR file

The INCAR file for PTFE calculation is shown below:

SYSTEM =C15F30

ISTART = 0;

ISMEAR = 0; SIGMA = 0.1

IBRION = 2; ISIF = 3; NSW = 30

NBANDS = 240; IALGO = 38

LREAL = .TRUE.; ISMEAR = 0

EDIFF = 1E-06; EDIFFG = 1E-05

b. POSCAR file

The POSCAR file for PTFE calculation is shown below:

C15F30:

5.660

1.0000000000000000 0.0000000000000000 0.0000000000000000

-0.5000000000000000 0.8660000000000000 0.0000000000000000

0.0000000000000000 0.0000000000000000 3.4452

15 30

Direct

0.5746 0.5000 0.0333

0.4360 0.5179 0.1000

0.5506 0.4650 0.1667

0.4650 0.5506 0.2333

0.5179 0.4360 0.3000

0.5000 0.5746 0.3667

0.4821	0.4181	0.4333
0.5350	0.5856	0.5000
0.4494	0.4144	0.5667
0.5640	0.5819	0.6333
0.4254	0.4254	0.7000
0.5819	0.5640	0.7667
0.4144	0.4494	0.8333
0.5856	0.5350	0.9000
0.4181	0.4821	0.9667
0.8321	0.7272	0.0333
0.6049	0.2728	0.0333
0.1604	0.3302	0.1000
0.4645	0.7747	0.1000
0.8321	0.6049	0.1667
0.4645	0.1898	0.1667
0.1898	0.4645	0.2333
0.6049	0.8321	0.2333
0.7747	0.4645	0.3000
0.3302	0.1604	0.3000

0.2728 0.6049 0.3667

0.7272 0.8321 0.3667

0.6698 0.3302 0.4333

0.2253 0.1898 0.4333

0.3951 0.7272 0.5000

0.8102 0.7747 0.5000

0.5355 0.2253 0.5667

0.1679 0.2728 0.5667

0.5355 0.8102 0.6333

0.8396 0.6698 0.6333

0.3951 0.1679 0.7000

0.1679 0.3951 0.7000

0.6698 0.8396 0.7667

0.8102 0.5355 0.7667

0.2728 0.1679 0.8333

0.2253 0.5355 0.8333

0.7747 0.8102 0.9000

0.7272 0.3951 0.9000

0.1898 0.2253 0.9667

0.3302 0.6698 0.9667

c. KPOINTS file

The KPOINTS file for PTFE calculation is shown below:

K-Points

0

Gamma

3 3 1

0 0 0

A.3.2 5Al+5Ni+PTFE VASP Input

a. INCAR file

general:

SYSTEM = Ni-Al (111) Ptfe

ENMAX = 400;

ISMEAR = 0 ; SIGMA = 0.2;

ISTART = 0;

IBRION = 2; ISIF = 3; NSW = 30;

LORBIT = .TRUE;

EDIFF = 1E-6; EDIFFG = 1E-5;

LREAL = Auto

ISYM = 0

LCHARG = F

NPAR = 1

b. POSCAR file

For VASP. System= nialcf

1.00000000000000

5.66000000000000 0.00000000000000 0.00000000000000

-2.83000000000000 4.90170378541992 0.00000000000000

0.00000000000000 0.00000000000000 42.51483540000001

15 30 5 5

Direct

0.57820020000000 0.49990810000000 0.55662080000000 a

0.43228150000000 0.51836690000000 0.58717860000000 b

0.55338270000000 0.46359220000000 0.61777210000000 c

0.46365560000000 0.55333610000000 0.64836790000000 d

0.51849600000000 0.43236180000000 0.67896040000000 e

0.50005020000000 0.57827390000000 0.70952350000000 f

0.48159130000000 0.41394760000000 0.74008410000000 g

0.53637410000000 0.58979960000000 0.77066390000000 h

0.44695200000000 0.41043280000000 0.80125870000000 i

0.56755950000000 0.58588330000000 0.83184950000000 j

0.42159960000000 0.42166070000000 0.86240190000000 k

0.58586160000000 0.56764720000000 0.89295080000000 l

0.41031610000000 0.44691900000000 0.92354110000000 m

0.58965840000000 0.53630470000000 0.95413780000000 n

0.41388870000000	0.48145320000000	0.98471790000000	o
0.83186050000000	0.72792020000000	0.55450890000000	p
0.60446630000000	0.27210050000000	0.55871900000000	q
0.15978080000000	0.32886940000000	0.58506890000000	r
0.46403450000000	0.77444720000000	0.58922240000000	s
0.83265660000000	0.60586730000000	0.61558290000000	t
0.46383380000000	0.18989690000000	0.61994290000000	u
0.18989480000000	0.46353370000000	0.64621450000000	v
0.60580660000000	0.83261010000000	0.65053840000000	w
0.77451200000000	0.46398090000000	0.67690820000000	x
0.32885260000000	0.15990500000000	0.68106820000000	y
0.27214580000000	0.60438660000000	0.70743560000000	A
0.72796100000000	0.83199760000000	0.71164350000000	B
0.67133300000000	0.33112120000000	0.73797760000000	C
0.22561860000000	0.18954150000000	0.74213660000000	D
0.39385640000000	0.72675330000000	0.76845320000000	E
0.80999540000000	0.77415310000000	0.77284250000000	F
0.53691940000000	0.22659280000000	0.79908070000000	G
0.16779650000000	0.27294650000000	0.80348160000000	H
0.53583480000000	0.81023710000000	0.82978730000000	I
0.83997010000000	0.66877910000000	0.83397610000000	J
0.39569500000000	0.16784620000000	0.86031980000000	K
0.16773060000000	0.39561450000000	0.86449390000000	L

0.66899250000000	0.84011110000000	0.89081950000000	M
0.81014130000000	0.53578560000000	0.89500720000000	N
0.27295970000000	0.16776190000000	0.92129590000000	O
0.22627070000000	0.53660600000000	0.92573700000000	P
0.77381040000000	0.80999570000000	0.95197310000000	Q
0.72672300000000	0.39390010000000	0.95632850000000	R
0.18945330000000	0.22553560000000	0.98265540000000	S
0.33122640000000	0.67131640000000	0.98682460000000	T
0.66666666666667	0.33333333333333	0.23165780000000	5
0.00000000000000	0.00000000000000	0.29107830000000	6
0.33333333333333	0.66666666666667	0.36744280000000	7
0.66666666666667	0.33333333333333	0.42797310000000	8
0.00000000000000	0.00000000000000	0.49376660000000	9
0.00000000000000	0.00000000000000	0.01739320000000	0
0.33333333333333	0.66666666666667	0.05810880000000	1
0.66666666666667	0.33333333333333	0.09834240000000	2
0.00000000000000	0.00000000000000	0.14030000000000	3
0.33333333333333	0.66666666666667	0.18518740000000	4

c. KPOINTS file

K-Points

0

Gamma

3 3 1

0 0 0

A.3.3 Aluminum large deformation VASP input

a. INCAR file

SYSTEM = fcc Al

ISTART = 1;

ISMEAR = 0; SIGMA = 0.1

IBRION = 2; ISIF = 2; NSW = 10

EDIFF = 1E-7; EDIFFG = 1E-6

b. POSCAR file

Al:

1

4.0494000 0.00000000 0.0000000000000000

0.00000000 4.0494000 0.0000000000000000

0.0000000000000000 0.0000000000000000 4.049400

4

Direct

0.0000000000000000 0.0000000000000000 0.0000000000000000

0.0000000000000000 0.5000000000000000 0.5000000000000000

0.5000000000000000 0.0000000000000000 0.5000000000000000

0.5000000000000000 0.5000000000000000 0.0000000000000000

c. KPOINTS file

K-Points

0

Monkhorst Pack

11 11 11

0 0 0

REFERENCES

[1] M. Born, R. Oppenheimer, *Ann Phys.*, 84, 457 (1927)

[2] P. Hohenberg, W. Kohn, *Phys. Rev.*, 136, B864 (1964)

[3] W. Kohn, L. J. Sham, *Phys. Rev.*, 140, A1133 (1965)

[4] F. Jensen, *Introduction to computational chemistry*, John Wiley & Sons, Chichester, New York (1999)

[5] Georg Kresse and Jürgen Furthmüller, *VASP the GUIDE*

[6] P.E. Blöchl, *Phys. Rev. B*, 50, 17953 (1994)

[7] G. Kresse, J. Joubert, *Phys. Rev. B*, 59, 1758 (1999)

[8] A. R. Champion, J. Appl. Phys. 42, 5546 (1971)

[9] J. N. Johnson, J. J. Dick, and R. S. Hixson, J. Appl. Phys. 84, 2520 (1998)

[10] C. E. Morris, J. N. Fritz, and R. G. McQueen, J. Chem. Phys. 80, 5203 (1984)

[11] X. Gonze, Phy. Rev. B 55, 10337 (1997)

[12] X. Gonze, and C. Lee, Phys. Rev. B 55, 10355 (1997)

[13] X. Gonze and J. P. Vigneron, Phys. Rev. B 39, 13120 (1989)

[14] Press w. H., Teukolsky S. A., Vetterling W. T. and Flannery B. P., Numerical Recipes, Cambridge: University Press, Cambridge, 1992, pp. 670

[15] G. Kresse and J. Jafner, Phys. Rev. B 47, 558 (1993)

[16] G. Kresse and J. Furhtuller, Phys. Rev. B 54, 11169 (1996)

[17] W. Frank, C. Elsasser and M. Fahnle, Phys. Rev. Lett. 74, 1791 (1995)

[18] B. B. Karke, S. J. Clark, et. al., J. Phys.: Cond. Matter 9, 375 (1997)

[19] G. J. Ackland, M. C. Warren, J. Phys.: Cond. Matter 9, 7861 (1997)

[20] K. Parlinski, Z. Q. Li and Y. Kawazoe, Phys. Rev. B 61, 272 (2000)

[21] B. Meyer, V. Schott and M. Fahle, Phys. Rev. B 58, R 14673 (1998)

[22] K. Parlinski and Y. Kawazoe, Phys. Rev. B 60, 15511 (1999)

[23] N. K. Bourne and G. T. Gray III, J. Appl. Phys. 93, 8966 (2003)

[24] L. Piseri, B. M. Powell and G. Dolling, J. Chem. Phys. 58, 158 (1972)

[25] M. S. Miao, P. E. Van, et. al., Intl. J. Quan. Chem. 64, 243 (1996)

[26] J. C. L. Hageman, Robert J. Meier, et. al., Macromolecules 30, 5953 (1997)

[27] F. Bartha, F. Bogar, et. al., Phys. Rev. B 62, 10142 (2000)

[28] M. S. Miao, M. L. Zhang, et. al., J. Chem. Phys. 115, 11317 (2001)

[29] M. D'Amore, G. Talarico, et. al., J. Am. Chem. Soc. 128, 1099 (2006)

[30] J. C.Boettger, S.B.Trickey, Phys. Rev. B 53, 3007 (1996)

[31] R.E.Cohen, O.Gulseren, Phys. Rev. B 63, 2241 (2001)

[32] B. K.Godwal, S.K.Sikka and R.Chidambaram, Phys. Rev. B 20, 2362 (1979)

[33] R.G.Greene, H.Luo and A.L.Ruoff, Phys. Rev. Lett. 73, 2075 (1994)

[34] M.I.Katsnelson, M.Sigalas, et. al., Phil. Mag. B 75, 407 (1997)

[35] W. J.Nellis, J.A.Moriarty, et. al., Phys. Rev. Lett. 60, 1414 (1998)

[36] S.K.Sikka, V.Vijayakumar, Phys. Rev. B. 38, 10926 (1988)

[37] J. Xie, S. P. Chen, et. al., J.Phys: Condens. Matter 12, 8953 (2000)

[38] Akber-Knutson, Bukowinski, et. al., Geophys. Research Letts 29 N3, 1034 (2002)

[39] Q.Lizhi, C.Wai-Yim, J.American Ceramic Soc. 84 N4, 801 (2001)

[40] V.Milman, M.C.Warren, J. Phys. Condens. Matter. 13 N24, 5585 (2001)

[41] S.S.Kushwah, J.Shanker, Physica B: Condens. Matter 253, 90 (1998)

[42] Swift, D. C. Ackland, et. al., Phys. Rev. B 64, 2141071 (2001)

[43] Baconi, S. de Gironcoli, et. al., Rev. Mod. Phys. 73, 515 (2001)

[44] B. K. Godwal, R. Jeanloz, Phys. Rev. B 40, 7501 (1989)

[45] Robert G. Schmitt, Paul A. Taylor, et. al., http://www.intdetsymp.org/detsymp 2002/PaperSubmit / FinalManuscript/pdf/Schmitt-133.pdf

[46] F. Jing, Introduction to Experimental Equation of State. Ed. 2, (Science Press, Beijing,1999), 197 (in Chinese)

[47] X. Xu and W. Zhang, Theoretical Introduction to Equation of State. (Science Press, Beijing,1986), P235

[48] H.Y. Geng, N.X. Chen and M.H.F. Sluiter, Phy. Rev. B 70, 094203 (2004)

[49] J.W.D. Connolly, A.R. Williams, Phys. Rev. B 27, 5169 (1983)

[50] Vikas Tomar, Min Zhou, Phys. Rev. B 73, 174116 (2006)

[51] Masataka Mizuno, Hideki Araki, et. al., Phys. Rev. B 68, 144103 (2003)

[52] B.L. Gyorffy, Phys. Rev. B 5, 2382 (1972)

[53] A. Mookerjee and R. Prasad, Phys. Rev. B 48, 17724 (1993)

[54] S.S.A. Razee, et. al., J. Phys: Condens. Matter 3, 3301 (1991)

[55] S.S.A. Razee, et. al., Phys. Rev.B 42, 9391 (1990)

[56] S.S.A. Razee and R. Prasad, Phys. Rev. B 48, 1361 (1993)

[57] S.S.A. Razee and R. Prasad, Phys. Rev. B 45, 3265 (1992)

[58] S.S.A. Razee and R. Prasad, Phys. Rev. B 48, 1349 (1993)

[59] S.S.A. Razee, et. al, J. Phys: Condens. Matter 3, 3301 (1991)

[60] S.S.A. Razee, et. al, Phys. Rev. B 42, 9391 (1990)

[61] D.D. Johnson, et. al, Phys. Rev. Lett. 61, 3712 (1987)

[62] S. Muller, and A. Zunger, Phys. Rev. Lett. 87, 165502 (2001)

[63] S. Muller, and A. Zunger, Phys. Rev. B 63, 094204 (2001)

[64] V. Ozolins, and A. Zunger, Phys. Rev. B 57, R9404 (1998)

[65] V. Ozolins, C. Wolverton, and A. Zunger, Phys. Rev. B 58, R5897 (1998)

[66] C. Wolverton, and A. Zunger, Phys. Rev. Lett. 75, 3162 (1995)

[67] A. Silverman, et. al., Phys. Rev. B 51, 10462 (1995)

[68] N. Martensson, J. Phys. F: Metal Phys. 8, N1 27 (1978)

[69] A. Zunger, et. al., Phys. Rev. Lett. 65, 353 (1990)

[70] J.C. Boettger and S.B. Trickey, Phys. Rev. B 53, 3007 (1996)

[71] J.C. Boettger and D.C. Wallace, Phys. Rev. B 55, 2840 (1997)

[72] G. Steinle-Neumann and L. Stixrude, Phys. Rev. B 60, 791 (1999)

[73] R.G. Greene, H. Luo, and A.L. Ruoff, Phys. Rev. Lett. 73, 2075 (1994)

[74] Nellis, et. al, Phys. Rev. Lett. 60, 1414 (1988)

[75] S.K. Sikka and V. Vijayakumar, Phys. Rev. B 38, 10926 (1988)

[76] Xie, et. al, J. Phys.: Condens. Matter 12, 8953 (2000)

[77] S. Akber-Knutson, et. al, Geophysical Research Letters 29, 1034 (2002)

[78] L. Ouyan and W.Y. Ching, J. Am. Ceram. Soc. 84, 801 (2001)

[79] Milman and Warren, J. Phys.: Condens. Matter 13, 5585 (2001)

[80] S.S. Kushwah and J. Shanker, Physica B 253, 90 (1998)

[81] A.D. Becke, Phys. Rev. A 38, 3098 (1988)

[82] W.Y.C. Lee and R.C. Parr, Phys. Rev. B 37, 785 (1988)

[83] J.P. Perdew and Y. Wang, Phys. Rev. B 45, 13244 (1992)

[84] J.P. Perdew, K. Burke, and M. Ernzerhof, Phys. Rev. Lett. 77, 3865 (1996)

[85] N.C. Handy and A.J. Cohen, Mol. Phys. 99, 403 (2001)

[86] A.J. Cohen and N.C. Handy, Mol. Phys. 99, 607 (2001)

[87] N.C. Handy and A.J. Cohen, J. Chem. Phys. 116, 5411 (2002)

[88] C.L. Fu, et. al., Phys. Rev. B 48, 6712 (1993)

[89] G. Bester, et. al., Phys. Rev. B 60, 14492 (1999)

[90] Mikkelsen and Boyce, Phys. Rev. Lett. 49, 1412 (1982)

[91] Kikuchi, Phys. Rev. 81, 988 (1951)

[92] Chen, Atago and Mohri, J. Phys: Condens. Matter 14, 1903 (2002)

[93] Colinet and Pasturel, J. Alloys Compd. 296, 6 (2000)

[94] Zhang, et. al., Acta Mater. 51, 207 (2003)

[95] Sluiter and Kawazoe, Mater.Trans. JIM 42, 2201 (2001)

[96] Sluiter, et. al., Phys. Rev. B 42, 10460 (1990)

[97] Sluiter, et. al., Phys. Rev. B 53, 6137 (1996)

[98] Garbulsky and Ceder, Phys. Rev. B 49, 6327 (1994)

[99] Zhang, et. al., Acta Mater. 51, 207 (2003)

[100] Kresse and Furthmuller, VASP, Wien, Austria (2005)

[101] Friedli and Ashcroft, Phys. Rev. B 12, 5552 (1975)

[102] Ross and Johnson, Phys. Rev. B 2, 4709 (1970)

[103] Lam and Cohen, Phys. Rev. B 25, 6139 (1982)

[104] Chisolm, Crockett and Wallace, Phys. Rev. B 68, 104103 (2003)

[105] Levy, barak, and Ashkenazi, Phys. Rev. B 35, 9474 (1987)

[106] Vargas, Christensen, Phys. Rev. B 35, 1993 (1987)

[107] Mainkar, Browne, and Callaway, Phys. Rev. B 53, 3692 (1996)

[108] Aryasetiawan, Phys. Rev. B 46, 13051 (1992)

[109] Manghi, Bellin, and Arcangeli, Phys. Rev. B 56, 7149 (1997)

[110] Lichtenstein and Katsnelson, Phys. Rev. Lett. 87, 0672051 (2001)

[111] Biermann, Aryasetiawan, and Georges, Phys. Rev. Lett. 90, 0864021 (2003)

[112] J.P. Perdew and A. Zunger, Phys. Rev. B 23, 5048 (1981)

[113] A.D. Becke, Phys. Rev. A 38, 3098 (1988)

[114] J.P. Perdew and Wang Yue, Phys. Rev. B 33, 8800 (1986)

[115] A van de Walle and M. Asta, Handbook of Materials Modeling, volume I, Kluwer Academic Publisher, 2005

[116] N.D. Mermin, Phys. Rev. 137, A1441 (1965)

[117] J.P. Boehler, ZAMM (Zeitschrift für angewandte mathematik und mechanik), 59, 157 (1979)

[118] O.S. Zheng, A.J.M. Spencer, Int. J. Engng Sci., Vol. 31, No. 4, 617 (1993)

[119] O.S. Zheng, A.J.M. Spencer, Int. J. Engng Sci., Vol. 31, No. 5, 679 (1993)

[120] N. Kambouchev, J. Fernandez, and R. Radovitzky, Modelling Simul. Mater. Sci. Eng., 15, 451 (2007)

[121] J. Schröder and P. Neff, Int. J. Solids and Structures, 40, 401 (2003)

[122] J. Schröder, P. Neff, and V. Ebbing, J. Mechanics and Phys. of solids, 56, 3486 (2008)

[123] S. Ogate, J. Li, and S. Yip, Science, 298, 807 (2002)

[124] K. Yashiro, M. Oho, and Y. Tomita, Computational Materials Science, 29, 397 (2004)

[125] M. Cerny, M. Sob, J. Pokluda, and P. Sandera, J. Phys.: Condens. Matter, 16, 1045 (2004)

[126] G.V. Sin'ko and N.A. Smirnov, J. J. Phys.: Condens. Matter, 14, 6989 (2002)

[127] J. Chen, L.L. Boyer, H. Krakauer, and M.J. Mehl, Phys. Rev. B, 37, 3295 (1988)

[128] M.J. Mehl, J.E. Osburn, D.A. Papaconstantopoulos, and B.M. Klein, Phys. Rev. B, 41, 10311 (1990)

[129] O.H. Nielsen and R.M. Martin, Phys. Rev. B, 32, 3780 (1985)

[130] O.H. Nielsen and R.M. Martin, Phys. Rev. Lett., 50, 697 (1983)

[131] Y.L. Page and P. Saxe, Phys. Rev. B, 65, 104104 (2002)

[132] Y.L. Page and P. Saxe, Phys. Rev. B, 63, 174103 (2001)

[133] K. Parlinski, PHONON manual, http://wolf.ifj.edu.pl/phonon/, Cracow, (2007)

[134] W. Koch and M. C. Holthausen, A Chemist's Guide to Density Functional Theory, (2001)

[135] M. Tuckerman, J. of Phys.: Condensed Matter, 14, R1297, (2002)

[136] J.A. White and D.M. Bird, Phys. Rev. B, 50, 4954, (1994)

[137] G.B. Bachelet, D.R. Hamann, and M. Schlüter, Phys. Rev. B, 26, 4199, (1982)

[138] S. Cottenier, http://www.wien2k.at/reg-user/textbooks, (2002)

[139] U.Von Barth, and C.D. Gelatt, Phys. Rev. B, 21, 2222, (1980)

[140] A.R. Verma and O.N. Srivastava, Crystallography for solid state physics, John Wiley & Sons, (1982)

[141] C. Kittel, Introduction to solid state physics, 4th ed, John Wiley & Sons, (1971)

[142] A.J.M. Spencer, Continuum mechanics, Longman Inc, (1980)

[143] R.P. Feynman, Phys. Rev., 56, 340, (1939)

[144] D.J. Griffiths, Introduction to Quantum Mechanics, Prentice Hall, (1994)

[145] R.K. Bel'Kheeva, J. of App. Mech. and Tech. Phys., 48, 664, (2007)

[146] R.G. Schmitt, P.A. Taylor, et. al., Application of a multiphase mixture theory with coupled damage and reaction to energetic material response, Sandia National Laboratories.

[147] X. Lu and S. Hanagud, Mat. Res. Soc. Symp. Proc., 800, AA8.3.1, (2004)

VITA

ZHIBO WU

Zhibo Wu received her Bachelor degree from Nanjing University of Aeronautic and Astronautics in June 1994, Nanjing, China. She received her Master degree in Automatic Control from the same university in April 1999. Then she came to the Unit States. She received her Master degree in Aerospace Engineering from Old Dominion University in May 2004 before coming to Georgia Institute of Technology to pursue a doctorate in Aerospace Engineering. In May 2009, she successfully defended her PhD thesis.